A PRACTICAL METHOD FOR FRICTION COMPENSATION IN RAPID POINT-TO-POINT MOTION

by

Brian A. Bucci

B.S. Mechanical Engineering, University of Pittsburgh, 2005

M.S. Mechanical Engineering, Univeristy of Pittsburgh, 2007

Submitted to the Graduate Faculty of

the Swanson School of Engineering in partial fulfillment

of the requirements for the degree of

Doctor of Philosophy

University of Pittsburgh

2011

UNIVERSITY OF PITTSBURGH

SWANSON SCHOOL OF ENGINEERING

This dissertation was presented

by

Brian A. Bucci

It was defended on

January 13th 2011

and approved by

Jeffrey S. Vipperman, Associate Professor, Swanson School of Engineering

Daniel G. Cole, Assistant Professor, Swanson School of Engineering

William W. Clark, Professor, Swanson School of Engineering

Stephen J. Ludwick, Lecturer, Swanson School of Engineering

Zhi-Hong Mao, Assistant Professor, Swanson School of Engineering

Dissertation Director: Jeffrey S. Vipperman, Associate Professor, Swanson School of Engineering

A PRACTICAL METHOD FOR FRICTION COMPENSATION IN RAPID POINT-TO-POINT MOTION

Brian A. Bucci, PhD

University of Pittsburgh, 2011

Rapid point-to-point motion of a servo mechanism has obvious industrial applications. Due to their low cost, simplicity, application flexibility, and position stability, rolling element bearings are often a good choice for servos used in such processes. As industrial processes begin to require nanometer tolerances, settling time of a servo after a step motion has significant impact on process throughput. For most servo problems, linear systems theory works well to describe and predict servo response. However, on the sub-micrometer length scale, friction causes the servo to become a highly nonlinear system. Thus, a linear representation of the system that works well to describe and predict system performance on a larger length scale, does not work for sub-micrometer displacements. This leads to servo settling times that are much longer than would be predicted by linear systems theory. While methods of friction compensation, such as feedforward and friction observers, have been investigated in other efforts, they may not be entirely appropriate for the point-to-point motion problem. Further, the apparent frictional parameters of the servo mechanism appear to change in a way that is not easily quantifiable. Analysis of previous methods of friction compensation is often based on the assumption of perfect model matching and the unavoidable error between the actual friction process and the modeled friction process can have large negative impact on the efficacy of these previous methods. Thus, this work aims to design a friction compensation method that realistically considers uncertainty in the friction process and performs robustly with one simple parameterization of the algorithm.

Keywords: friction, point-to-point motion, bearings, friction control, nonlinear control.

TABLE OF CONTENTS

LIST OF TABLES

LIST OF FIGURES

1.0 INTRODUCTION

1.1 PROBLEM STATEMENT

For a large class of basic servo problems, linear systems theory works very well to describe servo behavior. Figure 1 shows an example of a how a simple linear model appears to accurately capture an actual servo step response. However, if figure 1 is scaled to show only the final micrometer of settling, as shown in figure 2, it is clear that the linear model does not make a global description of the servo behavior. A key feature seen in figure 2 is the apparent slowing down of the settling process. This is seen as the periods of the oscillations that occur during settling become longer as the servo approaches the target location. The cause of this behavior is pre-rolling friction. As a consequence of this phenomenon, ultra-precision point-to-point motion is not as fast as linear system theory would suggest. This complicates the design of industrial servo processes and seriously impacts their efficiency.

The two most widely accepted methods of dealing with friction in precision motion applications are feedforward methods and observer methods. Literature states that feedforward methods offer little benefit when the servo's position reference does not have dynamics[1]. In the point-to-point motion problem, the position reference begins at a static value, changes while the system carries out the stepping motion, and resumes a static value during servo settling. The problem to be addressed occurs during the settling phase of the process thus, the position reference is static and feedforward methods are not applicable. Friction observers

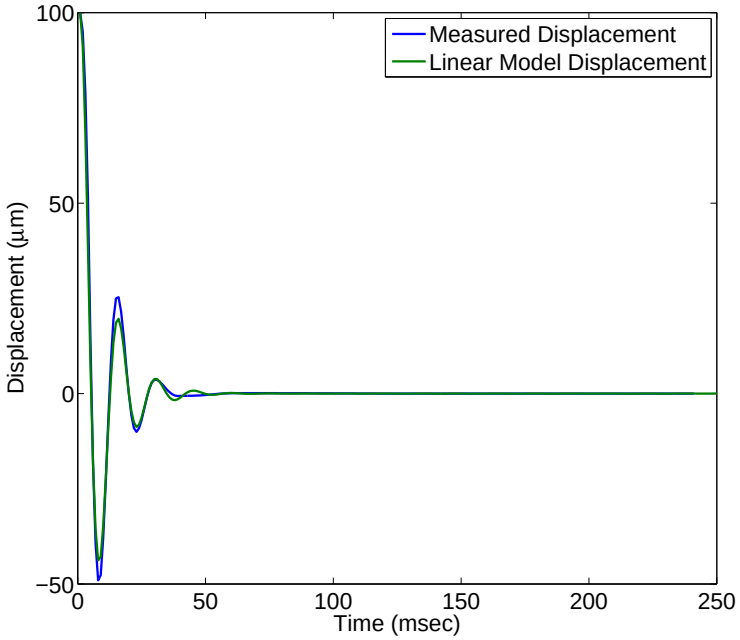

Figure 1: A basic linear model appears capable of capturing the majority of this 100 µm step response of a precision servo. A good model of servo behavior is useful in the design of industrial processes. (The measured data is from an actual step response of a crossed-roller linear stage)

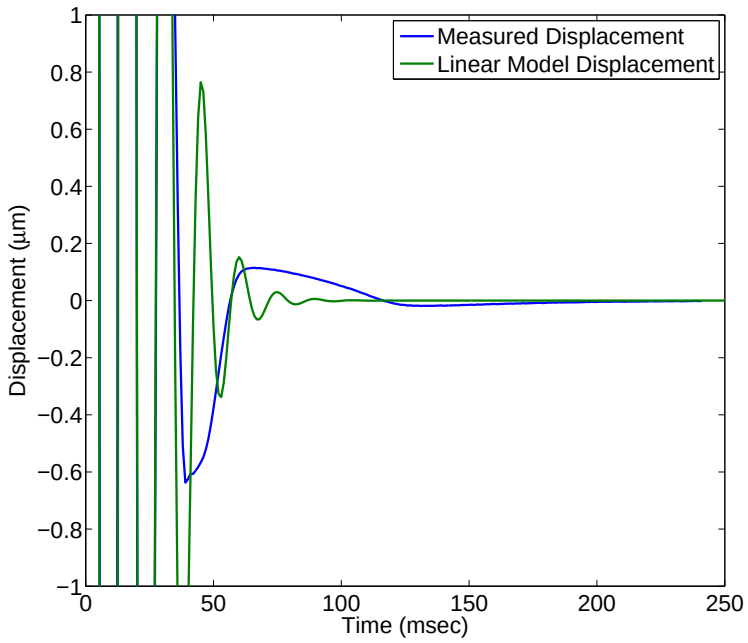

Figure 2: The basic linear model, that appeared to capture servo behavior in the previous figure, clearly does not make an accurate representation of servo response during the final micrometer of settling. The pre-rolling friction phenomenon causes this change in system response. This raises questions about the utility of linear systems theory methods for servo processes that require sub-micrometer precision. (The measured data is from an actual step response of a crossed-roller linear stage)

have been shown to improve accuracy at tracking tasks but, even some of the developers of friction observers show that they do not perform well at high accuracy servo settling for point-to-point motion[2]. With the deficiencies of these methods at the point-to-point motion control problem, precision point-to-point motion control is usually done with conventional linear PID control.

It is believed that a control design that realistically considers the behavior of pre-rolling friction and is specifically designed for servo settling will be able to offer better performance than linear PID control. *Thus, this effort aims to model the force of pre-rolling friction over these very small displacements and then incorporate this model of friction into a control algorithm to reduce point-to-point settling time for servo mechanisms. Additionally, it is theorized that pre-rolling friction is not a well behaved process. In short, the parameters of an advanced friction model for the global description of the pre-rolling phenomenon for a particular servo will only be available within some confidence bound. Thus, an effective point-to-point friction compensation method must be robust to parameter uncertainty.* Figure 3 shows that servo settling time from $\pm$ 3 nm to $\pm$ 100 nm can be reduced by up to 87.4%, compared the PID control, with use of such as algorithm.

1.2 OBJECTIVES

The goal of this research is to improve ultra-precision point-to-point performance of precision servo mechanisms. Toward this end, the objectives of this effort can be summarized as:

1. Determine the length scale at which linear control methodologies break down (Chapter 5).
2. Characterize the force of friction over sub-micrometer displacements (Chapter 6).
3. Generalize these observations to large length scales with full point-to-point motions and, if necessary, explain the effects of variables that may not be included in the original friction models (Chapter 6.3).
4. Develop, implement, and evaluate a feedback control algorithm to decrease the settling time for rapid point-to-point motion (Chapter 7-9).

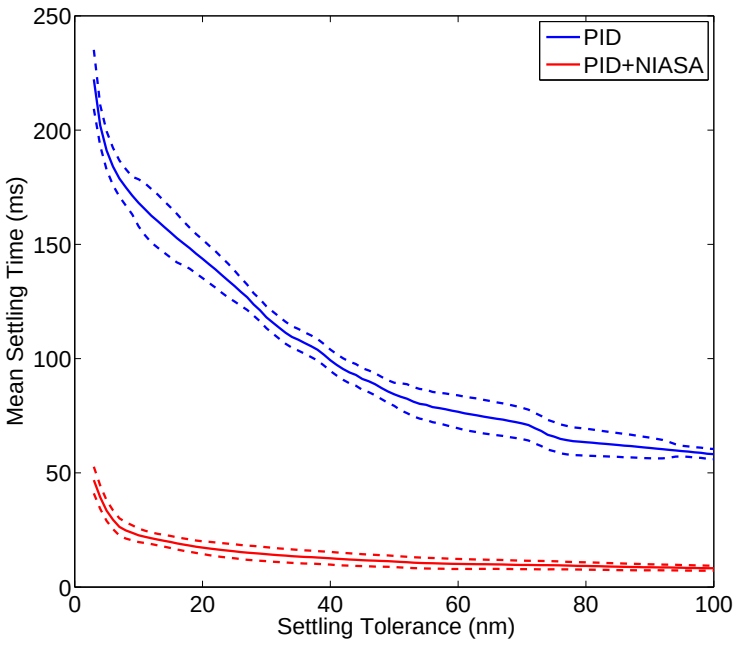

Figure 3: For 250 instances of 5 mm steps done on an actual precision servo, the mean servo settling time to tolerances of $\pm$ 3 nm to $\pm$ 100 nm can be reduced by up to 87.4% with use of the proposed friction model based settling algorithm. In this plot, the solid series represents the mean settling time to the specific tolerance and the dashed series shows one standard deviation from the mean value.

2.0 ADVANCED FRICTION MODELS

2.1 CLASSICAL MODELS AND THEIR LIMITATIONS

The two widely accepted classical friction models are the viscous model and the Coulomb model. Linear viscous friction can be approximated as,

$$F_r = \sigma_2 \dot{x}, \tag{2.1}$$

where F_r is the force of friction, σ_2 is the coefficient of viscous friction, and $\dot{x}$ is the velocity. Coulomb friction is defined as

$$F_r = \mu_k F_N \operatorname{sgn}(\dot{x}) \tag{2.2}$$

where F_r is the force of Coulomb friction, μ_k is the coefficient of kinetic friction, F_N is the normal force at the contact, and $\dot{x}$ is the relative velocity of the two surfaces at the contact. In a complex, multi-contact rolling contact mechanism such as a linear bearing, it becomes difficult to provide values for μ_k and F_N. However, continuous motion in one direction will usually cause a somewhat constant drag force. Thus, the Coulomb model could be expressed as

$$F_r = F_C \operatorname{sgn}(\dot{x}), \tag{2.3}$$

where F_C is the apparent level of Coulomb friction. The direction of this force will always be opposing motion.

The top plot in figure 4 shows an actual decaying sinusoidal motion profile and the bottom plot shows the computed force of friction versus displacement. The colored dots have been included to aid in visualizing how the time domain data translates into the spatial domain. Figure 5 shows a viscous model fit to the data from figure 4. The one problem with this

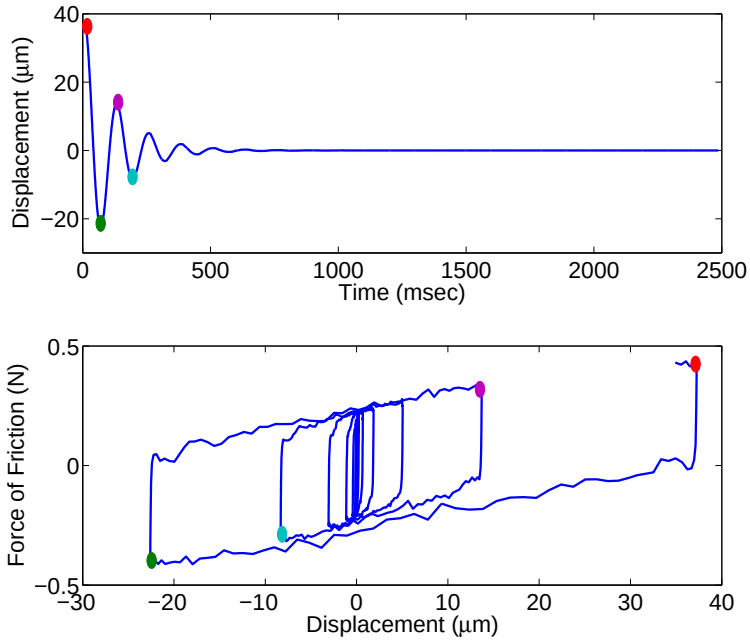

Figure 4: It is seen how the force of friction produces a family of hysteresis loops when the force of friction is plotted versus displacement for a sinusoidal displacement command with decaying amplitude(bottom plot). Colored dots have been included to aid in visualizing how the data maps between domains. (This plot shows actual data from a crossed-roller linear stage)

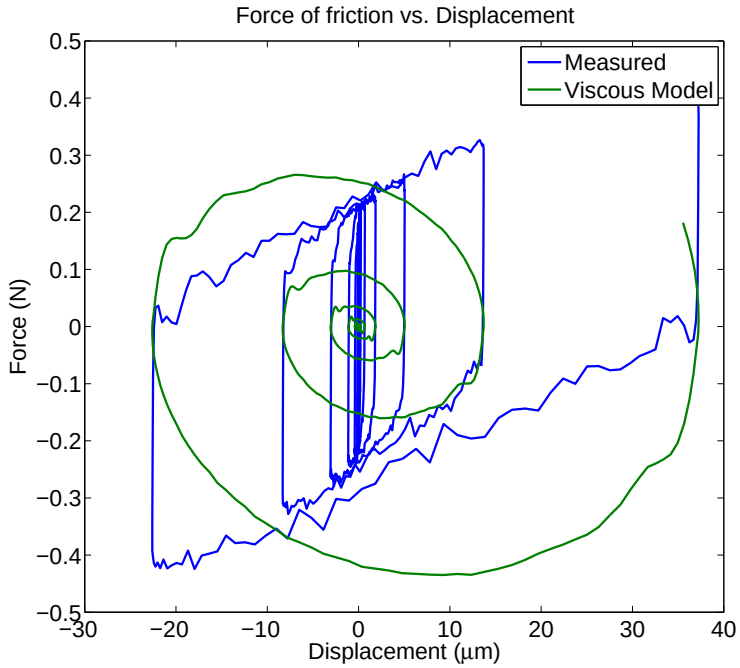

Figure 5: The viscous model linearly relates instantaneous velocity to the force of friction. While this model makes some approximation of the measured data, some key features are not captured. With the viscous model the force of friction is zero when velocity is zeros. However, the data does not suggest that the force of friction tends to zero when velocity goes to zero. Also, the viscous seems to over estimate the force of friction towards the beginning of the motion followed by a gross under estimation of the force of friction as the motion profile continues.

model is that viscous friction goes to zero when velocity is zero. The measured data suggests that the force of friction can have a non-zero value even if velocity is zero. Figure 6 shows the Coulomb model fit to the same data. The Coulomb model considers friction to be either a positive constant or a negative constant, depending on the direction of motion. However, the measured data indicates that the force of friction has some transition region after a velocity reversal occur and this transition is not instantaneous. The effects of combining the viscous and Coulomb model are shown in figure 7. While this combination of models offers a better representation of the experimental observations, there are still characteristics which could be improved upon. One serious issue is that the combined model still predicts the force of friction to significantly decrease when slowing down to approaching a velocity reversal while, the measure data indicates that the force of friction will continue to increase. On this length scale the system appears to have the characteristic of a hysteretic stiffness and neither the viscous model, the Coulomb model, nor a combination of the two are able to sufficiently describe the system behavior.

2.2 ADVANCED FRICTION MODELS

A useful friction model should be as simple as possible; while describing as much frictional behavior as possible. Therefore a balance must be struck between capturing the most frictional behavior and using the least amount of free parameters[3]. The viscous and Coulomb friction models were shown to not completely capture the behavior of the force of friction on sub-micrometer scale. Unfortunately, the link between the physics that govern this type of behavior on the microscopic scale and how this relates to somewhat larger scale observations is rather poorly understood. However, several useful phenomenological models have been developed to approximate this behavior.

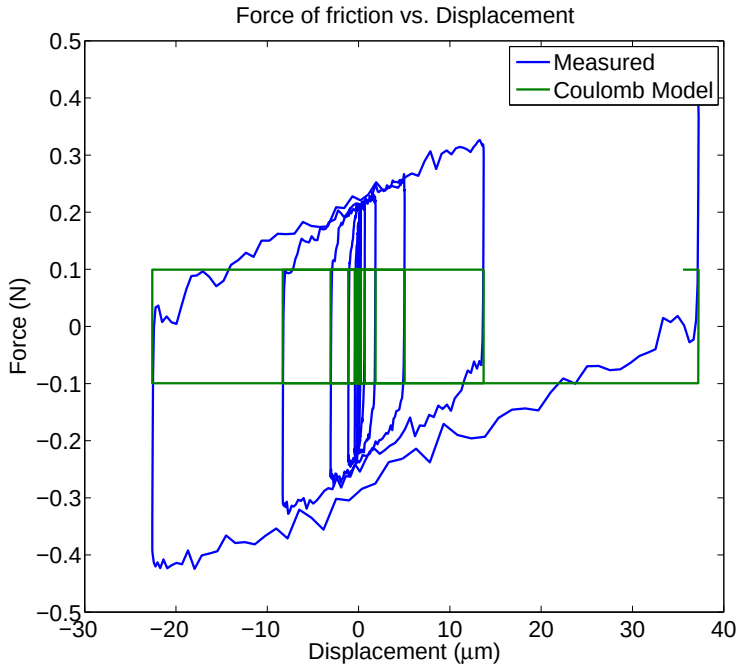

Figure 6: The Coulomb friction model relates the direction of the system velocity to the force of friction. This appears somewhat better at approximating the measured data than does the viscous model. However, the instant change in force, upon velocity reversal, that the Coulomb model yields does not agree with the gradual change in force seen in the measured data.

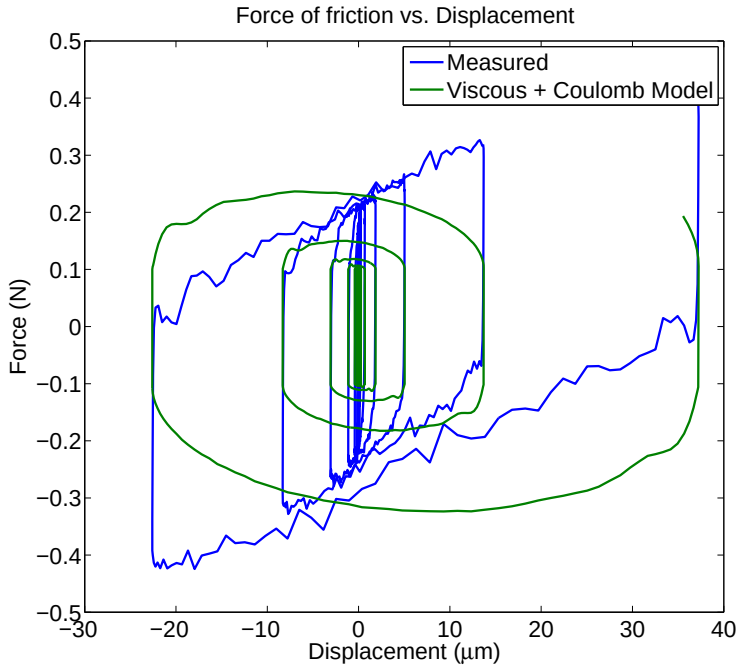

Figure 7: Combining the viscous and Coulomb models leads to a better fit to the measured data but, there are still problems with the characteristics of this fit. The combined model tends to predict the largest values for the force of friction in the middle of each oscillation, when the velocity is the largest. However, the measured data suggests that the force of friction tends to continue to increase as velocity decreases. Thus, relating the force of friction to simply the magnitude of velocity and the sign of the velocity does not provide a good representation of the pre-rolling friction process.

2.2.1 Stribeck Model

The first more complex description of the force of friction is the Stribeck model[4]. It is known from elementary physics that more force is needed to initiate sliding of a stationary object on a frictional surface than is needed to maintain sliding of the same object. This leads to defining a level of static friction, or force needed to initiate sliding, and a level of kinetic friction or Coulomb friction, or force needed to maintain sliding. This leads to model with discrete jumps in force making it difficult to apply in practice. However, Stribeck's work found that as the velocity of a sliding object decreases, at some velocity, the force of friction begins to increase from the Coulomb level to the static level[4]. This model is defined as

$$F_r = s(v) = F_C + (F_s - F_C)\exp\left(-\left|\frac{v}{V_s}\right|^{\delta}\right) \tag{2.4}$$

The model of the Stribeck effect includes the level of kinetic Coulomb friction, F_C, the level of static friction, F_s, the Stribeck velocity, V_s, and a shape factor, δ, which is typically set to 1. Defining the Stribeck effect as a function of velocity, $s(v)$, is a result that will become useful in other advanced friction models. This model is able to describe slip-stick behavior in frictional contacts but it is not able to describe the hysteretic stiffness behavior near velocity reversals.

2.2.2 Dahl Model

Hysteretic stiffness behavior near velocity reversals is also known as pre-rolling, pre-sliding, or micro-slip and is known to be observed for several micrometers following a velocity reversal[5]. Thus, if an object is moving along one axis subject to a constant frictional force and its direction is reversed, the object will have to travel at least several micrometers in the other direction before the force of friction can reach the same relative magnitude. The simplest and oldest of the more complex friction models capable of capturing this behavior is the Dahl model [6], defined as,

$$\frac{dF_r}{dx} = \sigma\left|1 - \frac{F_r}{F_C}\right|^{i}\operatorname{sgn}\left(1 - \frac{F_r}{F_C}\right) \tag{2.5}$$

where F_r is the force of friction, x is generalized coordinate defining the axis of motion, σ is the initial contact stiffness, F_C is the approximate level of Coulomb sliding friction, and i is a shape factor parameter. The Dahl interpretation of the force of friction may also be solved in time using the chain rule as

$$\frac{dF_r}{dt} = \frac{dF_r}{dx}\frac{dx}{dt} \tag{2.6}$$

This model is rate independent and does not account for possible Stribeck effect but, it does produce hysteretic behavior.

Figure 8 shows a fit of the Dahl model to the same friction data. While this fit is not perfect, some key characteristics of pre-rolling friction are able to be captured by the Dahl model. The Dahl model is the first model presented that is able to model a transition between opposite levels of Coulomb friction when velocity reversals occur. This allows the model to produce hysteresis loop structures that are characteristic of experimental observations. Additionally, when using the Dahl model, the force of friction can be a non-zero value when velocity is zero. This is also a characteristic that has been experimentally observed.

2.2.3 LuGre Model

The LuGre model was developed to include rate dependence and Stribeck effects[7]. The LuGre model approximates surfaces subject to a frictional contact as numerous contacting bristles which have individual stiffness and damping parameters. By averaging numerous individual interactions, the bulk phenomenon can be described by a simple model. The LuGre model is stated as,

$$\frac{dz}{dt} = v - \sigma_0 \frac{|v|}{s(v)} z \tag{2.7}$$

$$F_r = \sigma_0 z + \sigma_1 \frac{dz}{dt} + \sigma_2 v \tag{2.8}$$

where z is a hidden state describing the deflection of the bristles, v is the relative velocity between the surfaces, and the function $s(v)$ accounts for the Stribeck effect. The additional frictional constants are the micro-stiffness (bristle stiffness), σ_0, the micro-damping (bristle damping), σ_1, and the coefficient of viscous drag σ_2.

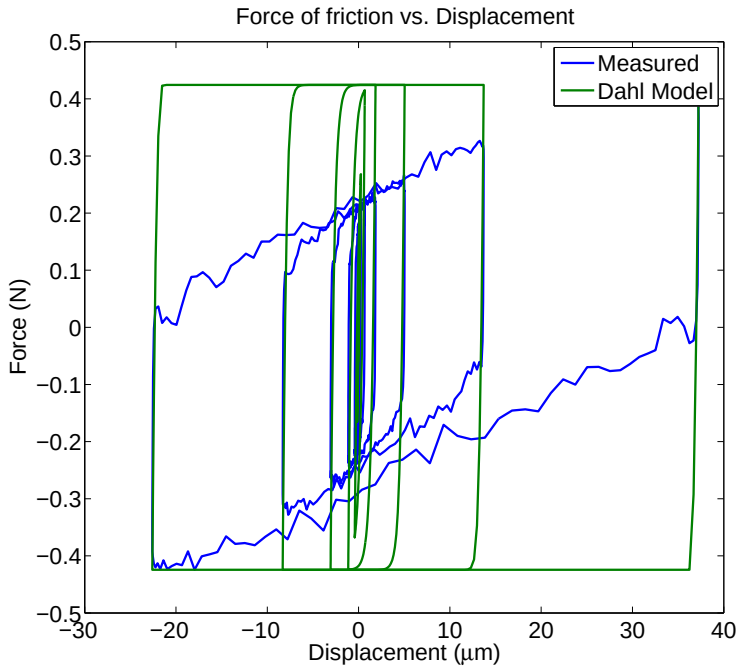

Figure 8: The Dahl model fit to this data set is far from perfect but, this increase in complexity is starting to be able to capture some of the key characteristics of pre-rolling friction. This model is able to express a transition in the magnitude of the force of friction that occurs at velocity reversals. Additionally, this model is able to produce the loop structures which are characteristic of pre-rolling friction.

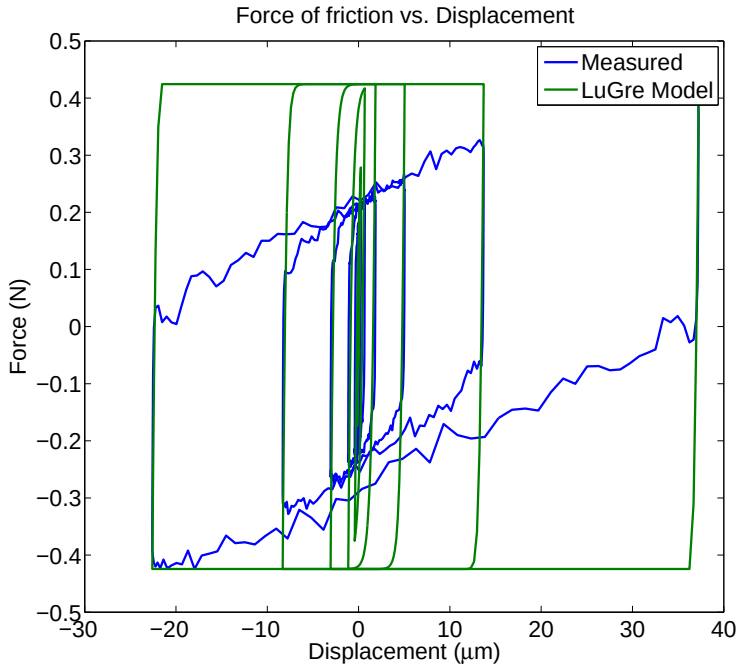

Figure 9: This fit of the LuGre model to the measured data is almost exactly the same as the Dahl model. This is because the difference between the LuGre model and the Dahl model is that the LuGre model also considers rate dependent effects and the Dahl model does not. Since this data did not show strong rate dependent characteristics, the rate dependent terms are found to be insignificant and the resulting fit appears much like the Dahl model fit. This case serves as a reminder that frictional phenomenon that are real and important in particular cases, may not be important in other cases.

Figure 9 shows a fit of the LuGre model to the same dataset. The first observation is that this model fit looks almost identical to the Dahl model fit. This is true because the Dahl model can actually be expressed as a special case of the LuGre model, a topic which will be discussed later. Recalling that the chief contribution of the LuGre model is the incorporation of rate dependent effects, the fitting algorithm was not able to detect rate dependent effects in this data and thus, the rate dependent terms become insignificant. This example serves as a cautionary reminder that although some frictional phenomenon are very real and have been legitimately identified by numerous researchers, there is no unifying theory of friction which covers all scenarios and a phenomenon that may be very important for one case of a type of contact may be undetectable in another. Thus, the behavior of the data should drive the effort, not the desire to use a particular model.

2.2.4 Generalized Maxwell Slip (GMS) Model

Keeping in mind the previous comments concerning frictional phenomenon and the lack of unifying theory of friction which covers all frictional scenarios, some efforts have observed pre-rolling friction to have arbitrarily shaped transition curves that are not well captured by the Dahl or LuGre models[8, 9, 10]. The chief contribution of the GMS model is the incorporation of a hysteresis function instead of the simple hidden state used in the LuGre model. The GMS model with the hysteresis function has non-local memory, meaning the model has memory of all velocity reversals while the system remains in the pre-sliding regime, as opposed to the Dahl and LuGre models which have local memory, meaning that the model only has memory of the last velocity reversal[8, 9]. Recent studies [8, 9] suggest that the force of friction in the pre-sliding regime shows non-local memory characteristics. This change affects the pre-sliding characteristics of the GMS model while the gross sliding characteristics are identical to the LuGre model. The GMS model is stated as

$$\frac{dz}{dt} = v\left(1 - \operatorname{sgn}\left(\frac{F_h(z)}{s(v)}\right)\left|\frac{F_h(z)}{s(v)}\right|^n\right) \tag{2.9}$$

$$F_r = F_h(z) + \sigma_1\frac{dz}{dt} + \sigma_2 v, \tag{2.10}$$

where z is a hidden frictional state, $F_h(z)$ is the hysteresis function, n is a shape factor, v is the relative velocity between the surfaces, and the function $s(v)$ accounts for the Stribeck effect. The additional frictional constants are the micro-damping (bristle damping), σ_1, and the coefficient of viscous drag σ_2. A Maxwell slip model is used to construct the hysteresis function. This model consists of a number of parallel saturating stiffness elements. In a single Maxwell slip element, the input is the hidden state, z, and the output is a force, which is one component of the overall force of friction. As the magnitude of the input z, increases, the magnitude of the output increases until a threshold is reached. At this point the element slips and force output will remain constant for any further increase in input magnitude. If at any point in time the rate of input, $\frac{dz}{dt}$, changes sign, stiffness behavior will resume until either the positive or negative threshold values are reached. Since the hysteresis function is likely to contain multiple Maxwell slip elements, the value of the hysteresis function can be written as

$$F_h(z) = \sum_{i=1}^{N} F_i \tag{2.11}$$

where N is the total number of Maxwell slip elements and F_i is the force output of each respective element.

Figure 10 shows the fit of a GMS model to the example data. In the case of this particular dataset the extra degrees of freedom provided by the GMS model offers the most accurate fit, compared to the other friction models. However, even a perfect fit of one friction model to one set of data does not imply that the frictional behavior for a particular device has been completely characterized.

Three friction models of increasing complexity have been introduced in the previous paragraphs. In an interesting result, the less complex friction models are special cases of the more complex models. The LuGre model is actually the GMS model when

$$F_h(z) = \sigma_0 z \tag{2.12}$$

and the saturation level is set to ∞. The LuGre model when $F_s = F_C$ and $\sigma_1 = \sigma_2 = 0$ is Dahl model with shape factor $i = 1$. These results are useful because; if a control algorithm can be developed around the GMS model, it could be easily generalized for evaluation with the other two models.

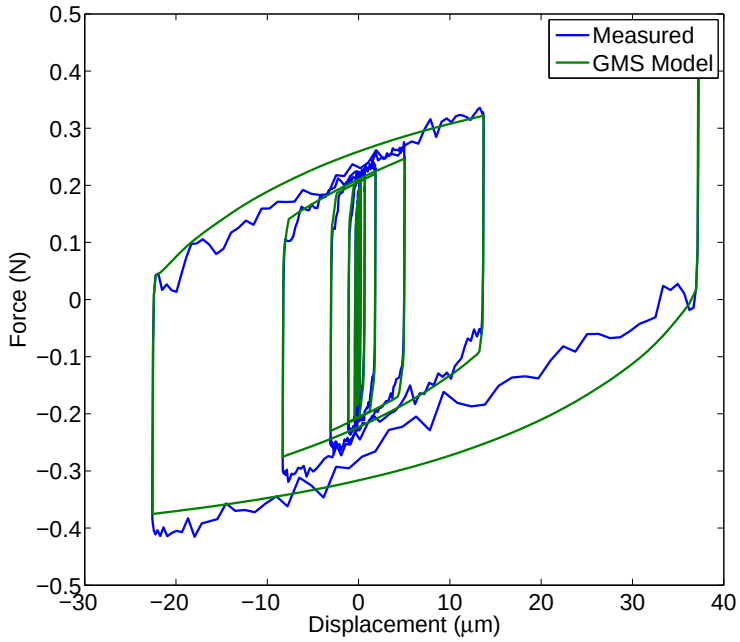

Figure 10: The extra degrees of freedom (N=8), provided by the GMS model, allow for the most accurate approximation of the measured data, compared to the other models which have been presented. However, this increase in modeling accuracy comes at the cost of increased complexity. It must also be considered that accurate fitting of a single set of data does not guarantee a complete characterization of frictional behavior of a device under all conditions.

3.0 THE ULTRA PRECISION RAPID POINT-TO-POINT MOTION PROBLEM AND EQUIPMENT

3.1 POINT-TO-POINT MOTION

In numerous applications, it is useful to have a servo mechanism rapidly move from one point to another. Initially, one may consider this motion analogous to the classical step response. In an actual precision industrial servo, a classical step in reference would almost never be used. Recalling that a classical step contains energy at all frequencies and that even the best designed servos and payloads will have undesirable high frequency resonances, it would be wise to avoid exciting these modes. Additionally, depending on the specifications of the system and magnitude of the step in reference, the undesirable condition of amplifier saturation is a possibility. In actual practice the position reference signal would be profiled to avoid these issues. Figure 11 shows an example of a profiled position reference signal.

The time when the position reference signal is changing will be known as the gross motion of the system. Once the position reference has stopped changing, the system will be said to have entered the settling phase of the motion. Every positioning system will still display some noise even when it has been commanded to stay in the same location for a very long time. This is known a in-position noise or jitter. Friction plays a role in all phases of system motion but, with regards to the ultra precision point-to-point motion problem, the behavior of pre-rolling friction during settling is most important to this work.

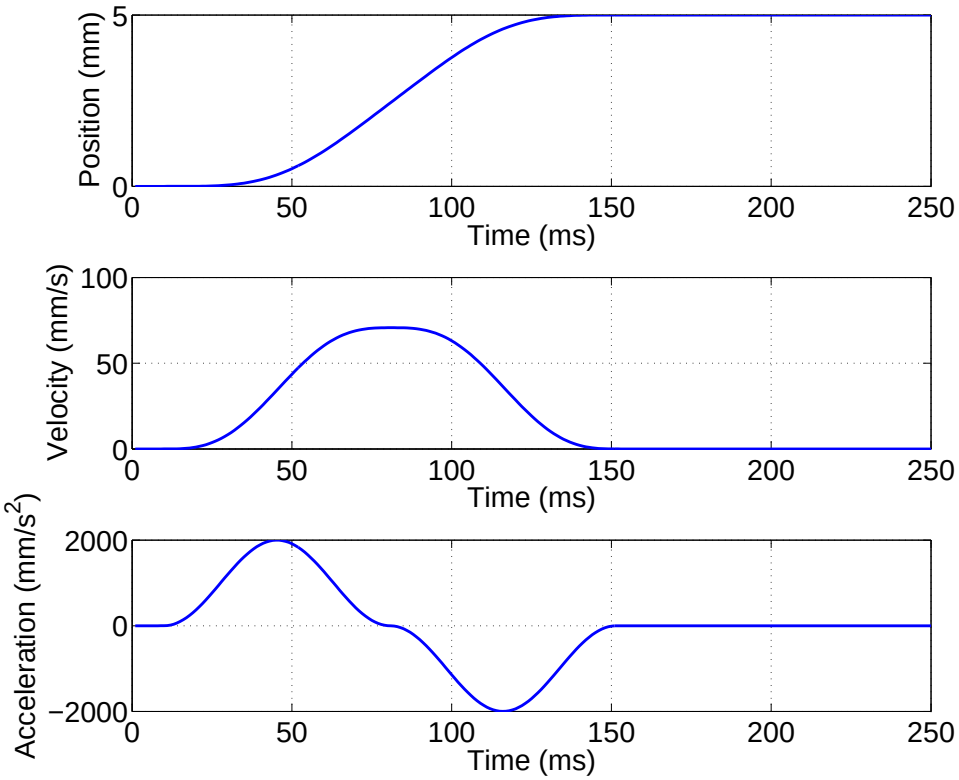

Figure 11: When rapid point-to-point motion is done on an industrial servo the position reference is typically profiled. The commanded displacement, velocity, and acceleration for a typical 5 mm step is shown in this plot.

Figure 12: The ALS-130H linear stage, by Aerotech Inc., is the precision servo used in this experimental study.

3.2 EQUIPMENT

The primary piece of equipment utilized in this study is an Aerotech ALS-130H. The stage provides 100 mm of linear travel with a carriage supported by linear crossed roller bearings. The stage has a moving mass of 1.8 kg and an encoder resolution of 61 pm. The stage is driven by an NDrive ML Linear Controller/Drive by Aerotech. This gives a servo sampling rate of 8 kHz. Figure 12 shows a picture of the ALS-130H linear stage.

4.0 FRICTION MEASUREMENT AND COMPENSATION

4.1 FRICTION MEASUREMENT

To model and eventually control systems with friction, it is necessary to measure the force of friction. Measuring the force of friction on the sub-micrometer length scale can prove quite challenging with conventional force sensors such as load cells. This is because most force senors rely on a deformation a part of the transducer to estimate force[11]. Even if the deformation of the transducer is only tens of nanometers, it may be too much to accurately capture the interesting components of pre-rolling friction. Thus, using a conventional force senor can add the mechanical dynamics of the sensor to the measurement, an undesirable situation.

To make measurement of pre-rolling friction behavior less obvious transducer configurations can prove useful. Harnoy et al. show an example of a method where an object is placed on an oscillating base and estimation of the force of friction can be made by measuring the acceleration of the object [12]. This is quite interesting because the measurement of the acceleration of the object should not interfere with the frictional process and, if the mass of the object is measured, a measurement of acceleration is enough to solve Newton's second law to determine the force of friction.

Bucci et al. applied this methodology to a fully assembled precision linear stage[10]. In this work, the stage actuator was disabled and the base of the stage was oscillated in the direction of intended motion. Friction in the precision linear stage was successfully measured using this method and the resulting data generally agreed with most previous descriptions of pre-rolling friction. The drawback of this method proved to be the lack of control over the motion of the carriage of the stage relative to the base of the stage. Since there was not

control of the carriage motion, there was no way to specify what range of displacement the force of friction was to be studied across. It was also troubling to find that if the carriage was placed in a particular location, as to study pre-rolling friction in that location, it would tend to wander to other locations. Thus, this method proved interesting as an academic exercise but, in its current state, was not a practical method of characterizing friction in precision servos.

The most simple way to estimate the force of friction in a precision servo is by the current scaling method. The equations of motion for an electric motor can be approximated as

$$m\ddot{x} + F_r = K_t i, \tag{4.1}$$

$$L\frac{di}{dt} + Ri + K_e\dot{x} = v\left(t\right), \tag{4.2}$$

where m is the mass or inertia, x is a generalized displacement, F_r is the friction force, K_t is the motor force constant, L is the inductance of the coil, i is the current in the coil, R is the resistance of the coil, K_e is the back EMF constant, and $v\left(t\right)$ is a voltage input. For the precision servo to be studied and the small motion to be considered, the K_e term tends to be insignificant. Also the electrical dynamics tend to be much faster than the mechanical dynamics so, equation 4.2 becomes insignificant. The servo control structure uses three cascaded loops. Starting from the outside and moving in, these loops are: the position loop, the velocity loop, and the current loop. Thus, in the control architecture the current in the motor coil is a controlled variable for which information is easily obtained. The force of friction can now be estimated as

$$F_r = K_t i - m\ddot{x}. \tag{4.3}$$

For small motions, in the pre-rolling regime, the $m\ddot{x}$ term is often very small compared to the other terms and can be ignored. However, it is better practice to either measure $\ddot{x}$ or estimate it from measurements of x. Measurement of acceleration may not be feasible because the use of additional sensors is usually not desirable. Estimation of acceleration from displacement data could present a problem because a twice differentiation of a discrete time signal is likely to add a substantial amount of noise to the estimate. However, if position measurement

resolution is small enough this issue can be minimized. Additionally, for characterization purposes, friction estimation can be done in post-processing so, acausal filtering methods can be used to eliminate phase loss. In the case of this effort, the current scaling method is used and no issues with excess noise in the estimation of acceleration are encountered.

4.2 FRICTION COMPENSATION

In general, nonlinear friction is viewed as an undesirable phenomenon in mechanisms. From the controls perspective, the main negative characteristic of friction is that it introduces a nonlinearity into systems and it is well known that analysis of nonlinear systems is generally more difficult than analysis of linear systems. Thus, most control related solutions to friction compensation involve minimizing the effects of friction by providing an opposing force that cancels the force of friction.

4.2.1 Feedforward Friction Compensation

For tracking problems, friction can be predicted and partially compensated by feedforward control[1]. However, it is only suitable for tracking since the desired velocity trajectory is known in advance[1]. Such a friction compensation method is shown in figure 13. In figure 13 the friction model could be the simple Coulomb model or any of the more advanced hysteretic models[6, 7, 8]. In the proper scenario of profile tracking applications tracking performance can often be significantly improved[1, 13, 14, 15, 9, 16, 8, 17, 18].

Though their efforts appear to focuses mainly on friction identification methods and a friction model without pre-rolling effects is used, Chen et al. demonstrate the ability to reduce tracking errors at velocity reversals with classical friction model feedforward[14].

The GMS model was introduced by Swevers et al[8]. It was first implemented as feedforward compensation for tracking of slow saw-tooth waves. The GMS model feedforward showed far better performance than the uncompensated system and a feedforward implementation of the Coulomb friction model. Jamludin et al. investigate GMS model feedforward

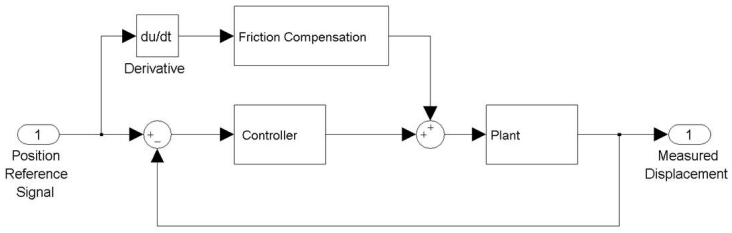

Figure 13: Feedforward friction compensation contributes to the control signal based on how the reference signal changes. This method is effective in reducing tracking errors, but since settling involves a static reference signal, it does not change the dynamics of system settling.

combined with a disturbance observer[15, 19]. They also make a comparison to a static friction model feedforward method combined with a disturbance observer. It should be noted that their observer is not a friction observer. The methods are evaluated at the task of tracking a circular trajectory with an XY table. While the disturbance observer combined with the GMS model feedforward yields the best tracking performance, it is not dramatically superior to the disturbance observer combined with the static friction feedforward.

Lampaert et al. conducted the first side by side comparison of the Dahl, LuGre, GMS, and static friction models in low velocity tracking applications[9]. In the case of this study the GMS model yields the best tracking performance. It is also interesting to note that using the static friction model actually makes the tracking performance of the system worse than without friction compensation. This may seem contrary to the results shown in [14, 15, 19] but, instead this illustrates how difficult it is to make fair comparisons between the utility of various friction models. Thus, what improves performance of one case study may degrade performance of another.

Some clarification of this concept was provided in Tjahjowidodo et al.[18], as tracking performance of feedforward of the Coulomb, LuGre, and GMS are compared for a smaller low velocity random profile and a larger high velocity random profile. For the smaller low velocity profile, the GMS feedforward clearly offered the best performance, with 89% decrease

in rms tracking error. The LuGre feedforward made significant improvement compared to the case of no friction compensation, with 71% decrease in rms tracking error. For the small displacement low velocity case, the Coulomb feedforward made only marginal improvement compared to no friction compensation, with 8% decrease in rms tracking error. In the large profile high velocity test the best tracking performance occurred with the GMS model, followed by the LuGre Model, followed by the Coulomb model. However, in this test case the increase in tracking performance was far less dramatic when comparing between the models to the uncompensated case, 56% decrease in rms tracking error for the GMS model, 55% for the LuGre model, and 45% for the Coulomb model. Thus, for motions with large displacement, the classical models such as the Coulomb model can give satisfactory results that are comparable to the more advanced models. However, at low displacements, which emphasize the pre-rolling regime, the more advanced models are superior.

Feedforward methods can also be extended to adaptive feedforward methods in effort to deal with the potentially changing frictional plant [13, 16]. Altpeter et al. develop a gradient decent method of tuning feedforward implementation of the LuGre model[13]. They show stability of their method and demonstrate a factor of three reduction of rms tracking error of sinusoid-like waveforms. Rizos et al. propose the idea of using the dynamic nonlinear regression with direct application of the excitation (DNLRX) method[16]. They use a GMS model as the basis for this grey-box method of identifying friction. The identified model is then used for feedforward control to track a random signal. In simulation, they show the ability to identify a friction model accurately even in the presence of noise.

Control system best practices would involve feeding forward any information that is available about the system that is controlled. Additionally, improved profile tracking is also desirable, as it may lead to the system being closer to the desired target location when the motion profile concludes. However, it is apparent, from the block diagram, that the contribution of the friction compensation to the control signal only changes when the position reference changes. Considering the rapid point-to-point motion problem, dynamic

friction compensation is needed during the settling portion of the motion. When the system is settling, the position reference signal has already been frozen to a constant value. This means that the friction compensation block is outputting a constant value at this point and is likely to have little or no effect on settling characteristics.

In summary, friction model feedforward should be used in the point-to-point motion problem. It is very important to use the appropriate level of model complexity with respect to the size of the step motion. Specifically, the simple classical friction models are likely to cause more harm than good when motion remains in the pre-rolling regime. Finally, feedforward of friction models has potential to reduce tracking error while the position reference is changing. This may lead to smaller position error at the conclusion of the step profile. However, feedforward friction compensation should not be expected to completely address the issue of settling after point-to-point motion.

4.2.2 Friction Observer

Another previously investigated method of friction compensation is the friction observer. As in feedforward compensation, the goal of the friction observer is to apply a force that cancels the force of friction. In most applications, it is not possible to directly measure the force of friction. However, other states of the system should be measurable. The friction observer takes measurements of other states, usually velocity, processes them through a friction model, and estimates the force of friction. In the ideal case, the force of friction is completely canceled leaving only the inertial dynamics of the servo which, can be effectively controlled using PD control[1, 5]. Friction observers have been successfully implemented with all significant friction models[1, 2, 7, 20, 3, 17, 21, 22, 23]. Several adaptive extensions have also been investigated[24, 25, 26, 27, 28]. The basic structure of the friction observer is shown in figure 14. In a position control application, the structure shown in figure 14 would have an outer PD loop wrapped around it. It is highly unlikely that the model of the frictional process will exactly match the actual frictional process thus, it is highly unlikely that the PD controller will be able to force the system to zero steady state error. An observer error term can be used to drive the observer to the actual plant. However, since there is no

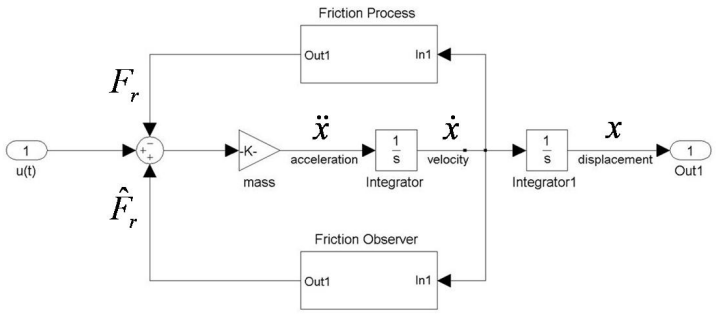

Figure 14: The previously discussed simple friction models and more advanced friction models depend on velocity. Therefore, some previously developed friction compensation methods fed back measured velocity into a friction observer in an attempt to cancel the effects of the real frictional process on the system.

real measurement of the force of friction, for the position control problem, the driving term is position error. Using the LuGre model, Olsson formulated an observer as

$$\frac{d\hat{z}}{dt} = v - \frac{|v|}{s\left(v\right)} + ke\left(t\right) \tag{4.4}$$

$$\hat{F} = \sigma_0 \hat{z} + \sigma_1 \frac{d\hat{z}}{dt} + \sigma_2 v, \tag{4.5}$$

where k is the observer gain, e is position error, and the hat notation indicates an estimated parameter. Thus, the driving term functions much like an integrator in forcing the system to zero steady state error. Very good analysis of the system's behavior can be done when it is assumed that the modeled frictional process is the same as the true frictional process[3, 20, 7]. However, when the modeled frictional process differs from the real frictional process, as it would in actual practice, analysis becomes considerably more difficult.

Using a friction observer based on the LuGre model, Olsson at al. and Canudas de Wit et al. demonstrate the ability to increase position tracking performance of sinusoid-like wave forms, on a real servo[1, 3, 20, 7]. In this work the possibility of parametric uncertainty

between the model of the friction process and the true process is acknowledged. The authors investigate this through time domain simulations and conclude that uncertainty in friction model parameters will degrade the observer performance but, due to the complexity of the problem, they are unable to concisely define the effects of modeling errors.

In later work by Canudas de Wit and Lischinsky[2], a very interesting result is seen. The data presented shows that the friction observer greatly improved performance when tracking a dynamic profile. However, when a point-to-point motion was executed, the system did not reach zero steady state error before the next step in the sequence was executed. While the friction observer offers increased tracking performance, this clearly raises questions about the suitability of the friction observer for ultra precision point-to-point motion.

Altpeter et al. also constructed a friction observer based on the LuGre model[21]. In their study, the performance of the observer is compared to a high bandwidth and a low bandwidth PID controller. The observer appears to have better responses to both high and low amplitude steps in reference but, it does not converge to zero steady state error, at least in the limited data that is presented. In later work [17], Altpeter states that methods such as friction model feedforward and observers give better results in sinusoidal tracking tasks than do PID and PD methods but, no current friction compensation method or linear control gives a satisfactory results for a simple step in reference.

Nilkhamhang and Sano propose an adaptive observer based on the GMS friction model[26]. They also propose a polynomial representation of the Stribeck function. This allows for the application of linear adaptive control methods. In their simulations, tracking of random velocity steps and sinusoidal velocity profiles is improved by these methods. However, position control is not considered and the algorithm takes several thousand seconds to converge even when the adapted parameters start in the neighborhood of their true values.

Martinez-Rosas and Alvarez-Icaza developed an adaptive observer based on an extension of the LuGre model[25]. They acknowledge that frictional parameters of a servo system are often subject to change for numerous reasons, both simple to quantify and difficult to quantify. Thus, there is a need to adapt the parameters used in a friction observer. Their

results suggest the algorithm is capable of driving the system to zero steady error with a static position reference, but examination of graphical results proves inconclusive due to the scaling. Also, the algorithm takes several seconds to adapt to new frictional conditions.

A common theme in friction observer efforts is the ability to increase tracking performance. As it relates to the point-to-point motion problem, observers show the ability to arrive near the target location but, convergence to zero steady state error is slow, if it even happens at all. When servo settling performance is best expressed in milliseconds, it would be more desirable to have an algorithm that is robust to parametric uncertainty instead of relying on time consuming adaption.

4.2.3 Other Methods

Helmik and Messner make use of a complex lag to increase gains at low frequency[29]. As a consequence some phase is given up. This work draws a distinction between elastohydrodynamic lubrication and boundary lubrication as two linear systems that approximate this nonlinear system. This assumption is based on the phenomenon illustrated by classic Stribeck curves. However, there is no definitive evidence presented that would show the system traveling along a Stribeck curve. Two linear system identification cases are presented. First, the case of a high amplitude stepped sine test is shown. This is called the elastohydrodynamic lubrication case. Next, a low amplitude stepped sine test is presented and called the boundary lubrication case. This assumption is based on the phenomenon illustrated by classic Stribeck curves. Judging by the loop transmission plots presented, it is possible that this method could increase system performance but, no temporal evidence is presented. Due to hardware limitations relating to the flexibility of controller designs available to the authors, it is stated that nonlinear and mode-switching controllers were not considered. Thus, it is quite possible that this solution was not the most desirable solution even to the authors.

Some previous efforts have investigated gain scheduling approaches to control systems subject to friction[30, 18, 31]. These efforts recognize that integral action is a good way to minimize steady state error but, they also mention that integral action generally slows the response of the system and carries a risk causing limit cycles[30, 18, 31]. They also

recognize that PD control will tend to have a higher steady state error, but with possibility of faster response and with reduced risk of limit cycle behavior. Thus, these efforts focus on scheduling controller PD action[18, 31] around frictional dynamics[32] to produce the desired behavior. This approach was shown to be successful in the task of rapid point-to-point motion [18] however, steady state error has not been completely eliminated and is still seen in the data. This method is probably very successful in settling drives with significant friction to micrometer scale precision. When nanometer precision is required, steady state error specifications drop to essentially zero. This makes any conventional PD or conventional scheduled PD method difficult to implement because these methods will almost always introduce some steady state error.

The most simple and practical way to achieve steady state error specifications is to include some controller integral action. The Yosida Nano-Mechanism Project presents the first case of a direct drive linear stage which is able to achieve nanometer accuracy with a single actuator[33, 34]. This project represents a very similar situation that is being studied in the current effort. Futami et al. do not explicitly discuss advanced friction models but, the data presented demonstrates a clear understanding of servo behavior over sub-micrometer displacements. It is emphasized that over sub-micrometer displacements, ball bearings show spring-like behavior. Futami et al. propose a multi-regime control algorithm where the final 100 nm of positioning is done mainly by integral control. Nanometer scale positioning is possible with the proposed mechanism and control algorithm but, the proposed algorithm appears rather complex and somewhat inefficient. As it relates to the current effort, the key concept from Futami et al. is that integral control was a major factor in achieving nanometer level positioning accuracy.

4.2.4 Summary

In summary, the two most widely accepted methods of friction compensation are friction model feedforward and the friction observer. However, friction model feedforward is not appropriate for issues to be addressed in this the point-to-point motion problem and friction observers have not shown favorable results in addressing this problem either. Most of the

less renown known methods of friction compensation would be considered gain scheduling or switched mode control methods. When nanometer precision is required, successful control methods tend to include some form of integral action. Recalling the problems with integral action discussed in previous efforts[30, 18], the challenge is to design controller integral action to avoid significantly slowing down the system, introducing limit cycles, or causing instability. This effort will focus on the design of the integral action to increase point-to-point settling performance while avoiding these potential problems.

5.0 IDENTIFICATION PROCEDURES AND TOOLS

In this chapter the procedures and tools to identify pre-rolling friction are discussed. Since linear systems theory works well to describe majority of servo motion, the basic concept of this procedure is to first identify the linear components of the system. With a good description of the linear components of the system, it is next desired to create a representation of the ideal linear system. Then, using knowledge of general behavior of pre-rolling friction, the length scale where the ideal linear approximation breaks down is to be determined. Next, knowing the length scale where pre-rolling effects are most significant, data that best illuminates the pre-rolling friction phenomenon can be collected. Finally, this data is to be used to identify the parameters of existing nonlinear pre-rolling friction models.

5.1 LINEAR SYSTEM IDENTIFICATION

Starting with an un-tuned precision servo, the first step is to construct a reasonable PID controller for the system using standard control system best practices (Gain Margin $\geq$ 6 dB, Phase Margin $\geq$ 30 degrees). At this juncture it is not important to maximize the bandwidth of the system, thus the term reasonable PID controller is used. In fact, if very large servo bandwidth is possible, the general characteristics of a lower bandwidth controller, such as greater overshoot, can actually prove advantageous in identifying pre-rolling friction. In the case of this study, it was found that the system could operate with open loop crossover frequencies up the 315 Hz, but, a tuning with an open loop crossover frequency of 100 Hz was sufficient to identify pre-rolling friction.

The linear component of the system can be identified with conventional stepped-sine analysis. Such a tool or software package is often used to produce loop transmission plots for PID tuning. The stepped-sine analysis should be done with the largest magnitude of excitation which is safely possible. The following is designed to explain what the a sufficient amplitude loop transmission should look like. Also, a brief description of the frictional artifacts of using a loop transmission of insufficient magnitude is included.

It is known that there is a nonlinearity in the system due to friction but, at this stage, it is desired to focus only on the linear components of the system and minimize the influence of the nonlinear part. To do this, the excitation given during identification should cause the system to leave the pre-rolling regime. When the system fails to leave the pre-rolling regime, the loop transmission will show a resonance due to pre-rolling friction. This could be confusing and counter intuitive to the control designer, as the designer would probably not expect a resonant mode at this frequency.

Helmick and Messner present a very interesting simulation of the resulting frequency response function of a mass subject to the Dahl friction model for various amplitudes of excitation[35]. For the lowest amplitude excitations, the system appears much like a spring-mass-damper. As the excitation amplitude is increased the response transitions to one which appears more like a free mass. However, in the course of this transition, there is a point where the system breaks free from the pre-rolling effects, with its stiffness-like behavior, and dramatically changes to a more mass-like system. It is this more mass-like regime which should be used in the initial identification. Figure 15 shows a family of loop transmission studies, of various amplitudes, conducted on the servo.

The loop transmission studies are conducted at 10%, 5%, 2.5%, 1.25%, 0.625%, 0.313%, 0.156%, and 0.078% of the maximum current output of the amplifier. Although these loop transmissions include the controller in their response, it is still clear that the simulations of Helmik and Messner[35] predict the behavior of the key features with respect to amplitude of excitation. Excitation of 0.625%, 0.313%, 0.156%, and 0.078% of the maximum current show the system response being dominated by pre-rolling effects, as there appears to be a resonance between 250Hz and 420Hz and the gain at low frequency is low. When the amplitude of the excitation is increased to 1.25% and higher, the resonance due to friction is

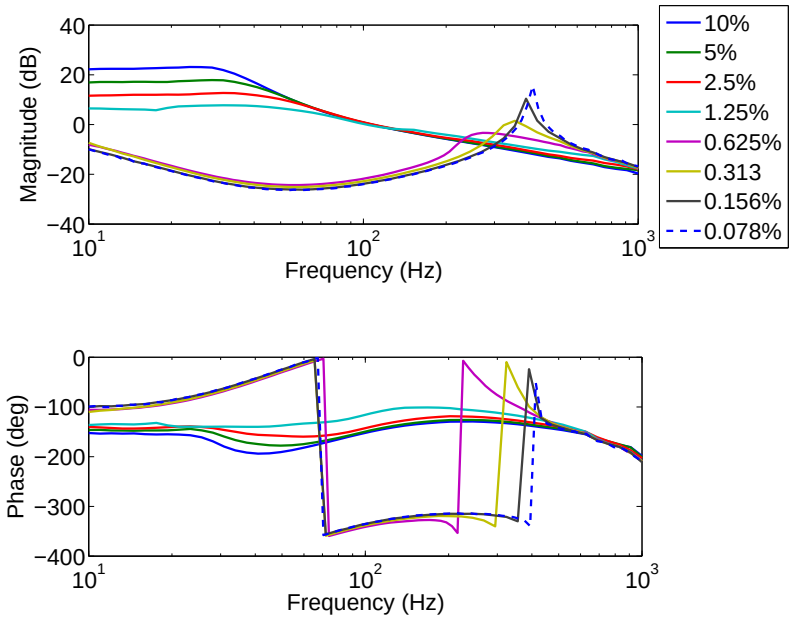

Figure 15: This plot shows the frequency response plot for loop transmissions with magnitudes of 10%, 5%, 2.5%, 1.25%, 0.625%, 0.313%, 0.156%, and 0.078% of the maximum current output of the amplifier. For low amplitude inputs, the servo remains in the pre-rolling regime and the response resembles that of a spring-mass-damper. For higher amplitude inputs, the servo leaves the pre-rolling regime and the system response appears more like a free mass. The frictional nonlinearity continues to effect the system response and the frequency response function remains amplitude dependent. However, the higher amplitude excitations, inspite of their apparent differences, will result in similar closed loop system approximations.

no longer seen and there is a significant increase in the gain at low frequency. This is because, at these amplitudes of excitation, the system has broken free of the pre-rolling regime and appears more mass-like.

With regards to the linear system identification of the servo, the loop transmission plots from the 5% or 10% of maximum current excitations are the best and safest options. In these cases, the system frequency cross over and phase margin are similar. Even though the low frequency gains are somewhat different, the resulting closed approximations will be similar.

5.2 IDEAL LINEAR SYSTEM REPRESENTATION

Typically, PID tuning with loop transmission plots is done with the open loop response of the controller and plant in series. However, the most convenient way to observe the effect of pre-rolling friction is during closed loop operation. Thus, it is necessary to create a closed loop representation of this ideal linear system to compare with the real servo data. This can be written as

$$\frac{Y(s)}{X(s)} = \frac{G(s)}{1 + G(s)}, \tag{5.1}$$

where $\frac{Y(s)}{X(s)}$ is the closed loop transfer function from the position reference to the position output and $G(s)$ is the open loop transfer function of the controller and servo in series. In most cases, the computed closed loop transfer function can be well approximated by a second order linear transfer function such as

$$\frac{Y(s)}{X(s)} \approx \frac{\omega_n^2}{s^2 + 2\zeta\omega_n s + \omega_n^2}, \tag{5.2}$$

where ω_n is the natural frequency and ζ is the damping ratio for this second order approximation of the closed loop system[36]. Figure 16 shows an example of the second order approximation of the closed loop system along with the closed loop response computed from the open loop frequency response data. At this point, it is now possible to simulate how the servo mechanism should behave if it were and ideal linear system. Examining how the actual servo behavior deviates from the ideal will show where the pre-rolling friction begins to dominate the system response.

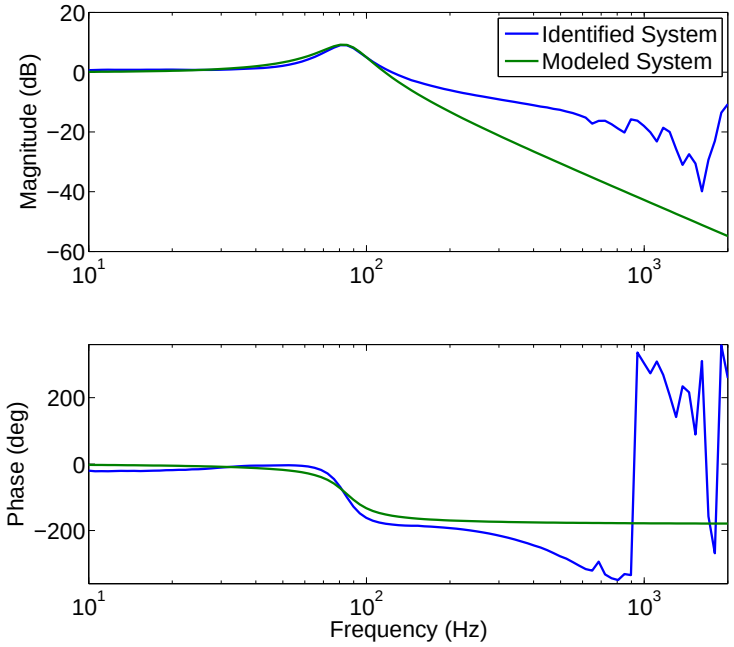

Figure 16: The closed loop behavior of the servo is well approximated by a second order linear system.

5.3 DETERMINING THE LENGTH SCALE OF PRE-ROLLING FRICTION

The next step in the pre-rolling friction identification procedure is to determine the length scale where pre-rolling effects significantly influence the system response. Recalling that pre-rolling friction has the greatest influence on system response near velocity reversals, this step aims to ascribe a value to the notion of near a velocity reversal. This is done by injecting the same motion profile into the actual system and the linear representation, constructed in the previous step, and comparing the responses. In this study, the motion profile was a simple step in reference. However, there are situations where a simple step in reference would be impractical, such cases may be when a step in reference would cause amplifier saturation or when the servo is carrying a payload with lightly damped modes. In these cases, a profiled step will suffice. The key feature to produce with this test is a number of velocity reversals which will occur at various distances from the target location. The step response of a second order under-damped linear system, which is what the closed loop system is approximated as, is good for producing this type of feature. Ideally, the step in position reference should be as large as possible but, possible amplifier saturation will limit the step amplitude. If the step amplitude is sufficient, the initial portion of the step response should be well predicted by the second order linear approximation.

As the oscillations from the step response decay, at some distance from the target location, the data from the real step response should significantly deviate from the ideal linear approximation. This is the regime where the servo response is dominated by pre-rolling friction. A key feature that can be used to differentiate two regimes is the time between the local minimums and maximums of the response. When the system is well approximated as a linear system the local minimums and maximums are regularly spaced with a frequency predicted by the linear model. As the nonlinearity of pre-rolling friction tends to dominate the system response, the locations of the local minimums and maximums will tend to spread out, leading to the long tails often characteristic of ultra precision settling. As a final note,

control system industry best practices would include feed forward of as many variables as possible. However, since it is desired to compare only the feedback control to an ideal representation of this feedback control, feed forward compensation should not be used in this step.

In an illustrative example of this step of the process a 100 µm step is executed on the servo mechanism. The data from this test are then compared to the same step executed on the ideal linear system as shown in figure 17. Upon first examination, one may conclude that the linear approximation worked rather well to prediction system settling. It is seen that the first few periods of oscillation are captured very well in terms of magnitude and temporal location. This is good because this test confirms that a nearly linear operating regime exists and is well predicted for this device.

However, when figure 17 is scaled to focus on the last micrometer of settling, as seen in figure 18, it is clear that the linear approximation does not capture the real system behavior. Considering the data presented in figures 17 and 18, the linear approximation predicts a local minimum or maximum about every 8 ms. This approximation holds until the system moves between the velocity reversals at -637 nm and 115 nm, where the system takes 23 ms to travel between these points. Pre-rolling effects are even more pronounced between the next set of velocity reversals where it takes 67 ms to travel between 115 nm and 19 nm. Thus, this step response has suggested that the servo behaves rather linearly in settling when velocity reversals are further than 3.81 µm from the target location and that there is a pre-rolling feature which is approximately 600 nm from velocity reversal that significantly affects settling performance.

To summarize use of the step response as a preliminary identification tool: the locations of local minimums and maximums of a step response are predicted by linear control theory, when these locations deviate from their predictions there is likely a pre-rolling feature with a length scale on the order of the last correctly predicted location. Given the simplicity of this method, it seems possible to automate this procedure. The deviation of time between predicted time between peaks and actual time between peaks which constitutes entering into a regime of significant pre-rolling effects is a tunable parameter.

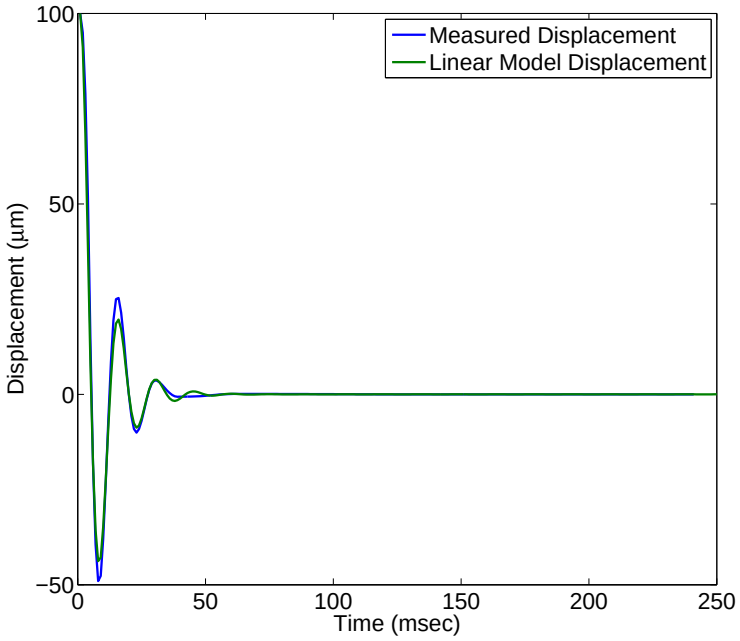

Figure 17: A second order linear system can be parameterized based on the open loop response data. Upon initial comparison to a real 100 µm step response, the linear approximation appears to predict the system settling behavior rather well.

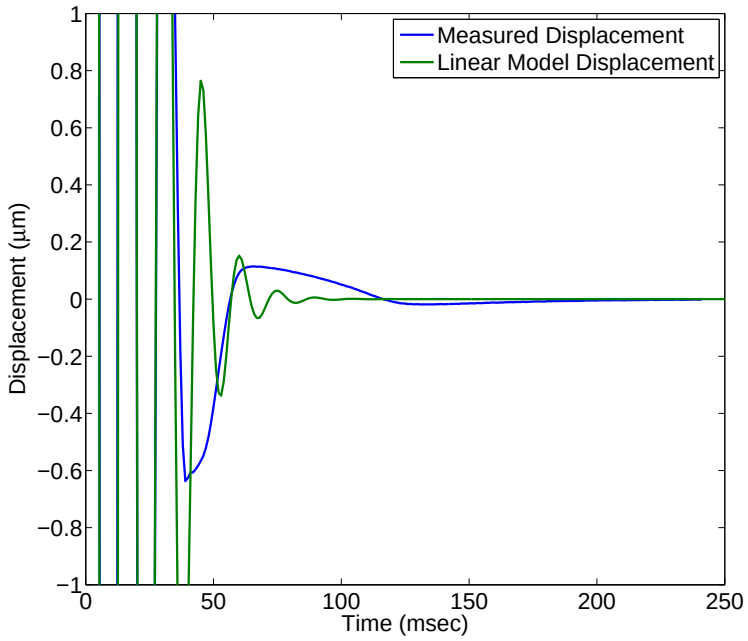

Figure 18: For the same data presented in figure 17, when the final micrometer of settling is studied, it is apparent that the linear approximation does not predict this phase of the settling process accurately.

5.4 IDENTIFICATION PROFILE

Since previous efforts have shown pre-rolling phenomenon to be relatively rate independent [37, 6], pre-rolling behavior can be identified by commanding a relatively slow, motion profile consisting of a decaying sinusoid. This proposed identification profile is thought to be well suited for this application because this profile shape mimics the decaying oscillations that are typical of system settling. However, by using this profile, the information contained in an identification signal can be controller to a greater extent as compared to simply letting the servo execute settling by itself. Such a profile is shown in figure 19. It is not possible to directly measure the force of friction in an industrial stage. However, it is possible to measure the electrical current in the motor. The motor force constant provides a way to approximate the force input to the system, yielding a conversion from Amperes to Newtons. As previously discussed, knowing the motion of the servo and the input force allows the separation of other force components, such as inertial or viscous components, and allows isolation of the force of friction. Figure 20 shows the force versus displacement results for such an identification profile. As suggested by the step response test, there is definitely a significant pre-rolling friction feature on the order predicted by the step response. To assure that pre-rolling friction is isolated from any other force components, the inertial response of the system can be computed with the second derivative of the position signal. Often it would be ill advised to use a second derivative of a digital signal but, given the small position resolution of 61 pm and low noise content, this does not appear to be a problem.

5.5 FRICTION MODEL PARAMETERIZATION

In adherence to good engineering practice, the most simple solution that accomplishes a task is usually best. For this case, the Dahl model was found to yield very good fits to the observed data. Thus, more complex models were not explored.

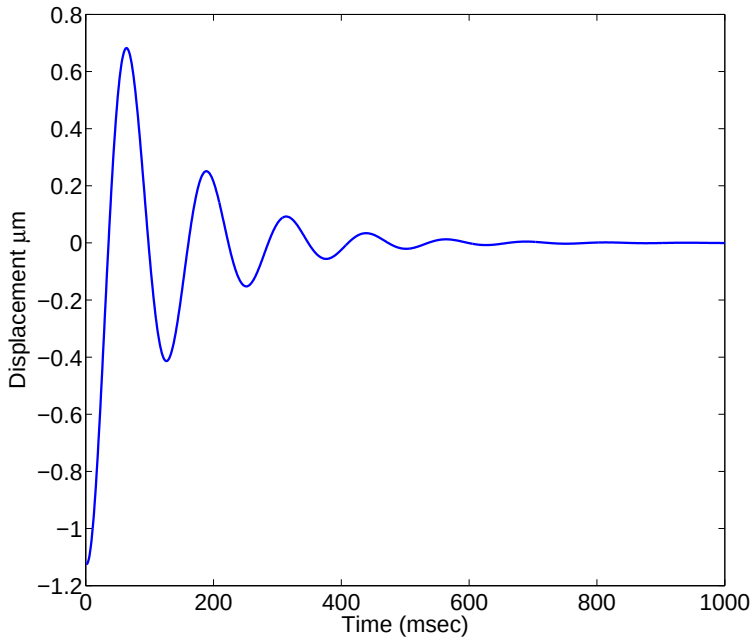

Figure 19: The identification profile consists of a sine wave multiplied by an exponential decay. For this example the sinusoidal component has a frequency of 8 Hz.

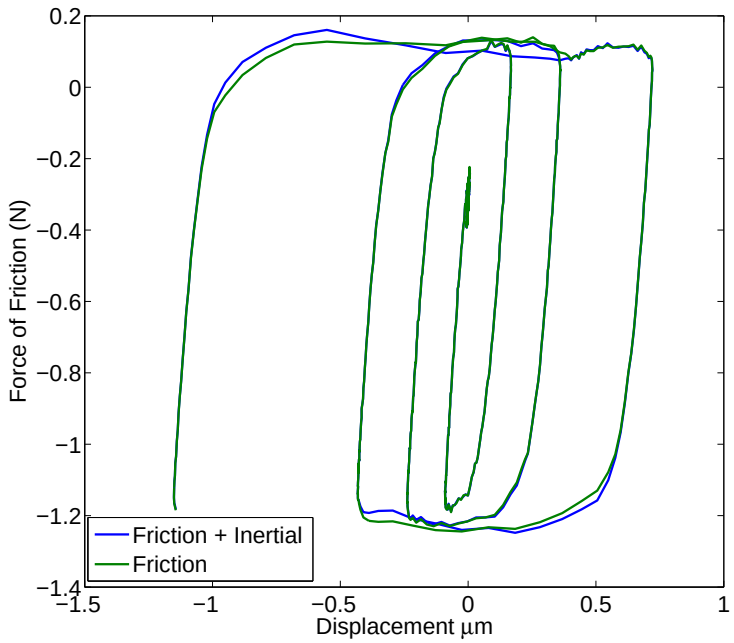

Figure 20: This plot shows an example of the force versus displacement curve which can be constructed from data generated by the identification profile. Since the mass of the system is known, the inertial component of the response can be computed and subtracted from the total force. The shape of this resulting curve is very good for pre-rolling friction identification.

Fitting a friction model to this data is a relatively easy task which can be accomplished by numerous gray-box identification methods. In the case of this effort, the data are fit using a genetic algorithm. Recalling the form of the Dahl model as

$$\frac{dF_r}{dx} = \sigma \left| 1 - \frac{F_r}{F_C} \right|^i \operatorname{sgn}\left(1 - \frac{F_r}{F_C}\right), \tag{5.3}$$

the free parameters are the initial contact stiffness, σ, the level of Coulomb friction, F_C, and the shape factor, i. As is often common practice, the shape factor is set to $i = 1$. This leaves two tunable parameters, σ and F_C.

The genetic algorithm is not the focus of this study but, a brief outline of its basic principle of operations is appropriate. First, the user selects a region where the optimal solution most likely resides. The algorithm then makes a series of random guesses of parameter sets within this space. This set of guesses is known as a generation. In keeping with the genetic terminology, each parameter set is referred to as an organism. In this case the fitness of each respective organism is defined as the mean square error between the force computed by the resulting parameterized model and the measured force of friction. The algorithm then selects the organisms with the highest fitness, or lowest mean square error, to breed. Breeding involves mixing the values of the highest utility parameters sets. This could be done by taking the average value of the two parameter sets to form a new organism. To avoid the prospect of the optimization becoming stuck in a possible local minimum, mutation can be applied to the new organisms. This is done by adding some random value to the parameters of the new organism. When a new generation of organisms has been constructed, their respective fitness is evaluated and the process is repeated. Typically, the fittest organisms of each generation are preserved in an un-mutated state in case that one may be the best overall solution.

There is nothing inherently special about the genetic algorithm which makes it the optimal choice of methods for fitting model parameters to the measured data. It is possible that most any optimization method suitable for nonlinear problems could be used. One potential drawback of the genetic algorithm is the lack of analysis that can be done on the optimization process and that it may not be possible to prove that a solution is optimal. Stepping back and considering the underlying philosophy of the proposed control algorithm as: Large variations in the plant's apparent parameters are to be expected and the algorithm

relies more on the general characteristics of the plant, (steeper transition curves are expected near velocity reversals and more shallow curves further away), as opposed to exact matching or cancellation of particular values. Thus, is it sufficient to find a solution that appears to capture the behavior of the measured data. In the case of this problem, the genetic algorithm produces good model fits very reliably and very quickly.

6.0 PRE-ROLLING IDENTIFICATION STUDY

6.1 INTRODUCTION TO IDENTIFICATION STUDY

The step response discussed in the previous section suggested that a significant pre-rolling friction feature on the order of 600 nm from velocity reversal is likely to be present in this system. Thus, the identification profile study will focus on displacement magnitudes of 1 micrometer and smaller. The identification profile is executed at 8 Hz, 16 Hz, and 32 Hz to check for any significant rate dependent characteristics. The highest identification frequency of 32 Hz was selected because the linear PID control began having trouble tracking identification profiles of higher frequencies.

The pre-rolling transition curve for this particular device proved to be fairly simple and was approximated quite well by the Dahl model. Fitting friction models to friction data is not a new development and in this effort nearly 1,000 datasets were approximated by friction models, thus, it is desired to expeditiously communicate that all of these model fits are reasonable. Let error for the model fits be defined as the difference between the modeled force of friction at a particular time sample and the measured force of friction at the same time sample. The mean squared error for all of the model fits is shown in figure 21. Figure 22 shows the model fit with the largest mean square error. Even though this is the worst model fit, the pre-rolling behavior behavior is still captured rather well by the friction model. Thus, if the worst model fit is still a good approximation of the system behavior, then all better model fits must also be good approximations of the system behavior. While it is

very convenient that the simple Dahl model was able to sufficiently capture the pre-rolling behavior of this device, there is no guarantee that the pre-rolling transition curves for other servo mechanisms would have such simple behavior. In the case of a more complex transition curve, the control algorithm should be formulated around a more complex friction model, such as the generalized Maxwell slip model.

6.2 PRE-ROLLING FRICTION IDENTIFICATION RESULTS

The pre-rolling identification test consists of 50 executions of the identification profile at six locations, five millimeters apart, at each of the three selected frequencies. The two free friction model parameters, σ and F_C, are then identified by the genetic algorithm. The results of this identification is presented in figures 23 through 28. A box plot is a convenient way to view these data sets. In the box plot the red center line indicates the mean of the dataset, the bottom and top of the box indicate the 25^{th} percentile and 75^{th} percentile, respectively, and the bottom and top whiskers indicate the 5^{th} percentile and 95^{th} percentile, respectively. Finally, the red crosses indicate points lying outside the 5^{th} percentile and 95^{th} percentile. This data has not been divided by location because it is desired to find patterns in behavior that are related to location. On the contrary, it is displayed in this fashion to show how inconsistently pre-rolling friction tends to behave and that attempting to correlate pre-rolling characteristics with a variable such as location could be difficult. Additionally, correlating observations to location adds complexity to the control algorithm and this is undesirable, especially if it turns out to offer no benefit. However troubling these inconsistent test results may be, repeating the test yields similar results in terms of inconsistency of the identified parameters. Formally, the cause of these inconsistent results must be attributed to unknown factors. To the best of the researchers' knowledge, there are not mechanical failures with the the servo but, the crossed roller bearings used in this stage do contain an anti-creep mechanism. The anti-creep mechanism is a small pinion in the center of the cage which holds the rolling elements. Two racks are machined into the non-bearing surfaces of the rails. Thus, the cage is not permitted to creep from its assembled

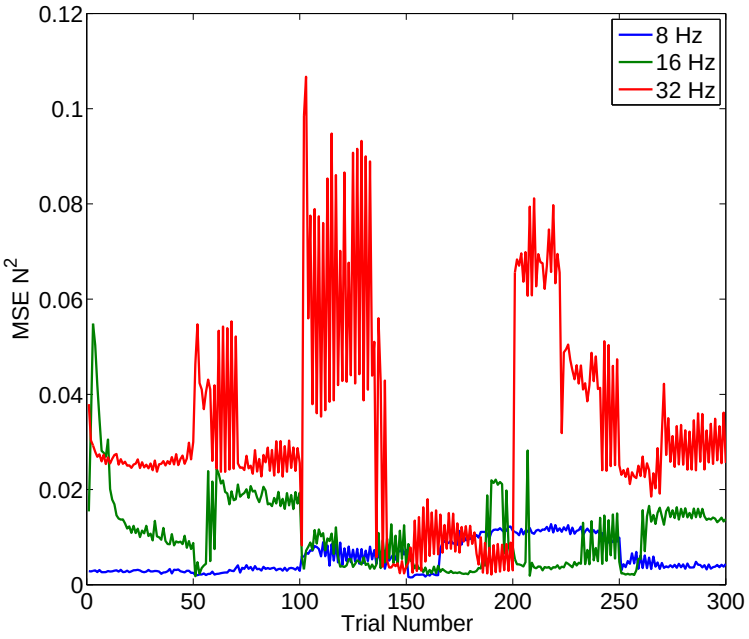

Figure 21: Computing the mean square error of the model fits to the measured data gives a metric of how well pre-rolling behavior is captured by the friction model. 300 trials are conducted at each identification frequency.

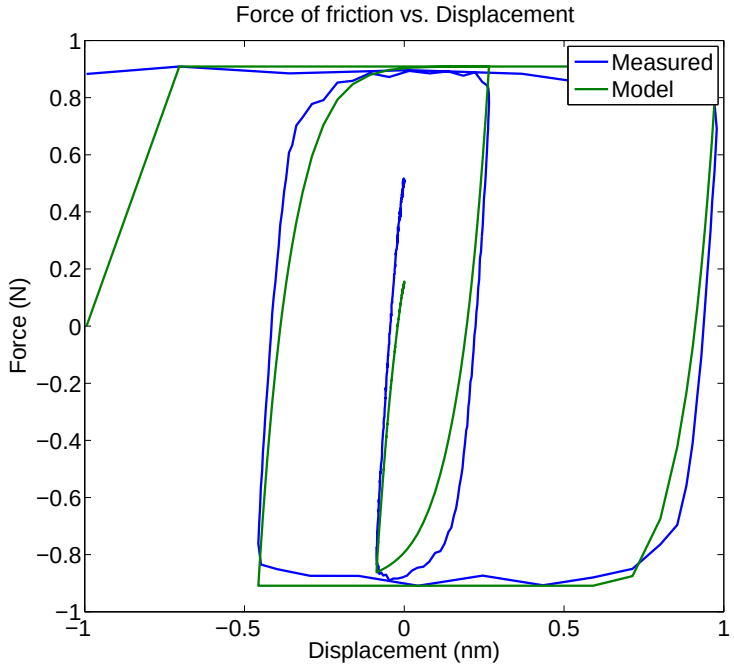

Figure 22: This figure shows the worst Dahl model fit over all of the identification data. The mean square error for this fit is 0.1067 N^2. Even though this is the worst model fit, it still captures an adequate amount of the pre-rolling friction behavior.

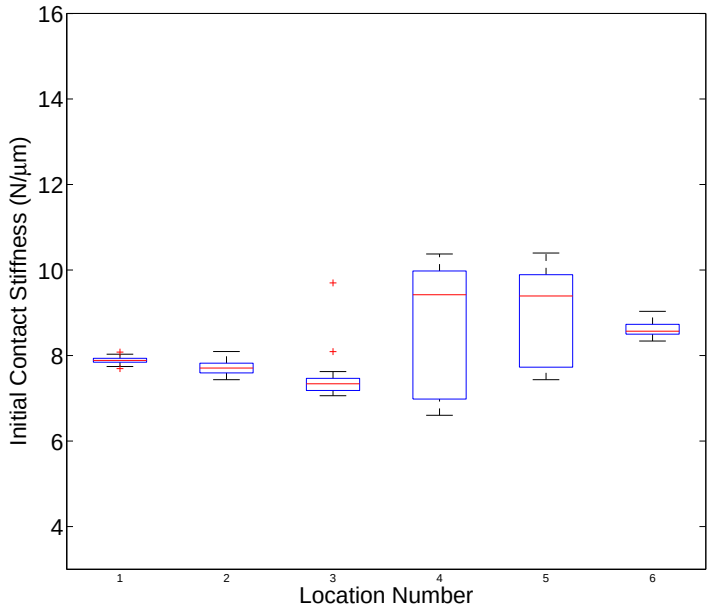

Figure 23: This box plot shows the distribution of the identified parameter σ for each of the six locations on the device travel. For this test an identification profile with a fundamental frequency of 8 Hz was used.

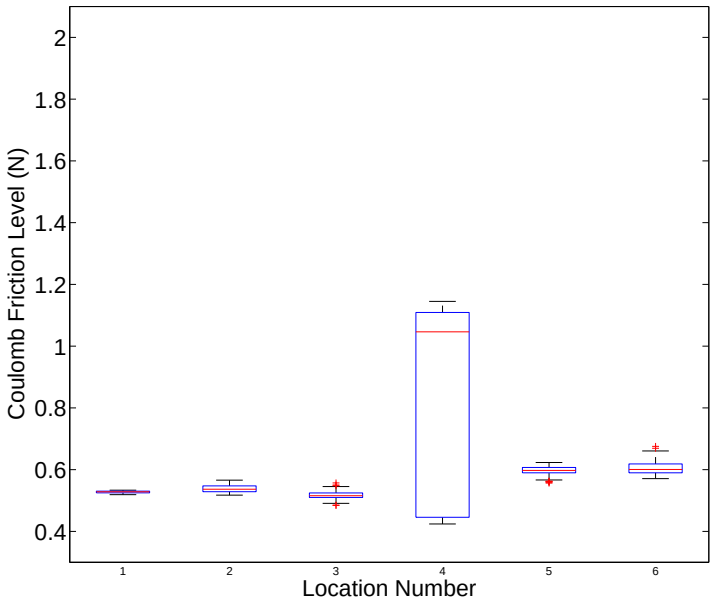

Figure 24: This box plot shows the distribution of the identified parameter F_C for each of the six locations on the device travel. For this test an identification profile with a fundamental frequency of 8 Hz was used.

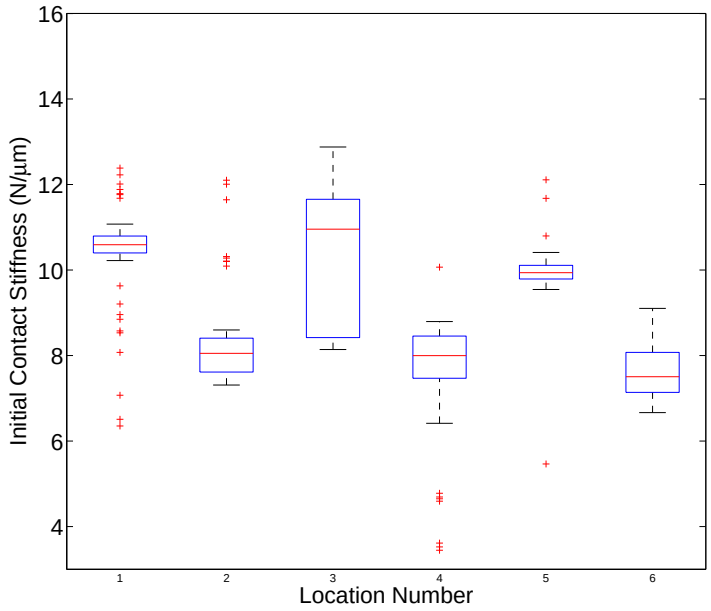

Figure 25: This box plot shows the distribution of the identified parameter σ for each of the six locations on the device travel. For this test an identification profile with a fundamental frequency of 16 Hz was used.

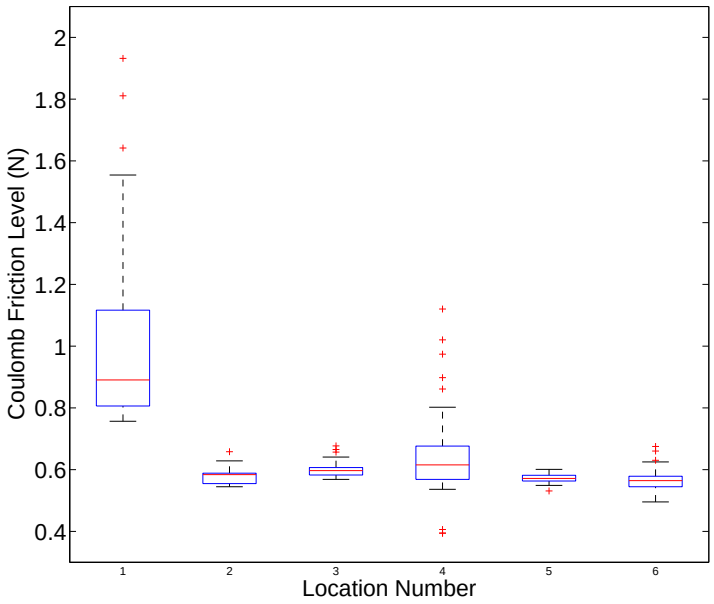

Figure 26: This box plot shows the distribution of the identified parameter F_C for each of the six locations on the device travel. For this test an identification profile with a fundamental frequency of 16 Hz was used.

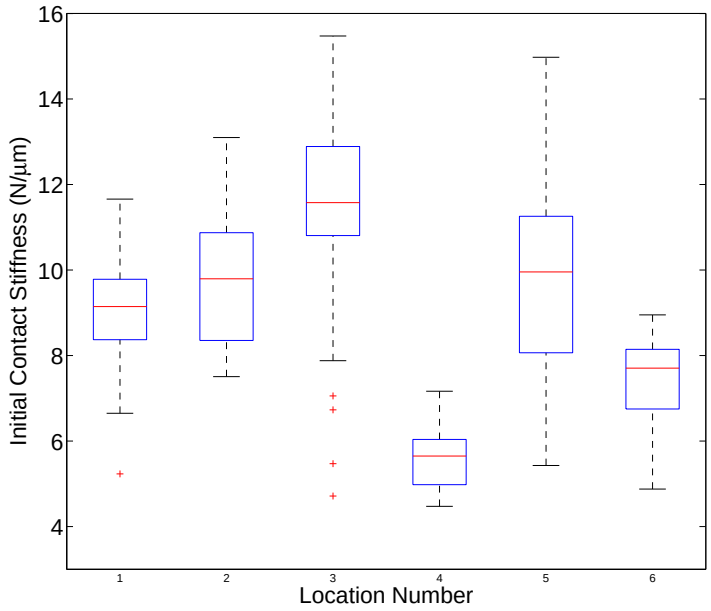

Figure 27: This box plot shows the distribution of the identified parameter σ for each of the six locations on the device travel. For this test an identification profile with a fundamental frequency of 32 Hz was used.

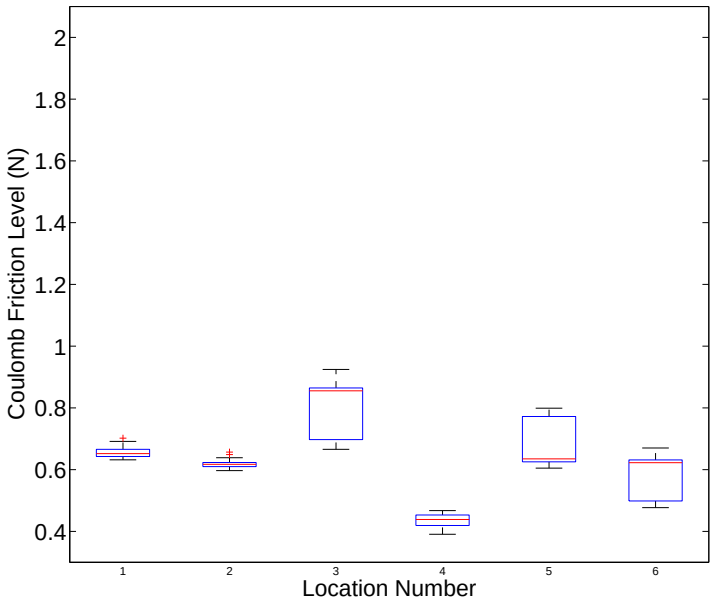

Figure 28: This box plot shows the distribution of the identified parameter F_C for each of the six locations on the device travel. For this test an identification profile with a fundamental frequency of 32 Hz was used.

position because it is constrained by the pinion and racks. This mechanism is not supposed to interfere with the bearing operation but, to keep the cage from creeping some force must be transmitted through this mechanism. Evaluating the anti-creep mechanism is not a subject of this work but, could be an avenue of future work.

In a different representation of the data, the data is only separated by frequency of the identification profile, 8, 16, and 32Hz. This is done to confirm the proposition the pre-rolling effects are mostly rate independent[37, 6]. Figure 29 shows histograms of the distributions σ for each frequency and figure 30 shows histograms of the distributions of F_C for the same frequencies. Additionally, basic statistics for this data are computed in table 1. When analyzing the data in figures 29 and 30 and table 1, there is not a clear shift in the mean values of σ or F_C. This implies rate independence of the friction model parameters. The only observable trend in the data appears to be an increase in the standard deviation of σ with increased identification frequency. This observation will be taken into account in the form of exercising increased caution during controller parameterization.

6.3 EXTENSION OF OBSERVATIONS TO ACTUAL POINT-TO-POINT MOTION

The goal of this section is to determine whether or not model parameterizations similar to those found in the previous step will describe the behavior of the force of friction during servo settling after a step motion. This effort theorizes that: As the servo settles after a step motion, there should be a region where the servo behavior is accurately described by a friction model parameterization similar to those computed in the previous step. To the best of the author's knowledge, no other efforts have attempted to fit a friction model to data collected during servo settling. Thus, it is not known if the system will smoothly transition into the, now familiar, pre-rolling behavior or if some other factors will tend to momentarily dominate the system response.

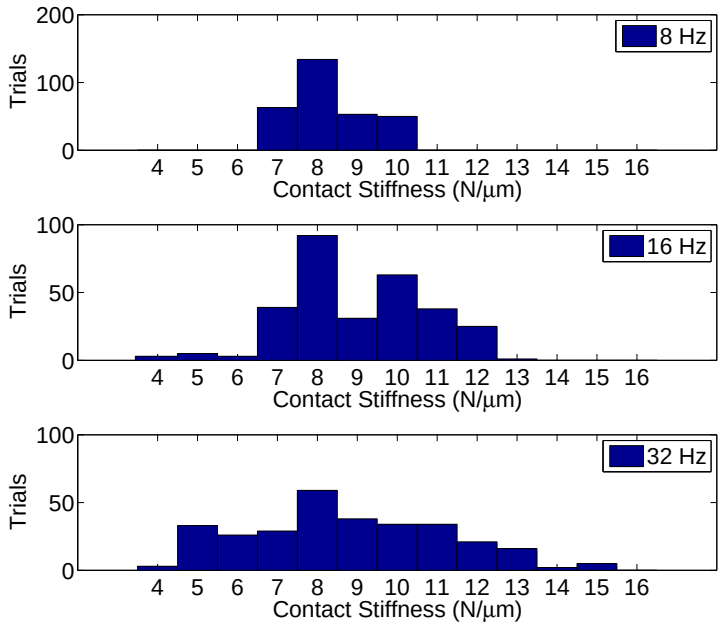

Figure 29: For each set of 300 trials, conducted at each frequency, there does not appear to be a significant change in the mean value value of σ. This would suggest that the parameter σ is indeed rate independent. However, the standard deviation of the data tends to increase with frequency. This does not have an explanation. However, a safe course of action in response to this observation is conservative friction model parameterization.

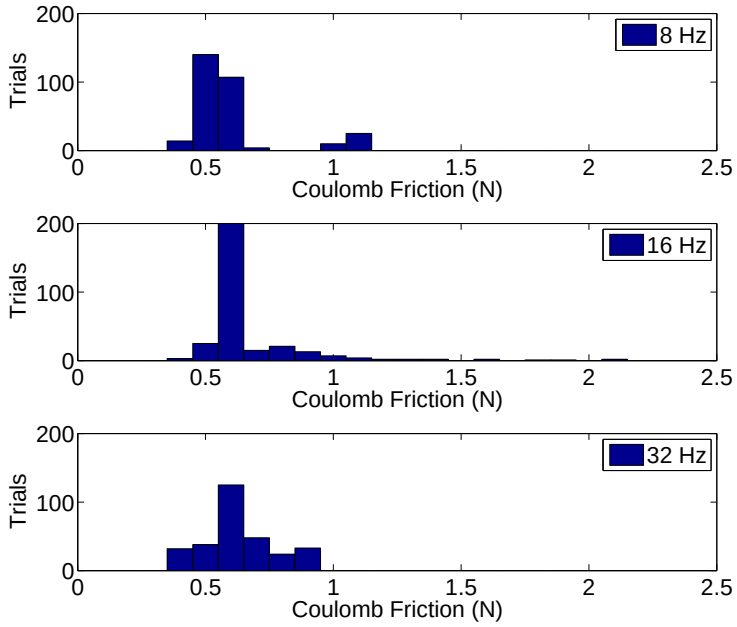

Figure 30: For each set of 300 trials, conducted at each frequency, there does not appear to be a significant change in the mean value value of F_C. This would suggest that the parameter F_C is also rate independent.

Table 1: In examining the statistics computed from the identified parameters σ and F_C there is not a clear trend in the mean values that would indicate significant rate dependence.

	8Hz		**16Hz**		**32Hz**	
	Mean	St. Dev.	Mean	St. Dev.	Mean	St. Dev.
σ	8.23	0.94	8.99	1.70	8.74	2.46
F_C	0.61	0.17	0.66	0.23	0.63	0.13

To investigate this proposition, 250 instances of 5 mm steps are conducted at the locations where the identification profile studies were performed. The data to be analyzed begins immediately after the motion command concludes. As with the identification profile studies, it is assumed that the only significant dynamics of the system are inertial and frictional. Thus, the inertial component can be subtracted from the system response leaving only the frictional component. Figure 31 shows an example of the frictional response being separated from the inertial response. From figure 31 it is clear that the inertial response of the system during settling tends to become insignificant, particularly as the system executes velocity reversals near the target location. It also appears that the frictional response could be approximated by the Dahl model. To further investigate this observation the identification algorithm is run on 250 settling data sets. Histograms of the identified initial contact stiffness and the identified level of Coulomb friction are shown in figure 32. Figure 32 appears to show similar parameter distributions as those seen in the identification profile tests. Table 2 shows basic statistics computed over all of the identified parameters from the profile tests and the identified parameters from the actual step and settle tests. When examining the statistics presented in table 2, it is seen that both methods yield very similar identification results. Finally, figure 33 shows the mean square error for the model fits to the settling data. In examining the mean square error for the model fits to the settling data, it is seen the the mean square error is actually smaller than for the identification profile tests. Thus, considering that force of friction versus displacement settling data appears to have the characteristics of the pre-rolling friction model, the settling data and the identification profile data result in statistically similar identified parameters, and the fits of the pre-rolling friction models to the settling data are as good if not better than the identification profile data; it appears that the system does move directly into understood pre-rolling behavior upon completing a rapid step motion.

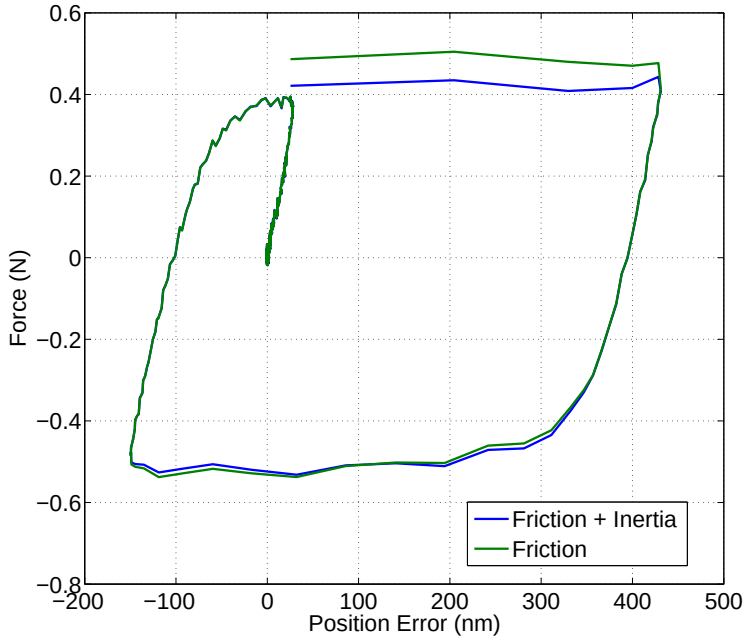

Figure 31: This data set is produced from force and displacement data collected immediately after the gross motion of a 5 mm step has concluded. Force versus displacement data for the force of friction combined with the system's inertial response and the force of friction separated from the inertial response are shown in this figure. This data suggests that the dominant dynamic during settling is indeed frictional and this frictional response resembles those produced by the identification profile.

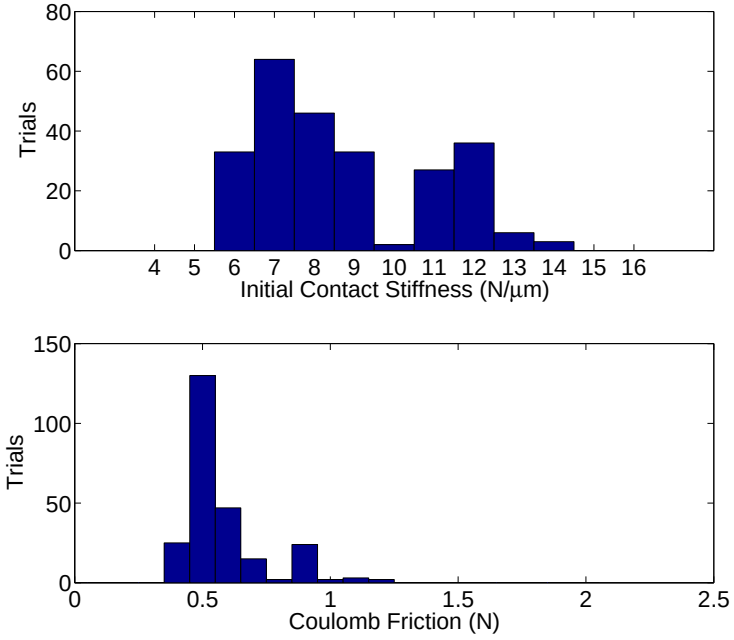

Figure 32: These histograms show the distribution of the identified Dahl model parameters for data sets collected during settling after a rapid step motion.

Table 2: This table shows the mean and standard deviation of the identified parameters from the identification profile tests and the actual step and settle tests. It appears that both methods have yielded very similar results in terms of the identified parameters.

	Identification Profile		**Step Tests**	
	Mean	St. Dev.	Mean	St. Dev.
σ	8.66	1.84	8.73	2.10
F_C	0.64	0.18	0.58	0.16

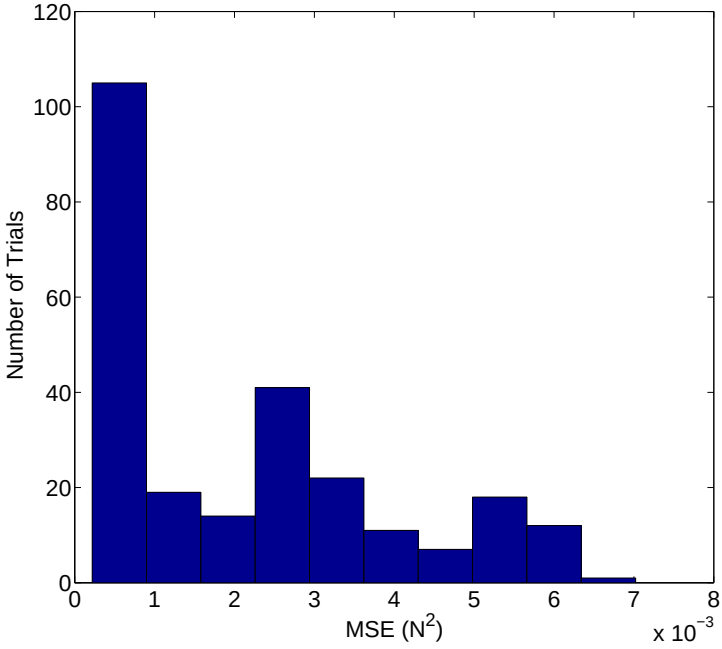

Figure 33: This plot shows the mean square error for the model fits to the settling after step motion data.

7.0 THEORETICAL DEVELOPMENT OF PROPOSED CONTROL ALGORITHM

7.1 CONSTRUCTING THE NONLINEAR ERROR DYNAMICS EQUATIONS

The aim of this section is to compare two approaches to friction compensation during settling for rapid point-to-point motion. The first method is the friction observer and the second is the Nonlinear Integral Action Setting Algorithm (NIASA) approach. Both of these methods make use of an advanced friction model as a key component of the compensator. Additionally, under the ideal conditions of a perfect friction model, both methods offer identical system behavior. However, it is highly unlikely that one single friction model will offer a complete description of the force of friction in a servo mechanism under all conditions. Thus, the plant to be controlled is subject to some measure of uncertainty in its parameters. While variations in plant parameters can sometimes be correlated to measurable quantities, such as position along the range of servo travel, a global description of these variations could prove exceedingly complex. Furthermore, the apparent plant parameters often change for reasons that are not understood. In the interest of providing a highly reliable friction compensation method, the conservative policy of considering the plant parameters to be subject to some measure of uncertainty for each instance of step-settle seems reasonable.

To compare these methods, it is useful to consider reexpressing the friction model equations in a form that is more convenient for analysis than the general differential equation expression. Next, useful assumptions for this problem are considered. With this framework progressively complex control algorithms are formulated and linearization of the nonlinear plant is explored. This leads to the formulation of the two methods to be compared, the

NIASA method and the friction observer. Finally, the effect of uncertainty on algorithm robustness is compared for both methods.

Starting with a simple Dahl model it is desired to express the force of friction, when moving in one direction, as a function of x. The Dahl model can be stated as

$$\frac{dF}{dx} = \sigma \left(1 - \frac{F}{F_C}\right), \tag{7.1}$$

where F is the force of friction, F_C is the level of Coulomb friction, and σ is the initial contact stiffness parameter. The Dahl model can be separated and integrated to solve for the resulting force of friction, F_2, given a displacement, from x_1 to x_2, and an initial force condition, F_1.

$$\int_{F_1}^{F_2} \frac{dF}{1 - \frac{F}{F_C}} dF = \int_{x_1}^{x_2} \sigma dx \tag{7.2}$$

$$-F_C \ln \left(1 - \frac{F}{F_C}\right) |_{F_1}^{F_2} = \sigma \left(x_2 - x_1\right) \tag{7.3}$$

$$\ln \left(\frac{F_C - F_2}{F_C - F_1}\right) = -\sigma \frac{(x_2 - x_1)}{F_C} \tag{7.4}$$

$$F_2 = F_C - (F_C - F_1) \exp \left(\frac{-\sigma}{F_C} \left(x_2 - x_1\right)\right) \tag{7.5}$$

To simplify initial analysis, let $x_1 = 0$ and $F_1 = 0$. Also, let only the trajectory in the positive direction be considered. For this specific case, the force of friction can be expressed as a function of x as

$$F\left(x\right) = F_C \left(1 - \exp \frac{-x\sigma}{F_C}\right). \tag{7.6}$$

The useful quantity, $\frac{dF}{dx}$, can be stated as

$$\frac{dF}{dx} = \sigma \exp \frac{-x\sigma}{F_C}. \tag{7.7}$$

The equation of motion for a single linear axis can be approximated as

$$m\ddot{x} + F\left(x\right) = u, \tag{7.8}$$

where m is the mass and u is the control signal. Now a very useful assumption about sub-micrometer servo dynamics is considered. At some point in sub-micrometer settling, the

frictional dynamics are likely to be substantially larger than the inertial dynamics. In this case the inertial term can be neglected and the equation of motion becomes

$$F(x) = u. \tag{7.9}$$

In application, the assumption presented in equation 7.9 is not meant to be made arbitrarily. It should be verified with actual data. With sufficient mass and sufficient bandwidth in displacement, even nanometer scale motion can have significant inertial response. Let the position error signal be defined as

$$e = r - x, \tag{7.10}$$

with r being the reference signal. If the reference signal is a constant, as it would be during settling, then

$$\dot{e} = -\dot{x}. \tag{7.11}$$

Integral control for this system could be written as

$$u = k_I \int_0^t e(t)dt, \tag{7.12}$$

where k_I is the integral gain. Thus, the system under integral control could be written as

$$F(x) = k_I \int_0^t e(t)dt. \tag{7.13}$$

To place the system in a more convenient form, both sides are differentiated with respect to time yielding,

$$\frac{dF}{dt} = \frac{dF}{dx}\frac{dx}{dt} = k_I e(t). \tag{7.14}$$

Applying the result from equation 7.7 leads to

$$\sigma \exp\frac{-x\sigma}{F_C}\dot{e} + k_I e = 0, \tag{7.15}$$

and

$$\dot{e} = -\frac{k_I}{\sigma \exp\frac{-x\sigma}{F_C}}e. \tag{7.16}$$

Since $\sigma > 0$, $\exp\frac{-x\sigma}{F_C} > 0$, $k_I > 0$, and the system is moving only in the positive direction,

$$\frac{k_I}{\sigma \exp\frac{-x\sigma}{F_C}} > 0. \tag{7.17}$$

Thus, the system is stable but nonlinear. This concept of integral control provides a framework that can be extended to other control methodologies.

PI control of this system can be expressed as

$$\left(\sigma \exp \frac{-x\sigma}{F_C} + k_P\right) \dot{e} + k_I e = 0 \tag{7.18}$$

or

$$\dot{e} = -\frac{k_I}{\sigma \exp \frac{-x\sigma}{F_C} + k_P} e, \tag{7.19}$$

where k_P is a proportional gain term. An interesting observation concerning this controller is that if k_P is always significantly larger than the term $\sigma \exp \frac{-x\sigma}{F_C}$ and both k_I and k_P are constants, the system will show nearly linear behavior. This case is linearizing the system with high gain feedback. While this theoretical result is nice, such a control method is not guaranteed to be feasible in actual practice.

7.2 FRICTION OBSERVER

If a friction modeled is constructed, an observer can be constructed to cancel the force of friction. This can be stated as

$$\left(\sigma \exp \frac{-x\sigma}{F_C} - \hat{\sigma} \exp \frac{-x\hat{\sigma}}{\hat{F_C}} + k_P\right) \dot{e} + k_I e = 0 \tag{7.20}$$

or

$$\dot{e} = -\frac{k_I}{\sigma \exp \frac{-x\sigma}{F_C} - \hat{\sigma} \exp \frac{-x\hat{\sigma}}{\hat{F_C}} + k_P} e, \tag{7.21}$$

where the parameters $\hat{\sigma}$ and $\hat{F_C}$ are modeled parameters. Since error in the context of this problem is position error, the driving term for the observer is the integral action. Proportional control action has been added to ensure that the denominator of equation 7.21 remains positive. Ideally, if the force of friction has been modeled perfectly, the resulting system is stated as

$$\dot{e} = -\frac{k_I}{k_P} e. \tag{7.22}$$

The control system designer can select select the desired time constant for the system, τ_d, and set the integral gain to

$$k_I = \frac{k_P}{\tau_d}. \tag{7.23}$$

7.3 NIASA COMPENSATOR

Returning to integral control shown in equations 7.12 through 7.16, suppose the integral gain, k_I, was not a constant but instead scheduled by the function

$$k_I = \frac{1}{\tau_d}\sigma \exp \frac{-x\sigma}{F_C}. \tag{7.24}$$

The integral gain function is developed from the friction model so, in the ideal case where the friction model is perfect, the resulting system will be

$$\dot{e} = -\frac{1}{\tau_d}e, \tag{7.25}$$

which is identical to the ideal friction observer.

A similar method could be applied to the PI controller that was first introduced in equations 7.18 and 7.19. Once again, if k_I is not a constant but, instead defined by the function

$$k_I = \frac{1}{\tau_d}\left(\sigma \exp \frac{-x\sigma}{F_C} + k_P\right), \tag{7.26}$$

in the ideal case, the resulting system will be identical to the ideal friction observer and identical to the ideal integral control shown in equation 7.25.

7.4 CONSIDERING UNCERTAINTY

At this point two model based control methods have been described as a means of controlling a precision servo during final settling after a step motion: the friction observer and the gain scheduled PI controller (the gain scheduled integral only control is grouped as a sub-set of gain scheduled PI controllers with $k_P = 0$). These have been shown to behave identically in the case of perfect system modeling, yet formulation of each controller is significantly different. Now it is desired to investigate the behavior of each in the presence of plant uncertainty. There are two parameters of this plant which could be subject to uncertainty, σ and F_C. Since it is desired to discuss uncertainty in the most simple yet relevant fashion, considering a realistic scenario for the system is useful. The key region where the behavior of the algorithms is most important will be for very small values of x. When x is small, all terms involving the exponential function approach one. Since the parameter F_C occurs only inside exponential functions it appears less important when x is small. Conversely, the parameter σ appears both inside of the exponential function and as a multiplying factor outside of the function so, it appears more important at small values of x. Thus, to simplify analysis, let only the initial contact stiffness be subject to multiplicative uncertainty as,

$$\sigma^+ = \sigma\left(1 + \delta\right), \tag{7.27}$$

where σ^+ is the perturbed plant and δ is the parameter uncertainty. Also, introduce the concept of describing pre-rolling friction in terms of a characteristic length as

$$x_c = \frac{F_C}{\sigma}. \tag{7.28}$$

Now consider that displacement and displacement based terms can be expressed as a function of the characteristic length as

$$X = \frac{x}{x_c}. \tag{7.29}$$

In further interest of making objective comparisons of methods let the proportional gain be defined in terms of initial contact stiffness as

$$k_{P\sigma} = \frac{k_P}{\sigma}. \tag{7.30}$$

The behavior of the error signal for the friction observer, when the plant is subject to uncertainty can now be written as

$$\dot{e} = -\frac{1}{\tau_d}\frac{k_{P\sigma}}{(1+\delta)\exp\left(-X\left(1+\delta\right)\right) - \exp\left(-X\right) + k_{P\sigma}}e. \tag{7.31}$$

Similarly, the behavior for the NIASA compensator is described by

$$\dot{e} = -\frac{1}{\tau_d}\frac{\exp\left(-X\right) + k_{P\sigma}}{(1+\delta)\exp\left(-X\left(1+\delta\right)\right) + k_{P\sigma}}e. \tag{7.32}$$

Most of the system specific information has been removed from the equations and methods can be evaluated objectively for the generalized case.

To develop bounds for reasonable choices of δ, real system data is considered. A set of 25 trails on a particular precision servo yielded a nominal value of $\sigma = 8.46$ N/µm, with maximum value of $\sigma = 16.79$ N/µm, and a minimum value of $\sigma = 4.17$ N/µm. Solving equation 7.27 leads to approximate bounds of $-0.5 < \delta < 1$.

7.5 SIMULATION OF MASSLESS APPROXIMATION

With the error dynamics equations for the simplified system defined, the next step is to analyze these equations. The solutions to equations 7.31 and 7.32 are still not simple and will be solved in relevant regions by numerical methods. There are several items that must be considered in producing proper solutions to these equations. First, manipulations used to construct 7.31 and 7.32 relied on the system starting at $x = 0$ (equivalent to $X = 0$), so at $t = 0$, $X = 0$. Starting at $x = 0$ was done to provide less cluttered equations and will not affect the final results. Also, the system is to be moving only in the positive direction, so the reference should be set to a positive value, which corresponds to a positive value for the error initial condition. Since frictional dynamics have the greatest effect on system behavior over displacements very near velocity reversals, the most relevant information to be gained from simulation would likely be over small displacements. Additionally, equations 7.31 and 7.32 vary with X. Thus, for this simulation, the initial conditions on error will contain a series of values of $e \leq x_c$.

With the space of the problem and initial conditions defined, the variables to be investigated should be discussed. As previously mentioned, it is important to investigate the space of uncertainty of the plant. This will be defined by $-0.5 < \delta < 1$, as derived from actual data. It is also desired to investigate the effect of changing the proportional gain, k_P. The values to be investigated will be between 5% and 100% of the initial contact stiffness, σ.

To make interpretation of the potentially large amount of simulation data more simple, a performance metric is considered. Since the fundamental problem to be addressed is system settling time, a metric of the percentage change in settling time for the perturbed plant to reach a given tolerance, compared to the nominal plant, is proposed. For this set of simulations, the settling tolerance is set to 2% of the initial error condition. Figures 34 through 44 show the results of these simulations in terms of this metric. Each plot compares the change in settling time across a range of initial error conditions and for the perturbed plant for both the friction model gain scheduling approach and the friction observer. The series of contour plots is neccessary because it is also desired to investigate the effects of varying the proportional gain. In the contour plots, each level curve cooresponds to a 10% change in system settling time. The level curve that denotes 0% change in settling time is marked in each plot for easier interpretation of the data. In the cases where the simulation was found to be unstable, these regions are denoted by the solid red regions.

When examining the series of plots presented in figures 34 through 44 several interesting observation can be made. First, it appears that the gain scheduled friction compensation method is far less sensitive to plant uncertainty than is the friction observer. This is apparent because there are significantly fewer level curves for the gain scheduling method as compared to the friction observer in each of the figures. Also, there are a significant number of cases where the friction observer becomes unstable while the gain scheduling method appears stable through all cases. This is not surprising because the value of the denominator in equation 7.31 can easily pass through zero and change signs while this is not true of equation 7.32. When comparing the overall performance of both methods across changes in the proportional gain, it is seen that increasing the proportional gain leads to less deviation from the nominal performance across the range of plant uncertainty. This is also expected since the effect of system nonlinearities can sometimes be minimized with high gain feedback.

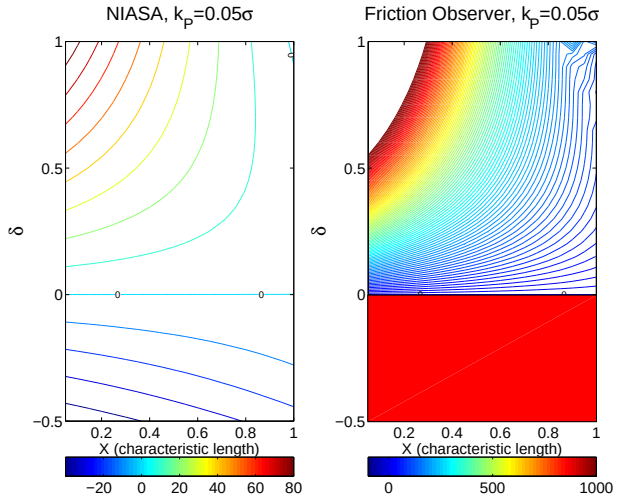

Figure 34: The percent change in settling time of the system, as compared to the nominal plant, is shown for the friction model based gain scheduling method (left) and the friction observer (right). For this case $k_P = 0.05\sigma$. The highest level curve is at 1000% increase in settling time from the nominal plant. The upper left corner of the friction observer contour plot contains settling times $> 1000\%$ of the nominal value. The friction observer contains an unstable region which is denoted by the solid red area.

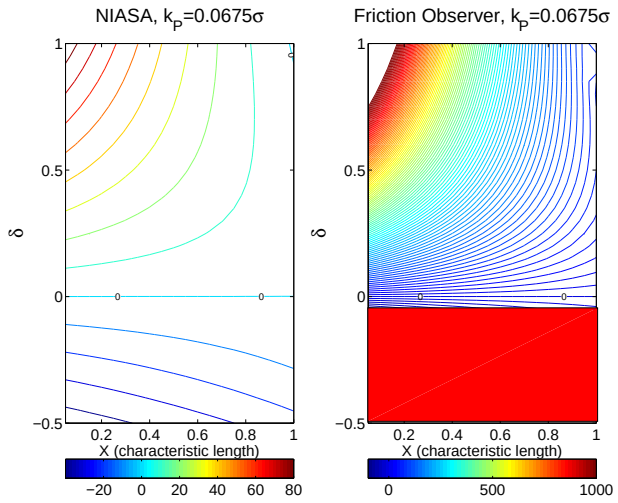

Figure 35: The percent change in settling time of the system, as compared to the nominal plant, is shown for the friction model based gain scheduling method (left) and the friction observer (right). For this case $k_P = 0.0675\sigma$. The highest level curve is at 1000% increase in settling time from the nominal plant. The upper left corner of the friction observer contour plot contains settling times $> 1000\%$ of the nominal value. The friction observer contains an unstable region which is denoted by the solid red area.

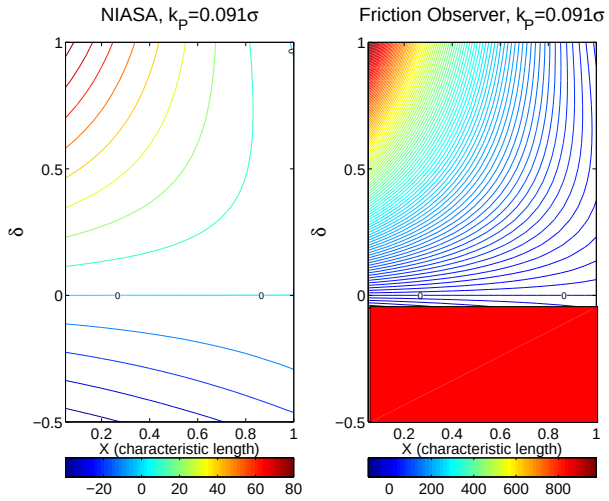

Figure 36: The percent change in settling time of the system, as compared to the nominal plant, is shown for the friction model based gain scheduling method (left) and the friction observer (right). For this case $k_P = 0.091\sigma$. The friction observer contains an unstable region which is denoted by the solid red area.

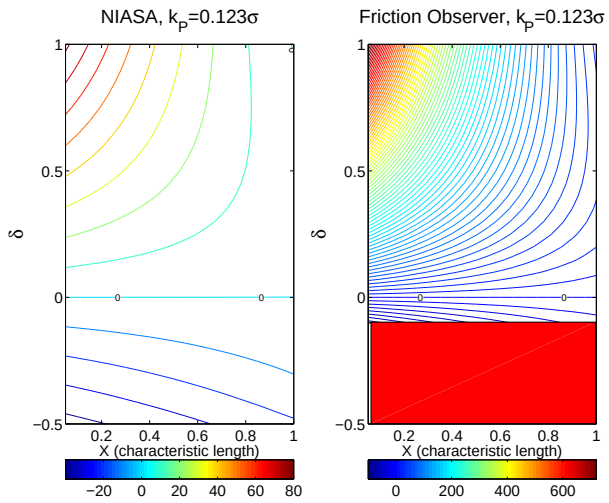

Figure 37: The percent change in settling time of the system, as compared to the nominal plant, is shown for the friction model based gain scheduling method (left) and the friction observer (right). For this case $k_P = 0.123\sigma$. The friction observer contains an unstable region which is denoted by the solid red area.

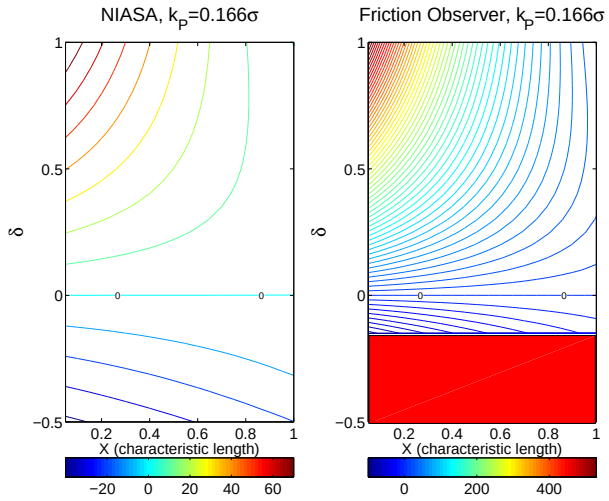

Figure 38: The percent change in settling time of the system, as compared to the nominal plant, is shown for the friction model based gain scheduling method (left) and the friction observer (right). For this case $k_P = 0.166\sigma$. The friction observer contains an unstable region which is denoted by the solid red area.

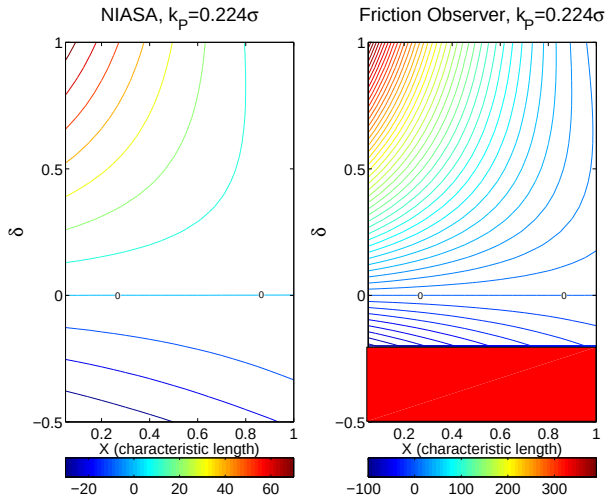

Figure 39: The percent change in settling time of the system, as compared to the nominal plant, is shown for the friction model based gain scheduling method (left) and the friction observer (right). For this case $k_P = 0.224\sigma$. The friction observer contains an unstable region which is denoted by the solid red area.

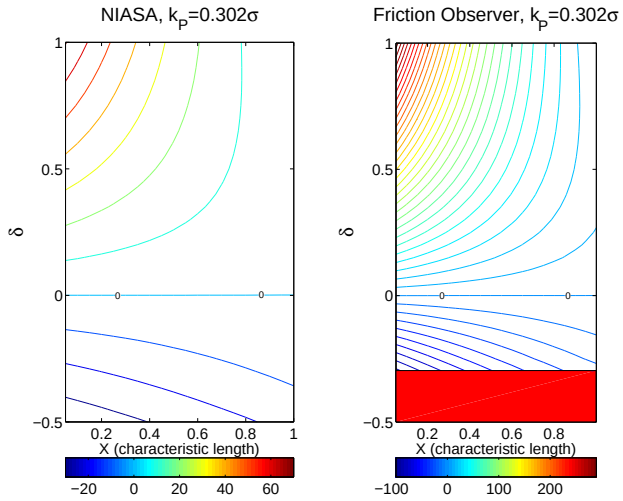

Figure 40: The percent change in settling time of the system, as compared to the nominal plant, is shown for the friction model based gain scheduling method (left) and the friction observer (right). For this case $k_P = 0.302\sigma$. The friction observer contains an unstable region which is denoted by the solid red area.

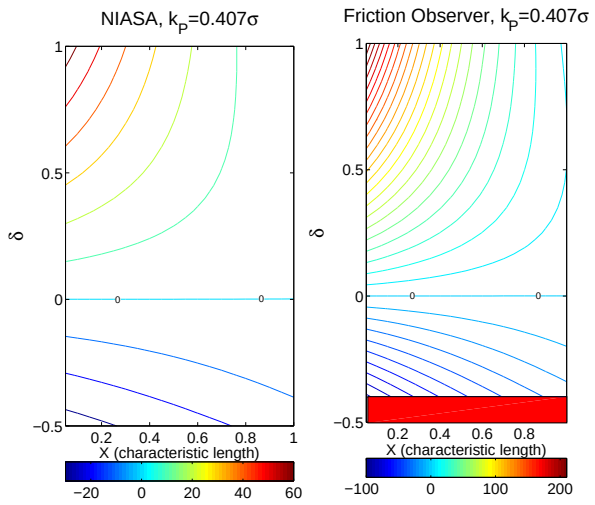

Figure 41: The percent change in settling time of the system, as compared to the nominal plant, is shown for the friction model based gain scheduling method (left) and the friction observer (right). For this case $k_P = 0.407\sigma$. The friction observer contains an unstable region which is denoted by the solid red area.

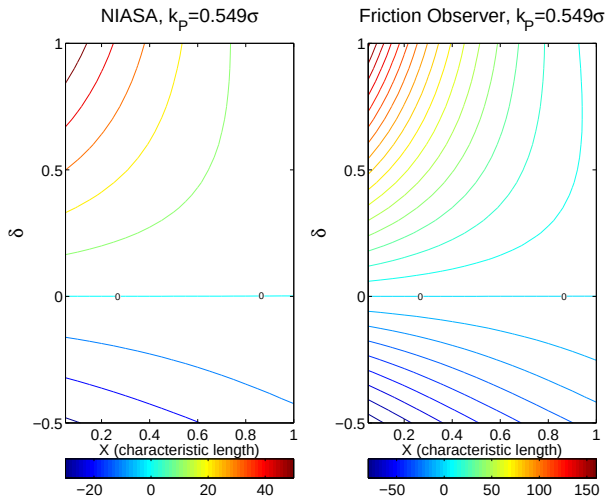

Figure 42: The percent change in settling time of the system, as compared to the nominal plant, is shown for the friction model based gain scheduling method (left) and the friction observer (right). For this case $k_P = 0.549\sigma$.

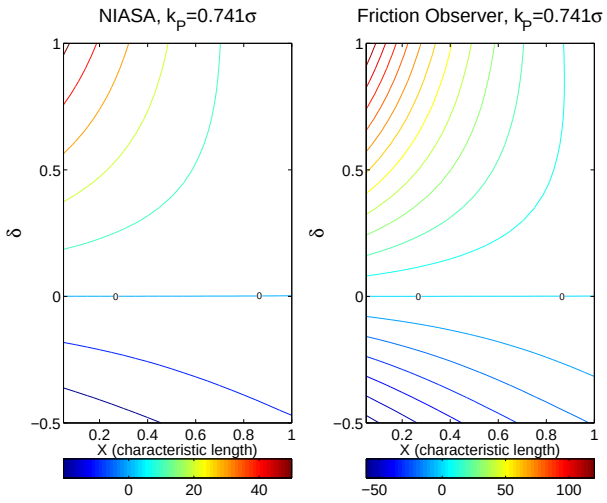

Figure 43: The percent change in settling time of the system, as compared to the nominal plant, is shown for the friction model based gain scheduling method (left) and the friction observer (right). For this case $k_P = 0.741\sigma$.

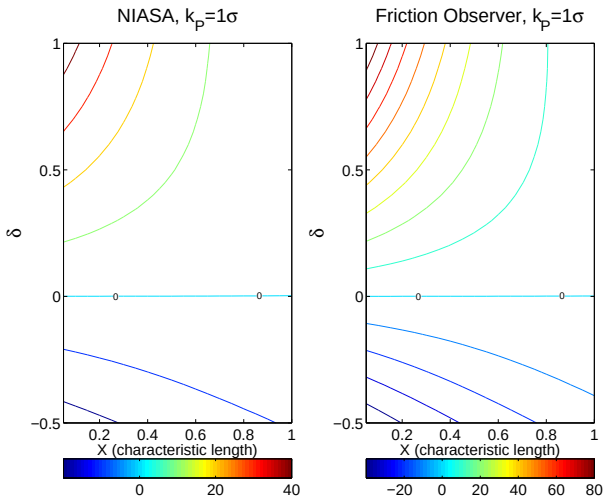

Figure 44: The percent change in settling time of the system, as compared to the nominal plant, is shown for the friction model based gain scheduling method (left) and the friction observer (right). For this case $k_P = 1.000\sigma$.

In this section the sensitivity to perturbations of the plant for two different methods of friction compensation during system settling have been compared. One key observation is that the friction model-based gain scheduling method appears to be far less sensitive to plant uncertainty than does the friction observer. Also, in this purely theoretical setting, the friction model based gain scheduling does not incur the risk of system instability while the friction observer can cause system instability. Additionally, it appears that increasing the proportional gain can minimize the effects of the nonlinearity in the system.

While these results are interesting and useful, for a practical implementation, more work is needed. It is clear that the massless approximation will only be valid under certain conditions. Thus, the effect of considering the mass of the system should be studied. In this theoretical setting, increasing proportional gain shows only positive effects. In actual application, there will be a practical limit to the amount of proportional gain which can be added. Finally, determining how an algorithm for increasing settling performances in the pre-rolling regime fits with control of gross motion and in-position performance must also be discussed. This will be discussed in later chapters.

7.6 SIMULATIONS INCLUDING MASS

The previous concepts of control in the presence of pre-rolling friction have been developed neglecting the inertial response of the system. However, real motion control systems always have mass. Thus, it is important to investigate how relevant the previous analysis is when the inertial response of the system is considered. First, the general form of the servo under PID control, subject to friction is introduced. Then the methods of solving around possible velocity reversals are discussed and parametric uncertainty is considered. Finally, the observer and gain scheduling methods are placed into this format and simulated. The equation of motion for this system, under PID control is

$$m\ddot{x} + F(x) = \int_0^t k_I e \, dt + k_P e + k_D \dot{e}. \tag{7.33}$$

As with the previous massless approximation, it is desired to eliminate the integral term on the right side of equation 7.33. Differentiating equation 7.33 leads to

$$m\dddot{x} + \frac{dF}{dx}\dot{x} = k_I e + k_P \dot{e} + k_D \ddot{e}. \tag{7.34}$$

With the third order dynamics of this equation it is quite possible that velocity reversals will occur during the settling process thus, a method to solve for these cases should be considered. In its most general form, for motion in the positive direction, the force of friction as a function of x can be expressed as

$$F(x)^{(+)} = F_C - (F_C - F_0)\exp\left(-\frac{\sigma}{F_C}(x - x_0)\right). \tag{7.35}$$

Similarly, for motion in the negative direction

$$F(x)^{(-)} = -F_C + (F_C + F_0)\exp\left(\frac{\sigma}{F_C}(x - x_0)\right). \tag{7.36}$$

In both cases, F_0 denotes the force of friction when motion is initiated in the given direction and x_0 is the location where this motion began. This allows solving for the force of friction through velocity reversals. Since $e = r - x$ equations 7.35 and 7.36 can be written in terms of e as

$$F(e)^{(+)} = F_C - (F_C - F_0)\exp\left(-\frac{\sigma}{F_C}(-e + e_0)\right), \tag{7.37}$$

for positive motion and

$$F(e)^{(-)} = -F_C + (F_C + F_0)\exp\left(\frac{\sigma}{F_C}(-e + e_0)\right), \tag{7.38}$$

for negative motion, where e_0 is the initial condition of error upon the start of motion or going through a velocity reversal. If equations 7.35 and 7.36 are differentiated with respect to x and the substitution $e = r - x$ is used, then for positive motion

$$\frac{dF}{dx}^{(+)} = \frac{F_C - F_0}{F_C}\exp\left(-\frac{\sigma}{F_C}(-e + e_0)\right) \tag{7.39}$$

and for negative motion

$$\frac{dF}{dx}^{(-)} = \frac{F_C + F_0}{F_C}\exp\left(\frac{\sigma}{F_C}(-e + e_0)\right). \tag{7.40}$$

Since r is assumed to be a constant during settling, $\dot{e} = -\dot{x}$, $\ddot{e} = -\ddot{x}$, and $\dddot{e} = -\dddot{x}$ become useful properties in expressing 7.34 in terms of only e and its derivatives. Thus, for positive motion, the error dynamics are

$$m\dddot{e} + k_D\ddot{e} + \left(\frac{F_C - F_0}{F_C}\sigma \exp\left(-\frac{\sigma}{F_C}\left(-e + e_0\right)\right) + k_P\right)\dot{e} + k_I e = 0 \tag{7.41}$$

and for negative motion the error dynamics are

$$m\dddot{e} + k_D\ddot{e} + \left(\frac{F_C + F_0}{F_C}\sigma \exp\left(\frac{\sigma}{F_C}\left(-e + e_0\right)\right) + k_P\right)\dot{e} + k_I e = 0. \tag{7.42}$$

If a velocity reversal was to occur during settling, e_0 for the new direction, is the value of e at the velocity reversal. F_0 for the new direction found by appropriately solving either equation 7.37 or 7.38 where, e is the value of e at the current location, e_0 is the value of e at previous velocity reversal or start of simulation, and F_0 is the value of the force of friction at the previous velocity reversal or start of simulation.

At this point let the same structured multiplicative uncertainty of σ be added to the system. For positive motion, this leads to

$$m\dddot{e} + k_D\ddot{e} + \left(\frac{F_C - F_0}{F_C}\sigma\left(1+\delta\right)\exp\left(-\frac{\sigma\left(1+\delta\right)}{F_C}\left(-e + e_0\right)\right)\right)\dot{e} + k_P\dot{e} + k_I e = 0 \tag{7.43}$$

and for negative motion the system becomes

$$m\dddot{e} + k_D\ddot{e} + \left(\frac{F_C + F_0}{F_C}\sigma\left(1+\delta\right)\exp\left(\frac{\sigma\left(1+\delta\right)}{F_C}\left(-e + e_0\right)\right)\right)\dot{e} + k_P\dot{e} + k_I e = 0. \tag{7.44}$$

Should a velocity reversal occur in this system, equations 7.37 and 7.38 must be modified to correctly solve for the initial conditions of the perturbed plant. This modification yields

$$F(e)^{(+)} = F_C - \left(F_C - F_0\right)\exp\left(-\frac{\sigma\left(1+\delta\right)}{F_C}\left(-e + e_0\right)\right) \tag{7.45}$$

and

$$F(e)^{(-)} = -F_C + (F_C + F_0)\exp\left(\frac{\sigma(1+\delta)}{F_C}(-e+e_0)\right). \tag{7.46}$$

Using the previous definition of the friction observer in the massless approximation, the friction observer for the case where system mass is considered can be written as

$$\begin{aligned} m\dddot{e} + k_D\ddot{e} + \left(\frac{F_C - F_0}{F_C}\sigma(1+\delta)\exp\left(-\frac{\sigma(1+\delta)}{F_C}(-e+e_0)\right)\right)\dot{e} \\ + \left(-\frac{F_C - F_0}{F_C}\sigma\exp\left(-\frac{\sigma}{F_C}(-e+e_0)\right) + k_P\right)\dot{e} + \frac{k_P}{\tau_d}e = 0 \end{aligned} \tag{7.47}$$

for positive motion and

$$\begin{aligned} m\dddot{e} + k_D\ddot{e} + \left(\frac{F_C + F_0}{F_C}\sigma(1+\delta)\exp\left(\frac{\sigma(1+\delta)}{F_C}(-e+e_0)\right)\right)\dot{e} \\ + \left(-\frac{F_C + F_0}{F_C}\sigma\exp\left(\frac{\sigma}{F_C}(-e+e_0)\right) + k_P\right)\dot{e} + \frac{k_P}{\tau_d}e = 0 \end{aligned} \tag{7.48}$$

for negative motion. Similarly, the gain scheduling approach becomes

$$\begin{aligned} m\dddot{e} + k_D\ddot{e} + \left(\frac{F_C - F_0}{F_C}\sigma(1+\delta)\exp\left(-\frac{\sigma(1+\delta)}{F_C}(-e+e_0)\right)\right)\dot{e} \\ + k_P\dot{e} + \frac{1}{\tau_d}\left(\frac{F_C - F_0}{F_C}\sigma\exp\left(-\frac{\sigma}{F_C}(-e+e_0)\right) + kp\right)e = 0 \end{aligned} \tag{7.49}$$

for positive motion and

$$\begin{aligned} m\dddot{e} + k_D\ddot{e} + \left(\frac{F_C + F_0}{F_C}\sigma(1+\delta)\exp\left(\frac{\sigma(1+\delta)}{F_C}(-e+e_0)\right)\right)\dot{e} \\ + k_P\dot{e} + \frac{1}{\tau_d}\left(\frac{F_C + F_0}{F_C}\sigma\exp\left(\frac{\sigma}{F_C}(-e+e_0)\right) + kp\right)e = 0 \end{aligned} \tag{7.50}$$

for negative motion. It is important to note that both of these methods actually contain two models of the frictional process each: the nominal model, which the control is designed around, and the true friction process, which is the nominal model along with the uncertainty. Thus, in the case of velocity reversal, the new initial conditions for the true plant come from

equations 7.45 and 7.46 while the new initial conditions for the control come from equations 7.37 and 7.38.

To explore the utility of the massless system approximation presented in the previous sections a simulation of a realistic system will be analyzed. The moving mass of the system is 1.5 kg. In the free mass, linear control approximation, the system has a cross-over frequency near 100 Hz with a phase margin of about 45 degrees. This leads to a proportional gain of $k_P = 900,000$ N/m and a derivative gain of $k_D = 850$ Ns/m. In the previous analysis derivative gain was not considered. It is hypothesized that derivative gain will not have a significant impact on the system response over very small displacements. It is also hoped that derivative action can add damping to the higher order dynamics introduced by now considering the mass of the system thus, minimizing oscillatory effects.

In the first simulation, figure 45, $\delta = 0$, thus it is assumed that the friction model exactly captures the real system behavior. In this case the massless observer and gain scheduling series are not visible because they are directly beneath the ideal case. The effect of adding mass to the system is clearly seen in the slight oscillations shown in these respective simulations. For the friction observer, this is not surprising since, the goal of the friction observer is to cancel the force of friction and leave only the inertial dynamics. It should also be noted that the period of oscillations of the friction observer considering mass suggest that this system is considerably less stiff than the gain scheduling method where mass is considered. This is because the observer has canceled the stiffness produced by pre-rolling friction. In a general sense, both stiffness and linearity are desirable characteristics in a servo mechanism. Pre-rolling friction is beneficial in that it contributes stiffness to the system but, it is potentially harmful to system performance because it introduces a nonlinearity to the system. The implied philosophy of the friction observer is that the potential problems of the nonlinearity outweigh the benefits of a stiffer system. However, the friction model-based gain scheduling method takes a different approach where, the positive characteristics of pre-rolling friction are preserved and a nearly linear response is still possible. This is seen as the period of oscillations of the gain scheduling approach considering mass suggest a significantly stiffer system than the friction observer. It should also be noted that, for this case, the massless simulations do provide a reasonable approximation of the system

behavior when mass is considered. The next four plots, figures 46 through 49, show the system response when δ=0.1, 0.25, 0.5, and 1.0. This corresponds to the true plant having an initial contact stiffness which in 10%, 25%, 50%, and 100% greater than the nominal model. From the data, it is apparent that the massless simulation provides a very good approximation of how each system behaves when mass is considered. Also, as predicted in the massless simulations, the system performance of the gain scheduling method is far less sensitive to perturbations in the nominal plant compared to the friction observer.

The next five plots, figures 50 through 54, show the system response when δ=-0.05, -0.1, -0.3, -0.5, and -0.65. When examining figure 50 the first noticeable feature is the ringing of the friction observer when mass is considered. While the massless simulation of the friction observer suggests that settling should be slightly faster than the nominal case, it is clear that when mass is considered, settling is actually much slower. When δ=-0.1, as in figure 51, the massless friction observer simulation again predicts settling faster than the nominal case. However, when mass is considered in the friction observer simulation, the result is a limit cycle with substantial amplitude. For further decreases in δ, the massless friction observer simulation predicts instability. When mass is considered, some of these cases did result in instability while others lead to large limit cycles. Both of these are not useful in addressing the settling problem and are not included on the remaining plots. In examining the behavior of model-based gain scheduling simulations, the simulations including mass tended to agree rather well with the massless simulations, for the anticipated range of parameter uncertainty, $(-0.5 < \delta < 1)$. There is some ringing of the system which tends to increase as δ decreases and this could degrade actual settling performance to some extent. When δ is decreased to -0.65 the gain scheduling approach with mass included shows signs of instability. Fortunately, this value was outside the estimated range of parameter uncertainty but, this test case was constructed to show that it is still possible to drive the system to instability with this algorithm. In summary, it appears that there are realistic cases where the friction control concepts developed in massless approximations provide a good representation of system performance when mass included. In an actual design situation it would probably be best to conduct simulations where the mass of the system is taken into account. Especially in the case of the friction observer, the designer should always be

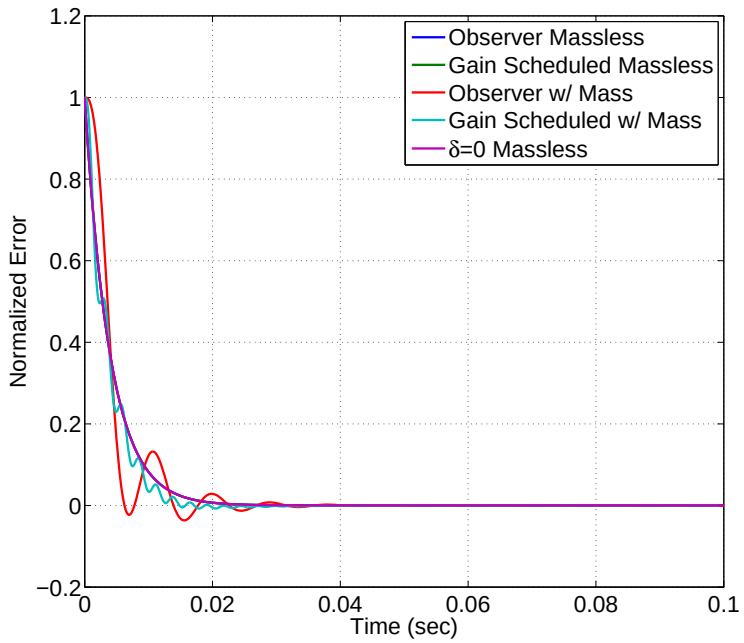

Figure 45: For the case where the friction model perfectly matches the friction process, δ=0, the massless observer and NIASA approximations are not visible because they are directly beneath the ideal massless approximation. The simulations of the observer and the NIASA where the mass terms are included are reasonably approximated by the massless approximations even though the effects of these additional terms are clearly seen in the slight oscillations of the approximations which include the servo mass.

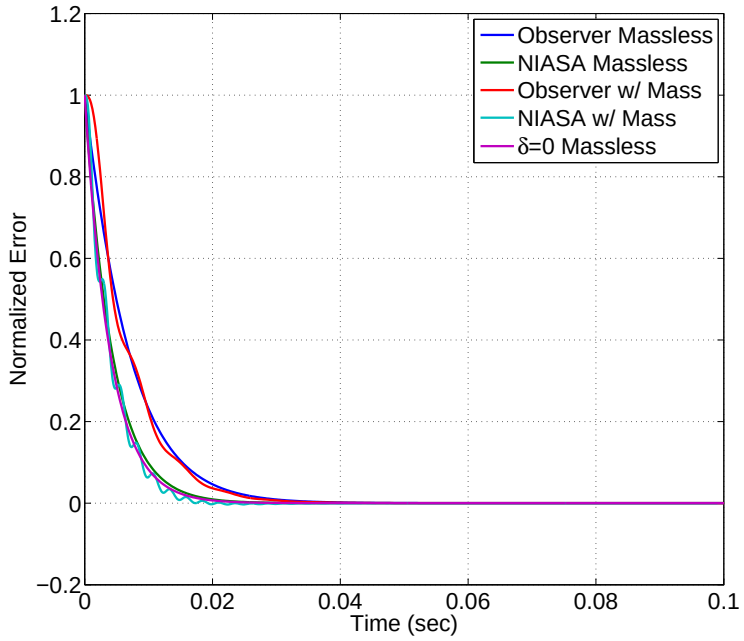

Figure 46: With a 10% underestimate of the initial contact stiffness parameter, δ=0.1, the NIASA compensator converges faster than the friction observer. For this case the massless approximations predict the full system response quite well.

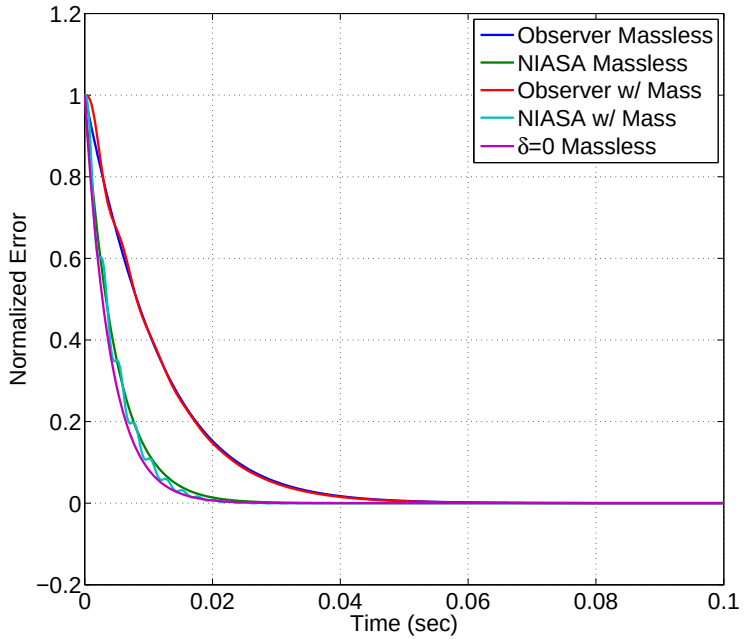

Figure 47: When δ=0.25, corresponding to a 25% underestimate of the initial contact stiffness, the NIASA compensator converges faster than the friction observer. Once again, the massless approximations predict the full system response very well.

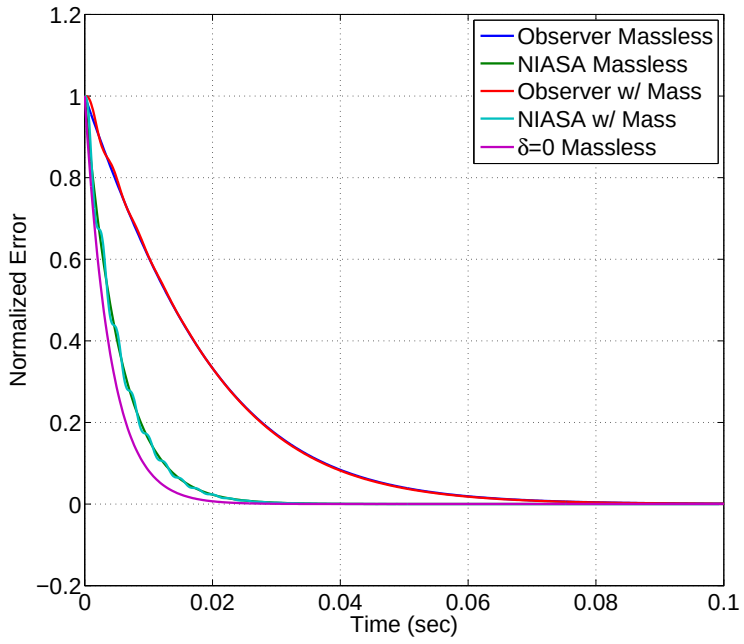

Figure 48: For a 50% underestimate of the initial contact stiffness, δ=0.5, the NIASA compensator still converges significantly faster than the friction observer.

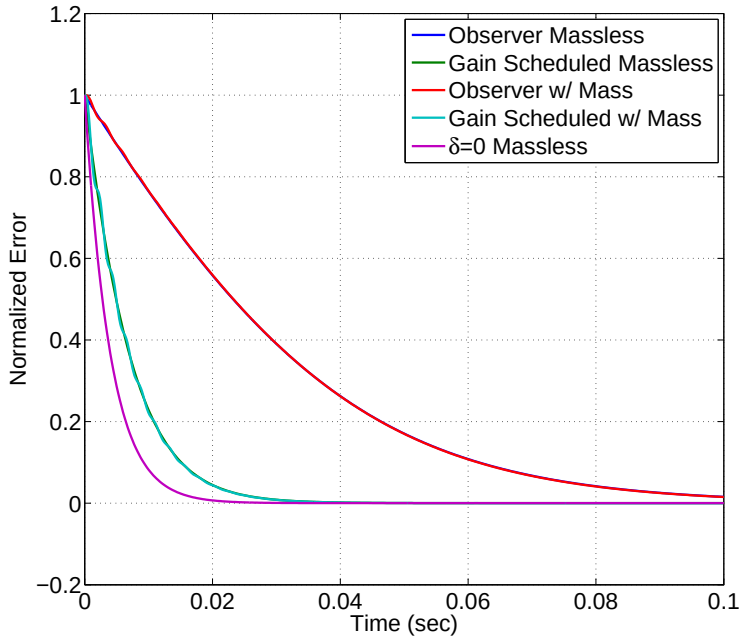

Figure 49: With δ=1.0, a 100% underestimate of the initial contact stiffness, the NIASA compensator again converges much faster than the friction observer. Again, the massless approximation is a good representation of the full system behavior.

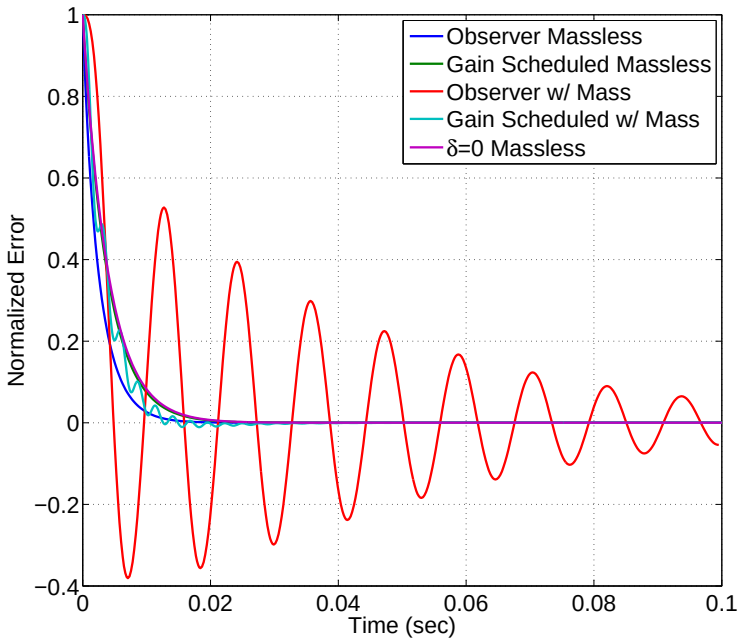

Figure 50: For a 5% overestimate of the initial contact stiffness parameter, δ =-0.05, the massless approximation of the friction observer predicts settling to occur faster than the perfect model case of δ =0. However, when the mass of the system is considered, the friction observer shows significant ringing and slower settling. The NIASA compensator still shows performance very near the perfect model case.

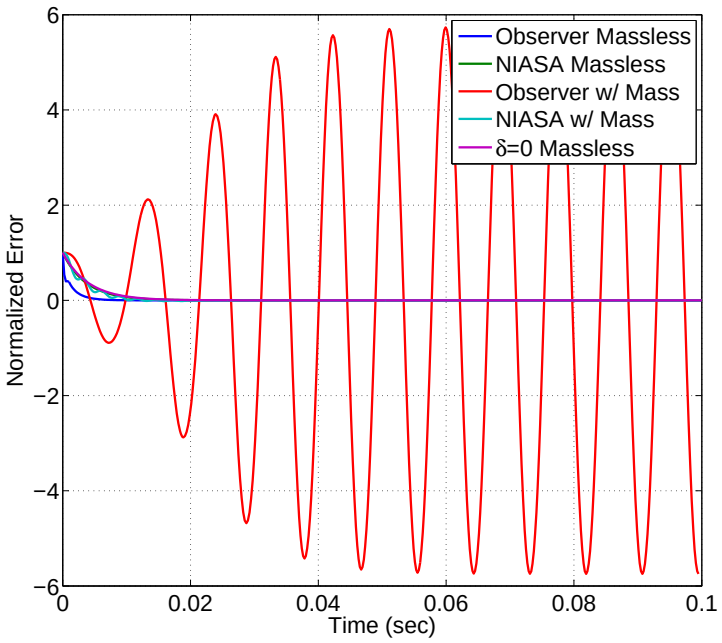

Figure 51: When δ=-0.1, a 10% overestimate of the initial contact stiffness, the massless approximation of the friction observer again predicts settling to occur faster than the perfect model case of δ =0. This time, instead of settling, the friction observer goes into a large limit cycle. This is an unacceptable situation for servo settling. Once again, the NIASA compesator has no issues with settling the system.

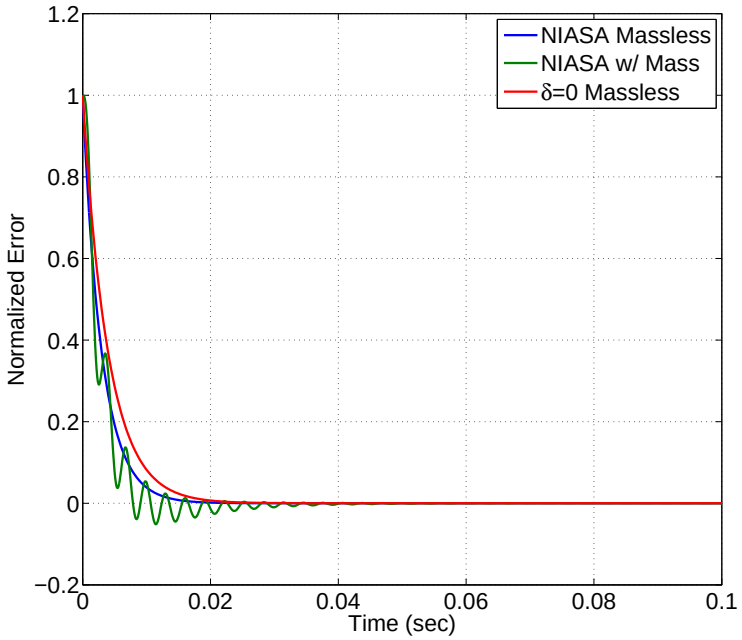

Figure 52: For the case of a 30% overestimate of the initial contact stiffness, δ=-0.3, the friction observer cases have been ommitted from the plot because they are unstable. Although there is a slight rining in the NIASA system response, this compensator still settles the system near the ideal rate.

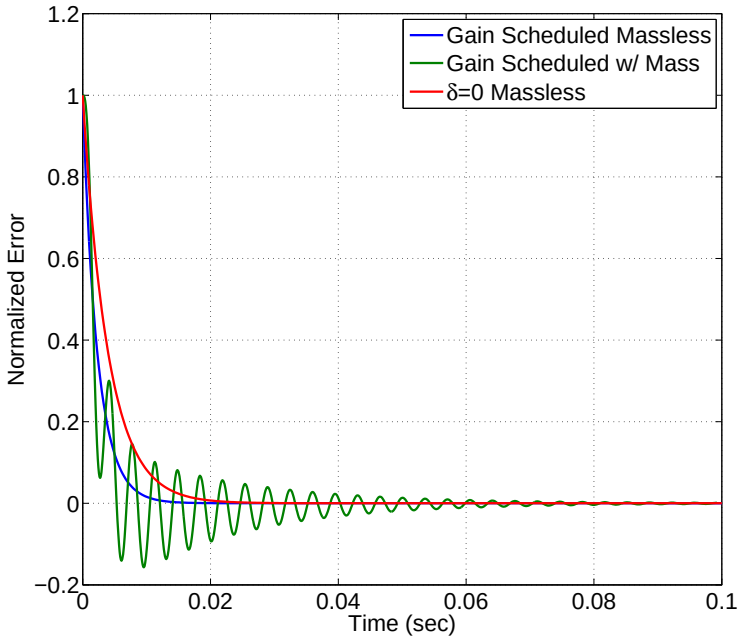

Figure 53: As a 50% overestimate of the initial contact stiffness parameter is considered, δ=-0.5, the friction observer cases are still ommitted because they are unstable. The NIASA compensator simulation including system mass shows significant ringing but, the system is still stable over the entire range of parametric uncertainty to be considered.

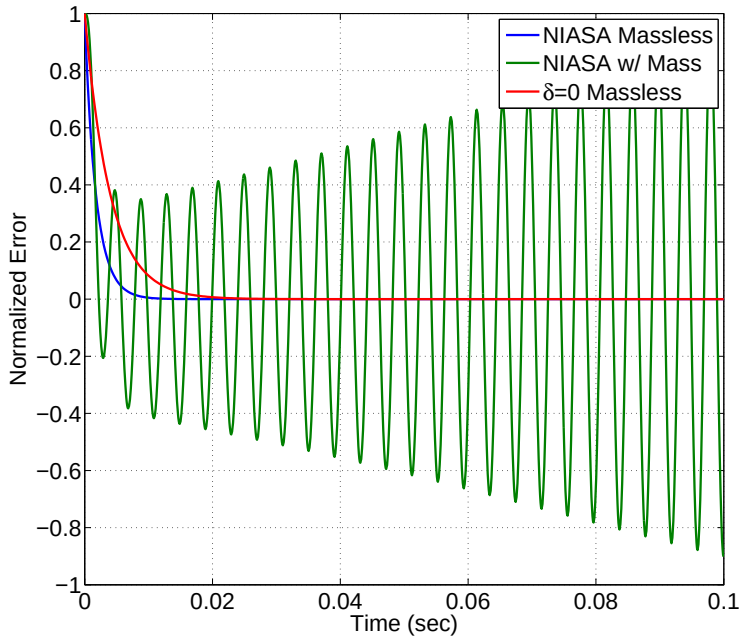

Figure 54: Considering a 65% overestimate of the initial contact stiffness, δ=-0.65, a value outside the range of parametric uncertainty for this experiment, finally moves the NIASA simulation including mass to instability.

cautious of cases where massless simulated performance appears to be better than nominal performance, as this seems to suggest the possibility of sustained oscillations or instability. Finally, as the massless simulations suggest, the simulations including mass confirm that the performance of the friction model-based gain scheduling method is much less sensitive to perturbations of the initial contact stiffness than is the friction observer.

7.7 CONTROL LAW

The proposed control law has been implied in the previous sections but, not yet explicitly stated. Recalling that PID control can be is stated as

$$u(t) = \int_0^t k_I e(t)\, dt + k_P e(t) + k_D \dot{e}(t). \tag{7.51}$$

Introduce $\frac{d\hat{F}_r(x,x_0,F_0)}{dx}$ as the modeled change in the force of friction with respect to change in displacement. The arguments x, x_0, and F_0 have been included to clarify that F_r is a function of these arguments. As first stated in equation 7.24, k_I is developed as a special case of $\frac{d\hat{F}_r(x,x_0,F_0)}{dx}$ specifically,

$$k_I = \frac{1}{\tau_d}\sigma \exp\frac{-x\sigma}{F_C} = \frac{1}{\tau_d}\frac{d\hat{F}_r(x,0,0)}{dx}. \tag{7.52}$$

More generally, k_I in the form of pure integral control can be defined as

$$k_I = \frac{1}{\tau_d}\frac{d\hat{F}_r(x,x_0,F_0)}{dx}. \tag{7.53}$$

The general form of k_I in terms of PI control, similar to equation 7.25 becomes

$$k_I = \frac{1}{\tau_d}\left(\frac{d\hat{F}_r(x,x_0,F_0)}{dx} + k_P\right). \tag{7.54}$$

Finally, the proposed NIASA compensator combined with PID control is stated as

$$u(t) = \int_0^t \frac{1}{\tau_d}\left(\frac{d\hat{F}_r(x,x_0,F_0)}{dx} + k_P\right) e(t)\, dt + k_P e(t) + k_D \dot{e}(t). \tag{7.55}$$

Figure 55 shows a block diagram representation of the NIASA compensator with a PID controller. The basic principal of the algorithm's operations is that the systems integral gain is adjusted using information from a model of the dynamics of the force of friction.

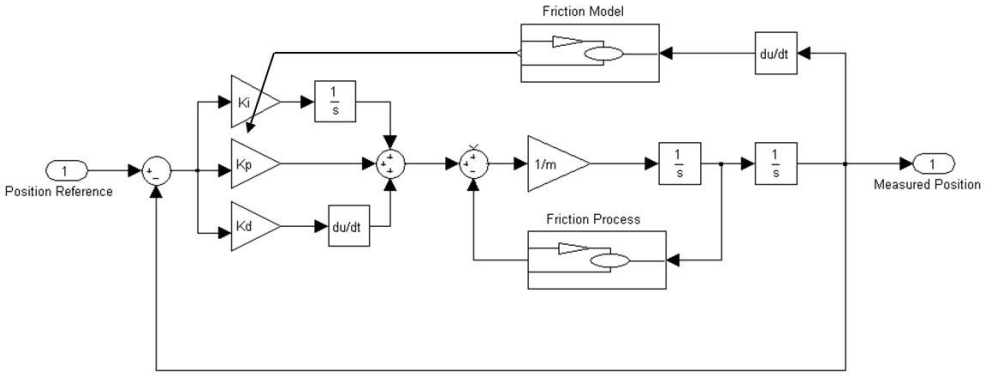

Figure 55: This figure shows a block diagram of the NIASA compensator implemented with a PID controller. The basic method of operation of the NIASA compensator is to adjust the system integral gain based on a model of the force of friction.

8.0 IMPLEMENTATION AND FREQUENCY DOMAIN ANALYSIS

8.1 IMPLEMENTATION

8.1.1 Friction Model for Compensation Parameterization

The highest priority when parameterizing the friction model at the heart of the friction compensation methods is to preserve stability of the system. Recalling the results of the control system simulations conducted in previous sections, it appeared that undesirable characteristics, such as ringing and instability, occurred when σ was over-estimated. Considering this observation, the friction model will use $\sigma = 4$ N/µm, a value near the minimum identified contact stiffness. The parameter F_C is thought to be somewhat less important when operating well inside the pre-rolling regime. Thus, a conservative value, slightly less than the mean values found in table 1, of F_C=0.6 N is used.

8.1.2 Limiting of Integration Rate

In the previous sections a control algorithm for settling a servo under a very specific condition has been proposed and analyzed. This specific condition is when pre-rolling friction dominates the system response. However, in the vast majority of servo operation, pre-rolling friction or even the whole friction process tends to be rather insignificant, as the system appears to be more like a controlled free mass. Applying integral action to such a system is likely to cause the resulting poles of this approximate plant to at least pass through the right half plane, resulting in instability. In a extremely brief summary of the workings of the proposed algorithm, very large integral gains are scheduled immediately after the servo has a velocity reversal and as the servo moves further from this velocity reversal, this additional

integral gain is reduced. The reduction in integral gain as the system moves further from velocity reversals should aid in preserving system stability but, there still is a brief instant, immediately after the reversal occurs, when the integral gain is very large and it is possible that position error could also be large. Thus, the contents of the additional nonlinear integrator could become very large within a few samples. This is clearly a potential problem that must be addressed.

For the initial rapid point-to-point studies conducted in this effort the solution proved rather simple. Since the problem of extended settling times only manifests after the motion profile has concluded, the value in the nonlinear integrator was frozen during the gross motion of the servo. When the motion profile concluded, the servo was typically within a few hundred nanometers of the target location. This is within the pre-rolling regime. Thus, pre-rolling friction tended to dominate the system response and the proposed algorithm was again activated. Settling occurred faster than with only the linear PID control and no stability issues were encountered. While this is a simple and fortunate solution, a better solution may be possible.

The NIASA compensator was designed to increase the rate at which the pre-rolling regime is traversed during final settling. Thus, the largest desired application of force, while traveling in one direction, would be moving the system from $-F_C$ to F_C, or the opposite. Recalling that the NIASA compensator attempts to introduce a first order linear convergence to the target locations, the rate at which force is applied by the nonlinear integrator could be approximated as a first order linear linear system with a time constant of τ_d. Figure 56 is provided to aid in visualizing this concept. The servo sampling rate should be smaller than the friction compensation time constant, τ_d, and is shown as such in figure 56. Since this is approximated as a first order process, the largest change in the value of the integrator will occur in the first sample. This value can be computed as

$$\Delta I_{max} = 2F_C \frac{\Delta t}{\tau_d}, \tag{8.1}$$

where Δt is the servo sample time and ΔI_{max} is the maximum amount that the integrator should change, in one sample, while traveling in the pre-rolling regime. Thus, by considering the purpose of the NIASA compensator, a good justification for limiting the rate at which

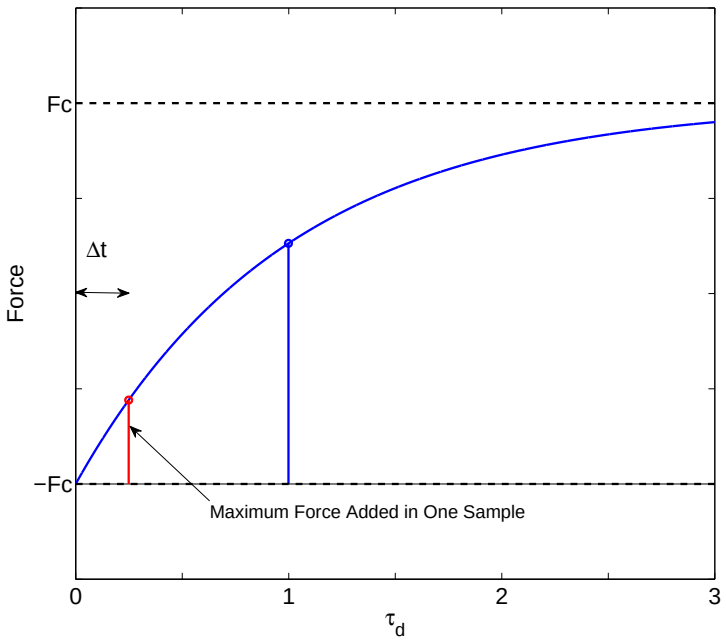

Figure 56: Since the NIASA compensator is designed to efficiently move the system throughout the pre-rolling regime, the furthest the compensator is designed to move the system is from one level of Coulomb friction to the opposite level. The application of force by the NIASA compensator is approximated as a first order process. From this model it is possible estimate the maximum rate of force application per time sample. To preserve stability outside of the pre-rolling regime, the rate at which the integrator of the NIASA compensator increases, per time sample, is limited to this worst case value.

the nonlinear integrator changes can be produced. In depth analysis of limiting the rate of integration is a subject of future research. However, limiting the rate of integration does not appear to have significant impact on settling performance but, it has been shown to make the system stable under disturbance where the compensator without rate limitation became unstable.

8.2 FREQUENCY DOMAIN ANALYSIS

Frequency domain analysis of a nonlinear system, such as a servo subject to friction, is not the best way to study such a system. However, frequency domain tools, such as loop transmissions, are often easily available and well understood by control system engineers. While these tools are not the final word on performance and stability when a system is not linear, they do provide some insight into system behavior and it would be useful to have some understanding of the outputs of such tools when applied to precision servos. Further, applying the loop transmission tool to the NIASA compensator helps to show how the compensator deceases servo settling time.

In this study, stepped sine system identification is conducted on the servo with the NIASA compensator enabled and also with it disabled. All of the tests are conducted sequentially and in the same location on the device travel to minimize uncontrolled factors. The PID controller used for comparison and also in conjunction with the NIASA compensator is what will be known as the high performance tuning. This tuning is used because it best showcases the limitations of linear control best practices. Two amplitudes of excitation are given to the system in separate tests, a large amplitude excitation, where the system leaves the pre-rolling regime, and a small amplitude excitation, where the system remains in the pre-rolling regime. For an in depth theoretical explanation of many of the features seen in the loop transmissions, it is suggested to read Helmick and Messner[35].

Figure 57 shows typical loop transmissions for high amplitude and low amplitude inputs. For the high amplitude input, which would probably be used in conventional tuning practices, it appears that the system has a frequency cross over at 315 Hz. However, when the low

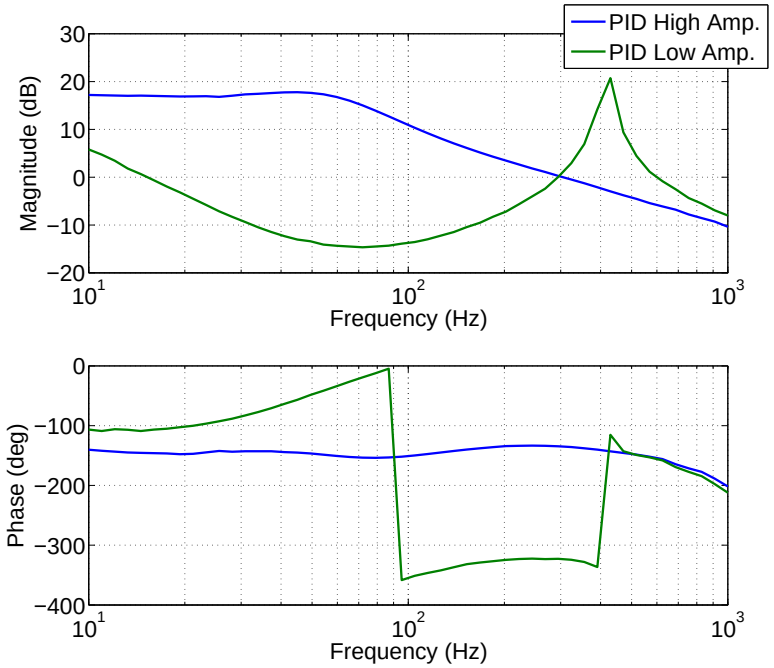

Figure 57: When comparing the loop transmissions for high amplitude inputs (motions that leave the pre-rolling regime) and low amplitude inputs (motions that remain in the pre-rolling regime), it is seen that the apparent bandwidth of the servo drops dramatically for low amplitude inputs. This is due to the effects of pre-rolling friction. Pre-rolling friction appears to have characteristics of a stiffness when viewed in the frequency domain.

amplitude excitation is applied, the frequency cross over is reduced to 15 Hz and a resonant peak appears near 400Hz. This is because, at low amplitude excitation, pre-rolling friction appears to have the effect similar to adding a stiff spring to the system. Although these two test cases do not provide a global description of the frictional process in of themselves, it is intuitive that a system will not settle as quickly as might be expected if the frequency cross over suddenly changed from 315 Hz to 15 Hz.

When the NIASA compensator was first tested with high amplitude excitation the system became unstable. Thus, integration rate limiting method described in the previous section was developed and used in the tests of the NIASA compensator. In the NIASA compensator loop transmission tests, the design time constant, τ_d, is set to $\frac{1}{100}$ s for all trials. In the first trial the conservative value of $\hat{\sigma} = 4$ N/µm is used and in the second trial the more aggressive value of $\hat{\sigma} = 8$ N/µm is used. It should be noted that the system has shown a mean value of $\sigma = 8.66$ N/µm and $\sigma = 8.73$ N/µm for the identification profile method and the step test method, respectively.

Figure 58 shows the system response to high and low amplitude excitation with the NIASA compensator enabled and $\hat{\sigma} = 4$ N/µm. One key characteristic is that the frequency cross over frequency of the low amplitude case has been increased to about 50 Hz as compared to the 15 Hz seen in figure 57. However, when doing a side by side comparison of the high amplitude inputs to the system with only PID control and PID with the NIASA compensator, as shown in figure 59 it is found that there is very little difference in the loop transmission response. This is desirable since the original, PID, high amplitude loop transmission is a good system response.

In a second NIASA compensator experiment, the friction model is changed so that $\hat{\sigma} = 8$ N/µm. The low amplitude loop transmission for this case is compared to that of the $\hat{\sigma} = 4$ N/µm case in figure 60. It is interesting to see that doubling the contact stiffness parameter used in the model adds about 6 dB to the response at low frequencies and the frequency crossover is increased to about 90 Hz. With this increase of low amplitude bandwidth the high amplitude loop transmission still remains very similar to the original PID controller, as shown in figure 61.

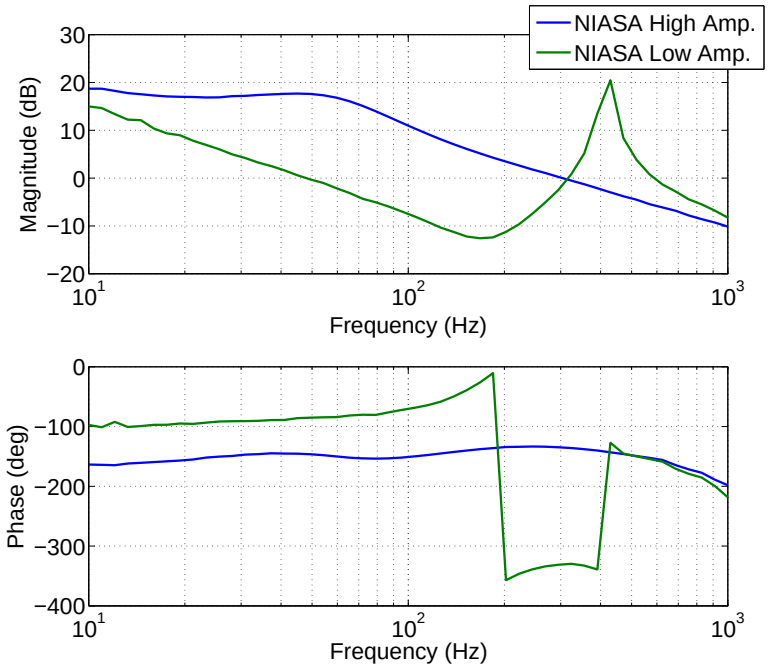

Figure 58: When using the NIASA compensator with $\hat{\sigma} = 4$ N/µm the frequency cross over at low amplitude excitation is increased to almost 50 Hz from 15 Hz using only PID control. Also, the desirable high amplitude loop transmission is relatively unchanged by the additional compensation.

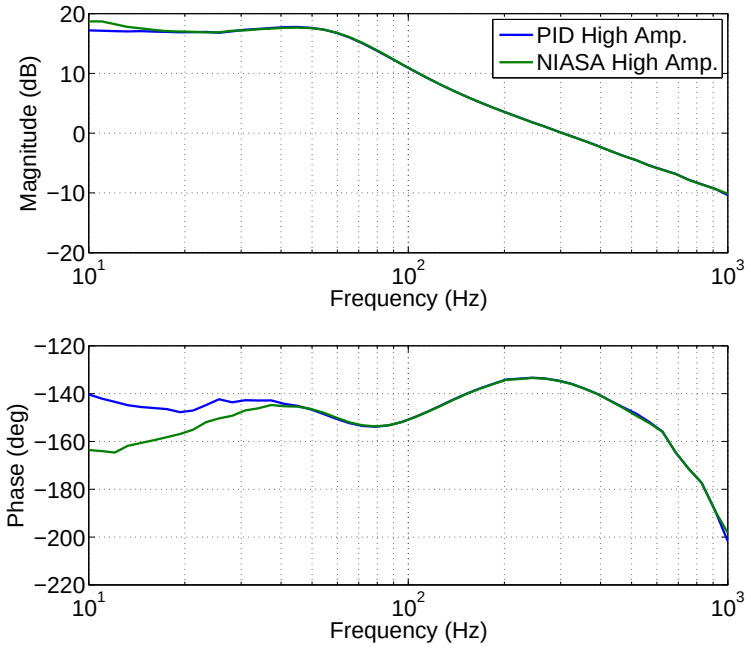

Figure 59: Conducting a side by side comparison of the loop transmission for high amplitude inputs shows that the PID controller and the PID controller with the NIASA compensator yield very similar results. There is some phase is lost at low frequency with the NIASA compensator but, this does not occur near the frequency cross over so it is not a concern.

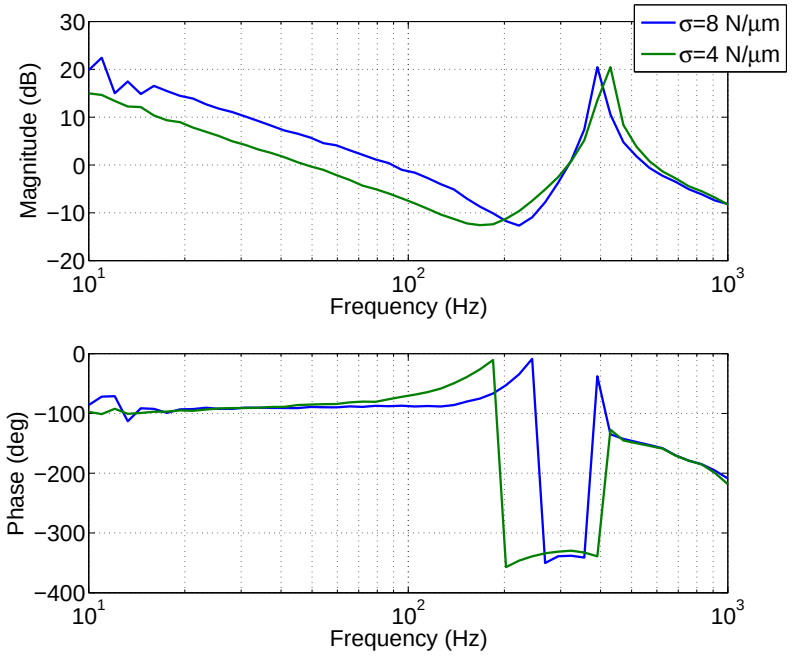

Figure 60: Doubling the value of $\hat{\sigma}$ to 8 N/µm adds approximately 6 dB of gain to the low frequency section of the loop transmission and the frequency cross over has been increased to approximately 90 Hz.

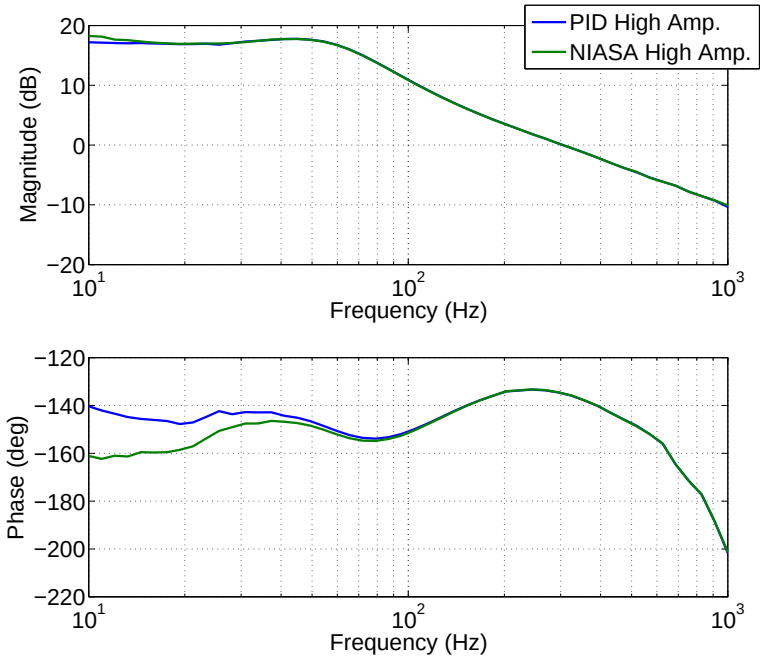

Figure 61: With $\hat{\sigma} = 8$ N/µm there is slightly more phase loss at low frequency than with $\hat{\sigma} = 4$ N/µm but, the phase margin at frequency cross over is still approximately the same as with only PID control.

Given the nature of these frequency domain tests, it was not possible to analyze displacement versus force data, as was done in the previous friction identification studies. Thus, it was not possible to determine the frictional parameters of the system in these studies. It is interesting to see that the NIASA compensator with $\hat{\sigma} = 4$ N/µm lead to a frequency cross over near 50 Hz and $\hat{\sigma} = 8$ N/µm lead to a frequency cross over near 90 Hz. Recall that the concept behind the NIASA compensator is to design a first-order-like system response, at least for low frequencies, where inertia is small. Assuming that the initial contact stiffness was near the observed mean value of either 8.66 N/µm or 8.73 N/µm and that the design time constant was $\frac{1}{100}$ s, using $\hat{\sigma} = 4$ N/µm lead to an effective time constant of $\frac{1}{50}$ s, about half as fast as the design time constant, while using a $\hat{\sigma}$ value that was probably half of the true σ value. Using $\hat{\sigma} = 8$ N/µm lead to an effective time constant of $\frac{1}{90}$ s, slightly less than the design time constant, and the value of $\hat{\sigma}$ was probably slightly less than the true value of σ. Thus, the frequency domain observations tend to agree with the proposed theory.

In summary, the NIASA compensator when used in conjunction with PID control has been shown to increase the bandwidth of control for small amplitude motion while preserving the desirable behavior already seen in loop transmission studies at large amplitude motion. By properly limiting the rate of the integral action in the NIASA compensator stability is possible for a wide variety of conditions. While these frequency domain observations are not the best way to view this nonlinear process, they do provide useful insight into how the NIASA compensator is able to reduce servo settling time.

9.0 POINT-TO-POINT EXPERIMENTS AND RESULTS

The rapid point-to-point motion experiments are divided into two distinct sets of experiments. The first set of experiments used a factory tuned PID controller without acceleration feed forward as a baseline for comparison. The second set of experiments used a high performance PID tuning constructed by an industry expert control system engineer with 10+ years of experience. In addition to this aggressive tuning, tuned acceleration feed forward was also implemented. The second case was designed to represent the limits of conventional linear control system best practices. In all tests settling to tolerances of +/- 3 nm to 100 nm will be studied. The +/- 3 nm minimum settling tolerance was selected because it is the listed amount of expected peak-to-peak in-position noise for a comparable servo.

9.1 FIRST EXPERIMENT

The first PID tuning should not be thought of as bad or flawed but, only as less aggressive. Depending on the design of the servo, task of the mechanism, and payload, such a tuning may actually be a high performance tuning. Figure 62 shows the loop transmission plot for this particular tuning. The move studied in this experiment is a 5 mm step with acceleration and deceleration rate of 1 m/s^2. In the center of the step a maximum velocity of approximately 70 mm/s is achieved and the motion profile takes 143 ms to complete. This test consists of 250 steps conducted on a 25 mm section of the device travel, (25 passes, 5 steps up, 5 steps back). In this parameterization of the NIASA compensator $\tau_D = \frac{1}{100}$s, $\sigma = 4$ N/µm, and F_C=0.6 N.

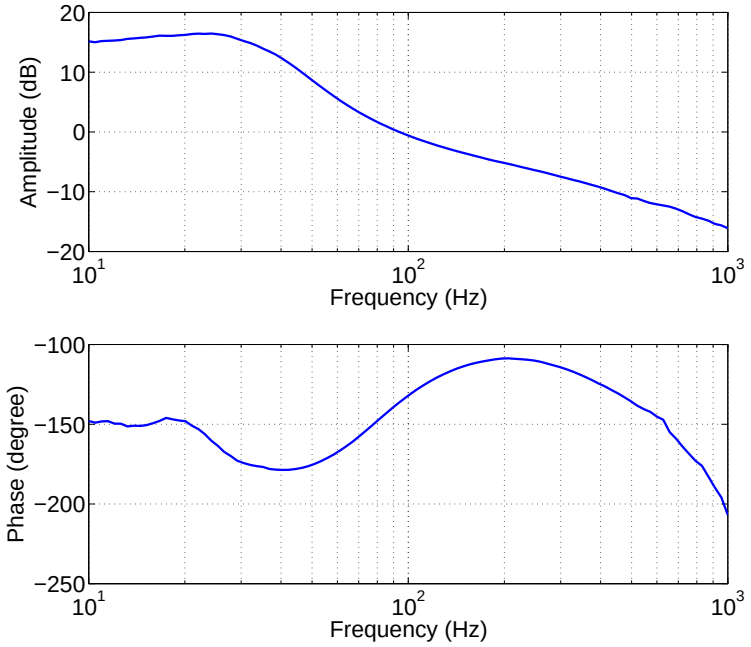

Figure 62: A loop transmission plot for the first PID controller shows the system to have a cross-over frequency near 100 Hz and a phase margin of about 45 degrees.

Figure 63 shows the mean time to settle to tolerances of +/- 3 nm to 100 nm for the first PID tuning, the same tuning combined with the NIASA compensator. Dashed lines have been added to figure 63 to indicate one standard deviation in settling time as computed across the data set. For different perspective on the improvements made by the NIASA compensator the percentage reduction of settling time for each respective tolerance is shown in figure 64. In figure 64 it is seen that, for this range of settling tolerances, this controller tuning, and this particular motion profile, servo settling time is reduced by between 80.5% and 87.4% for all settling tolerances.

Examining a few time series plots of the position error signal also proves interesting. Figure 65 shows six randomly selected time series of position error during settling for the PID controller. The common feature amongst each of these series is that the system appears to be significantly slowed down at each velocity reversal that occurs. This behavior is identical to that seen in figure 18 and exactly how pre-rolling friction reduces servo settling performance. With this performance baseline in consideration the NIASA settling compensator is now considered.

In examining time series of the position error figure 66 shows the algorithm settling the system in a manner that is very close to how the proposed theory suggested that it should. Apart from a slight undershoot, this settling profile looks very much like a first order decay. Not all settling responses proved to be as clean and ideal as that shown in figure 66 but, the algorithm proved to be surprisingly resilient and their time responses also prove to be interesting. Figure 67 shows the settling responses for the same sequence of randomly selected moves presented in figure 65. As this data suggests, it is not uncommon for overshoots and undershoots to occur during the settling process even with the NIASA compensator. However, compared to the original PID tuning, the NIASA compensator appears effective at quickly tuning the system around when velocity reversals occur in the final few hundred nanometers of settling.

This experiment shows that the NIASA compensator works quite well to reduce system settling time when used with this particular controller tuning. However, one can still make the valid argument that, by using stiffer control, the effects of pre-rolling friction can be minimized. While it is true to stiffer control will reduce pre-rolling effects, there is a practical

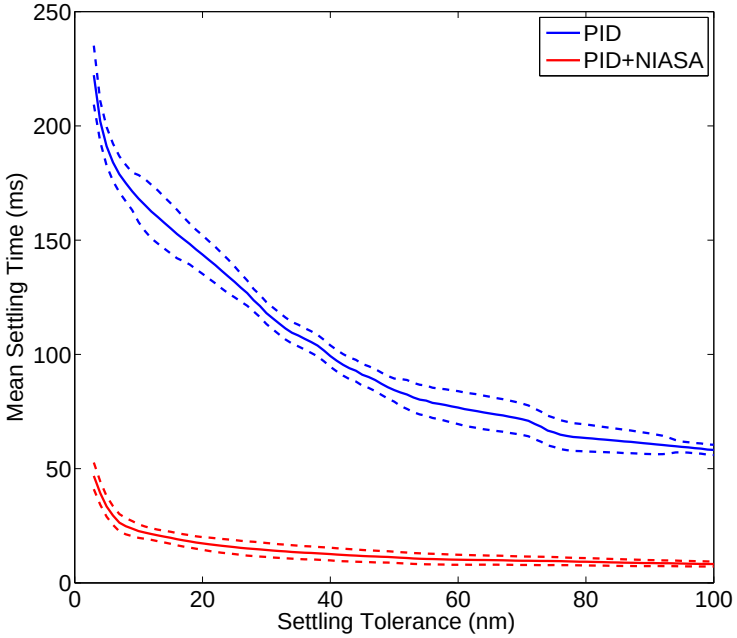

Figure 63: The solid line series show the mean settling time to given tolerances and the dashed lines show one standard deviation from the mean settling time. For this first controller parameterization, the NIASA compensator combined with the PID controller is able to settle the servo to all tolerances significantly faster than the PID controller by itself.

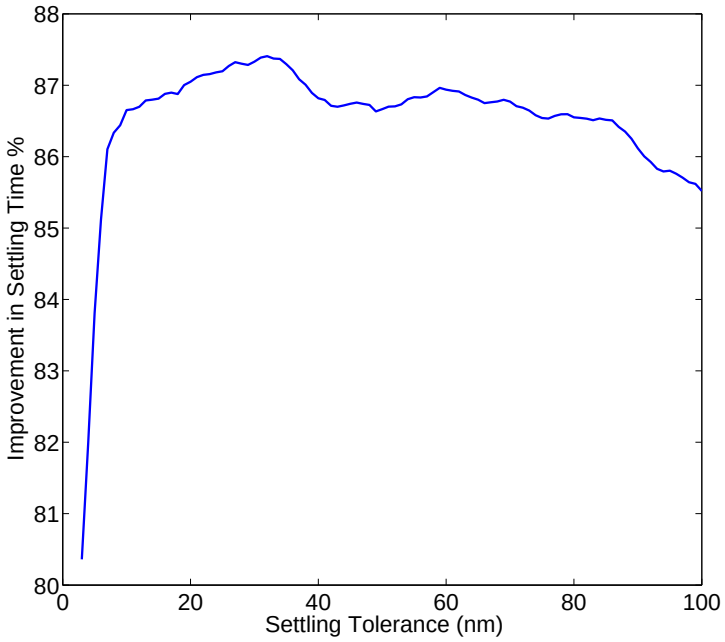

Figure 64: The data from figure 63 is processed to show the percentage reduction in settling time that is accomplished by using the NIASA compensator. Across all settling tolerances, the NIASA compensator is able to reduce the servo settling time by between 80.5% and 87.4%.

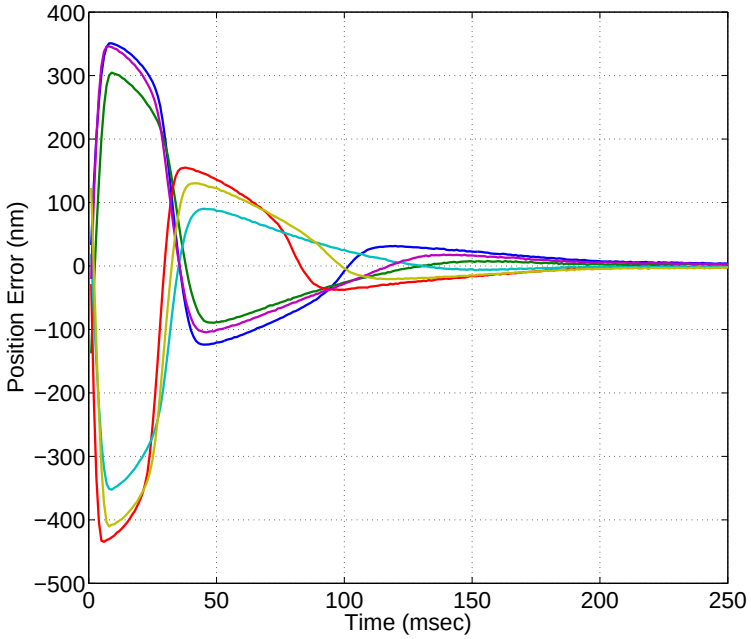

Figure 65: In examining some typical position error signals during servo settling, with only PID control, a common feature is the tendency for the system to be slowed down when a velocity reversal occurs. This is due to pre-rolling friction. The closer the velocity reversal is to the position set point, the more pronounced the slowing of the system due to pre-rolling effects. This is because the comparatively small integral gains needed to maintain stability over all conditions take time to build up the control system integrators when operating in the pre-rolling regime. This plot clearly shows the long settling tails when velocity reversals occur in the final 100 nm of settling.

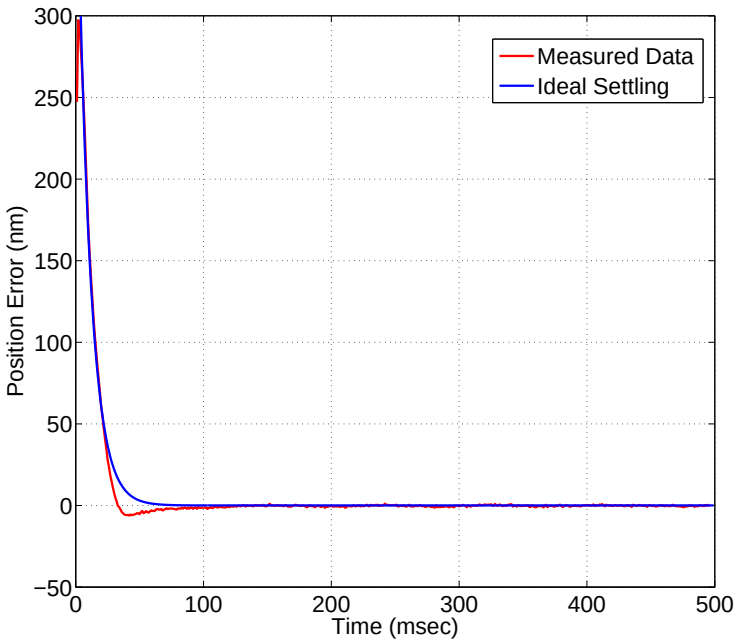

Figure 66: In this example a response from the PID controller combined with the NIASA compensator, the system response closely resembles the ideal, first order, system responses constructed in the previous simulations. For this test τ_D is set to $\frac{1}{100}$ s and the ideal settling profile is approximated as a first order system with a time constant of $\frac{1}{100}$ s. This would suggest that the modeled parameters for this case are very close to the true system parameters.

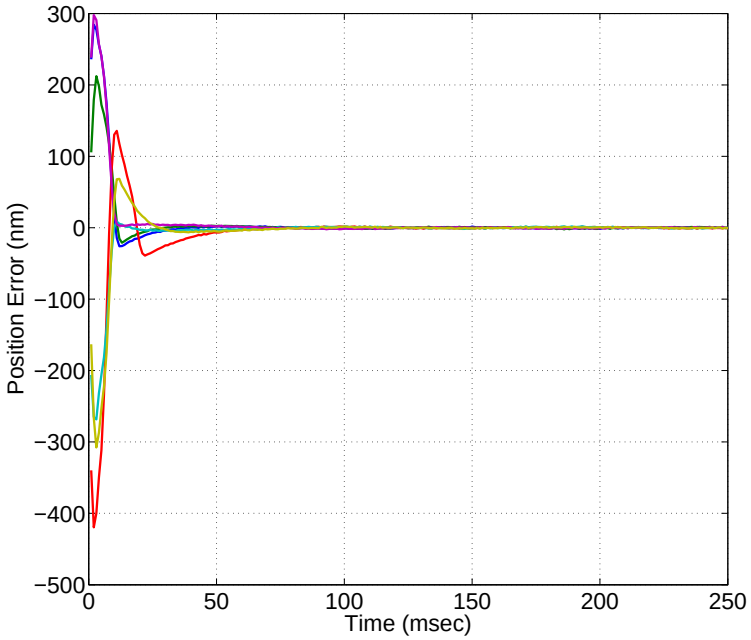

Figure 67: When observing a set of settling responses most are not as well behaved as the previous figure. However, the NIASA compensator works well to quickly reverse the direction of the system when an overshoot of the position reference occurs.

limit to the amount of stiffness which can be added to the system and it is still possible that pre-rolling effects will be significant even with the stiffest feasible controller. A second valid argument is, properly tuned feed forward of the acceleration of the moving mass should leave the system much closer to the target location when the motion profile ends. In fact, according to experienced control system engineers, the majority of the control effort supplied to the system should come from feed forward methods. However, there is always some measure of uncertainty within the system and some small changes are continuously occurring within the system. Thus, consistent and reliable nanometer precision is not likely to be possible using only feed forward methods. Taking a realistic perspective of the point-to-point motion task, it would be very nice for the system to be within a few hundred nanometers or less of the final target location but, this region is also exactly where pre-rolling effects tend to dominate the system response. Thus, final servo settling, done by conventional PID methods could still suffer from the same problems. This discussion raises a very interesting question: Could a high bandwidth control combined with properly tuned feed forward, now coupled with a specialized settling algorithm, be used to achieve even better point-to-point performance?

9.2 SECOND EXPERIMENT

In contrast to the first PID tuning, this high performance tuning should not be thought of as the best tuning for all devices in all situations. It just happens that this was the best tuning that could be done on a very simple, yet well designed servo, with no payload. Figure 68 shows the loop transmission plot for this particular tuning. The move studied in this experiment is also a 5 mm step but, with acceleration and deceleration rate of 10 m/s^2 (the maximum rate of acceleration of this device). In the center of the step a maximum velocity of approximately 223.5 mm/s is achieved and the motion profile takes 46 ms to complete. This test consists of 500 steps conducted on a 25 mm section of the device travel, (50 passes, 5 steps up, 5 steps back). In this parameterization of the NIASA compensator $\tau_D = \frac{1}{100}$s, $\sigma = 4$ N/µm, and F_C=0.6 N.

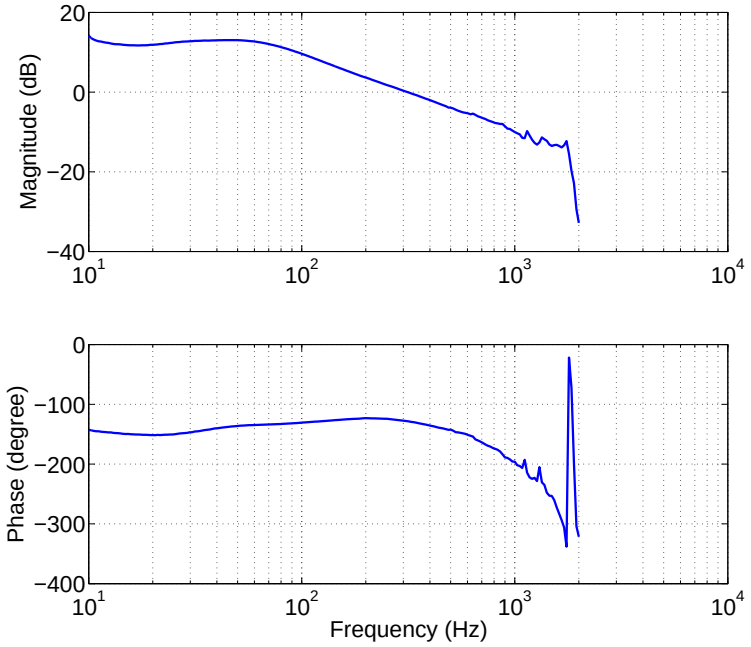

Figure 68: A loop transmission plot for the second PID controller shows the system to have a cross-over frequency near 315 Hz and a phase margin of about 50 degrees.

Figure 69 shows the mean time to settle to tolerances of +/- 3 nm to +/-100 nm for the high performance PID controller with feed forward and also this same tuning with the addition of the NIASA compensator. Dashed lines have been added to figure 69 to indicate one standard deviation in settling time as computed across the data set. For different perspective on the improvements made by the NIASA compensator the percentage reduction of settling time for each respective tolerance is shown in figure 70. In figure 70 it is seen that, for this range of settling tolerances, this controller tuning, and this particular motion profile, servo settling time is reduced by between 50.5% and 73.0% for all settling tolerances.

Figure 71 shows the position error during settling for the high performance PID controller for six randomly selected step moves. Figure 72 zooms in on the final 100 nm of figure 71 and is provided to better present the settling process. Using figures 71 and 72 as a baseline for comparison, figure 73 shows the settling of the same six moves from the sequence with the NIASA compensator and figure 74 zooms in on the final 100 nm of settling. In examining these figures, it is clear that the high performance PID controller settles better than the first PID controller but, it still suffers from the same pre-rolling friction issues. This is seen as the still significantly slowed down when velocity reversals occur during settling. In contrast, the NIASA compensator responses were able to reduce these counter productive velocity reversals and draw the system into the target position much quicker and in a fashion similar to the theoretical prediction. Thus, it appears that the NIASA settling compensator has the ability to make improvements to even a very high performance PID controller with properly tuned feed forward compensation.

9.3 IN-POSITION NOISE

There was some concern that the adjustment of system gains done with the NIASA compensator could increase the in-position noise of the system. Measures of transitioning out of the settling compensation to a separate in-position compensation were even considered. However, at least for the case of this servo, there was no significant difference in in-position noise with or without the settling compensation be active. To confirm this observation the

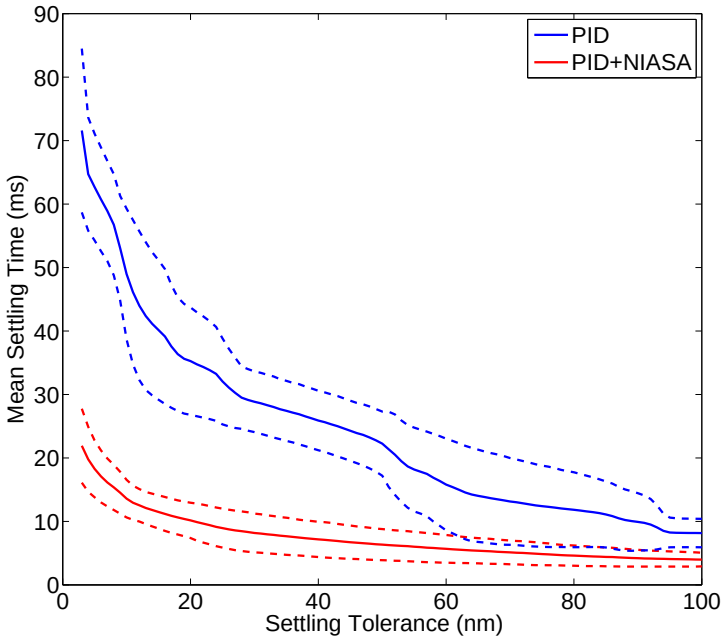

Figure 69: The solid line series show the mean settling time to given tolerances and the dashed lines show one standard deviation from the mean settling time. For this first controller parameterization, the NIASA compensator combined with the PID controller is able to settle the servo to all tolerances significantly faster than the PID controller by itself.

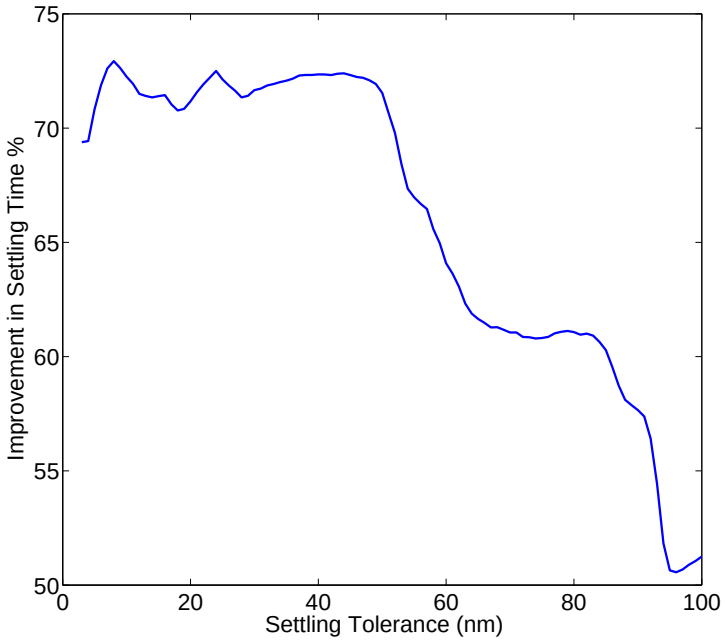

Figure 70: The data from figure 63 is processed to show the percentage reduction in settling time that is accomplished by using the NIASA compensator. Across all settling tolerances, the NIASA compensator is able to reduce the servo settling time by between 50.5% and 73.0%.

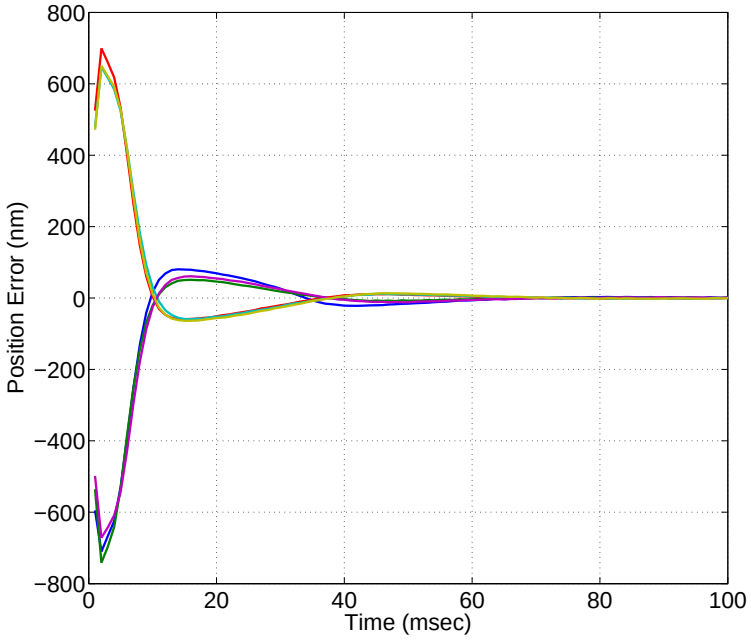

Figure 71: While this controller performs significantly better than the first tuning, the velocity reversals, that occur during settling, still show slowing of the system.

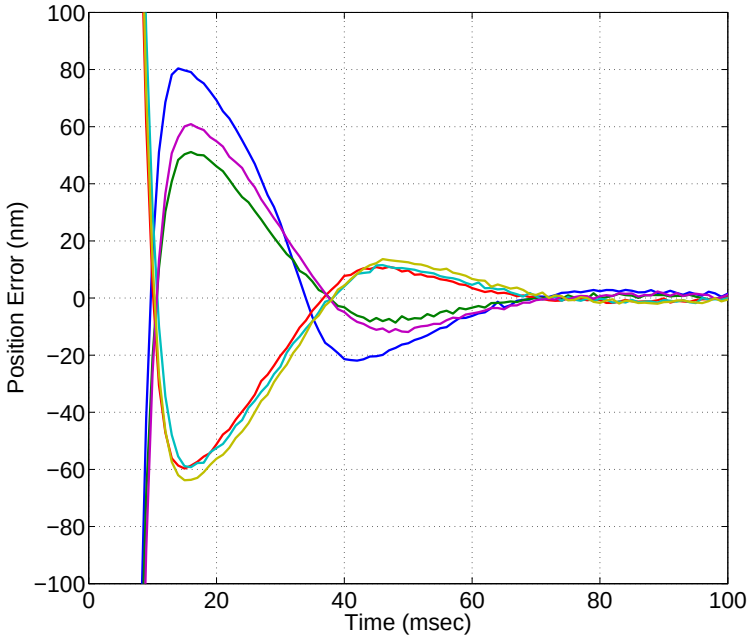

Figure 72: Zooming in on the final 100 nm of settling from figure 71 better illustrates the typical settling behavior of the high performance PID tuning.

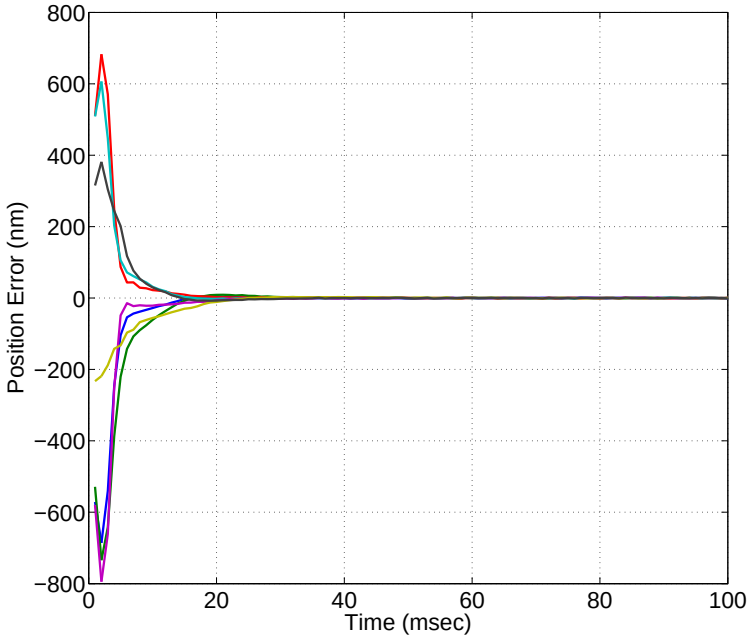

Figure 73: As compared to figure 71 the servo appears to take a more direct path to the target location when the NIASA compensator is added to the control system.

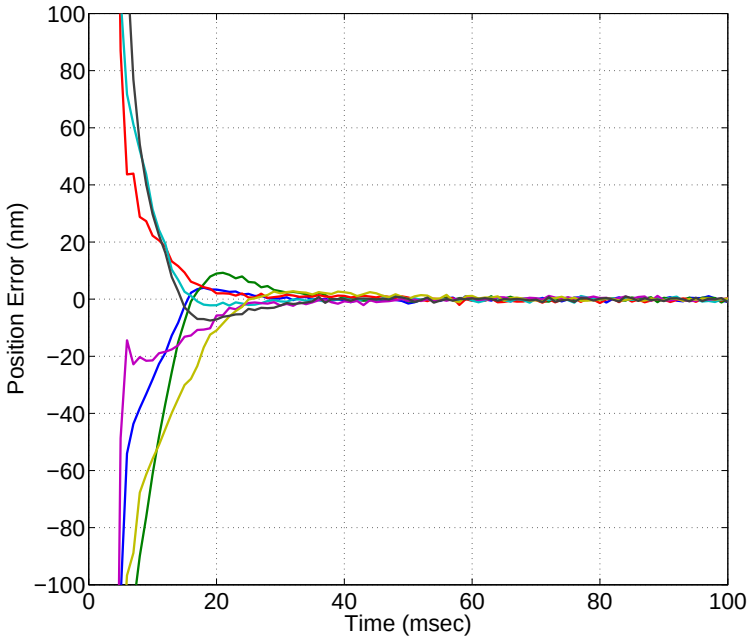

Figure 74: Focusing on the final 100 nm of servo settling shows that the drawn out velocity reversals that occurred with PID control have been nearly eliminated by the NIASA compensator. This leads to significantly increased servo settling performance.

Table 3: Analysis of the root mean square in-position error shows that all of the controller configurations have very similar in-position characteristics.

Controller	In-Position Noise (nm_{rms})
Regular PID	0.48
Regular PID + NIASA	0.50
High Performance PID	0.49
High Performance PID + NIASA	0.48

root mean square of the position error 500 ms after settling to +/- 3 nm was analyzed for all of the steps in each test. The results shown in table 3 show that there is no significant change in the in-position characteristics of the servo with or without the settling compensation being active.

9.4 SMALL STEP EXPERIMENTS

At the beginning of this effort, the targeted application for this control algorithm was a step motion of several millimeters with a settling tolerance of a few nanometers. Recalling the previous discussion of how some compensations methods are only useful in specific situations, to answer the question of when the NIASA compensator is useful additional tests are conducted. In the first set of tests, where the 5 mm move is used, the servo moves well outside the pre-rolling regime for the gross motion of the step. As this occurs, it is safe to assume that the system experiences fully developed rolling friction before the settling phase. Thus, testing larger displacement step motions is not interesting because they would involve nearly the same frictional conditions as the 5 mm step. However, testing of smaller displacement steps, motions that just leave the pre-rolling regime or possibly remain entirely in the pre-rolling regime, would constitute a frictional scenario that has not yet been experimentally explored.

The small step experiments consist of 500 instances of 5 µm steps and 500 instances of 50 nm steps. The tests will be performed with the standard PID controller and the high performance PID controller for cases when the NIASA compensator is active and when the NIASA compensator is disabled. These step tests will use a similar format as the previous test, five steps in one direction followed by five steps in the returning direction. The 5 µm steps use an acceleration and deceleration rate of 100 mm/s^2, which leads to a maximum commanded velocity of approximately 698 µm/s and a motion profile lasting 15 ms. The 50 nm steps use an acceleration and deceleration rate of 1 mm/s^2. This yields a maximum commanded velocity of 6.98 µm/s and a motion profile lasting 15 ms.

The 5 µm step represents a case where the gross motion of the step may take the system just outside the pre-rolling regime and into nearly fully developed rolling friction. In this experiment the mean time to settle to ±3 nm to ± 50 nm is calculated. Figures 75 and 76 show the settling performance of the system for the standard PID controller and the high performance controller respectively. As seen in figures 75 and 76, the NIASA compensator is effective in reducing servo settling times for step motions that are just outside the pre-rolling regime, when combined with either PID controller.

The 50 nm step test is designed to show a case where the step motion may not exit the pre-rolling regime. Since the magnitude of the step motion is only 50 nm, settling to tolerances of ±3 nm to ± 10 nm is calculated. Figures 77 and 78 show the settling performance of the system for the standard PID controller and the high performance controller respectively. Once again, the NIASA compensator is seen to be effective in reducing servo settling time when combined with either PID controller. In figure 78 a 0 ms settling time is listed for the NIASA compensator, for tolerances between ± 6 nm and ± 10 nm. This is because the NIASA compensator was able to keep the system within ± 6 nm before the motion profile ends. This interesting result leads to examination of the temporal results of the 50 nm step test to determine how such a result is achieved. Figures 79 and 80 show some example time series from the tests using the standard PID controller and the high performance PID controller respectively. Figures 81 and 82 show example time responses from the same respective controllers combined with the NIASA compensator. As compared to either PID controller, the NIASA compensator appears to significantly reduce the position error when

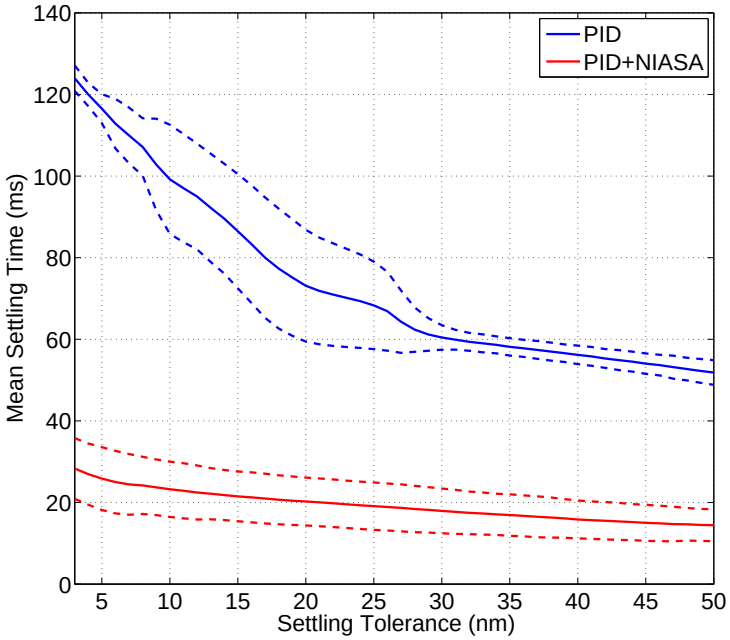

Figure 75: The settling performance for 500 instances of 5 µm steps, with the standard PID controller (frequency cross over of 100 Hz and phase margin of 45 degrees), is shown in this figure. The solid series shows the mean settling time to the given tolerance and the dashed series shows one standard deviation from the mean value. Across all settling tolerances, the NIASA compensator combined with the PID controller demonstrated the ability to reduce servo settling time, as compared to the PID controller by itself.

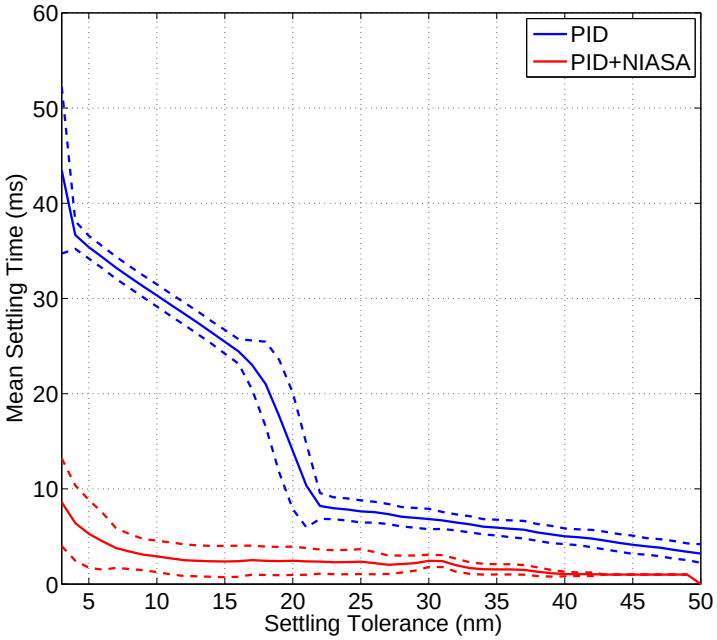

Figure 76: The results of using the high performance PID controller (frequency cross over of 315 Hz and phase margin of 51 degrees), for 500 instances of 5 µm steps, is presented in this figure. The solid series shows the mean settling time to the given tolerance and the dashed series shows one standard deviation from the mean value. Across all settling tolerances, the NIASA compensator combined with the PID controller demonstrated the ability to reduce servo settling time, as compared to the PID controller by itself.

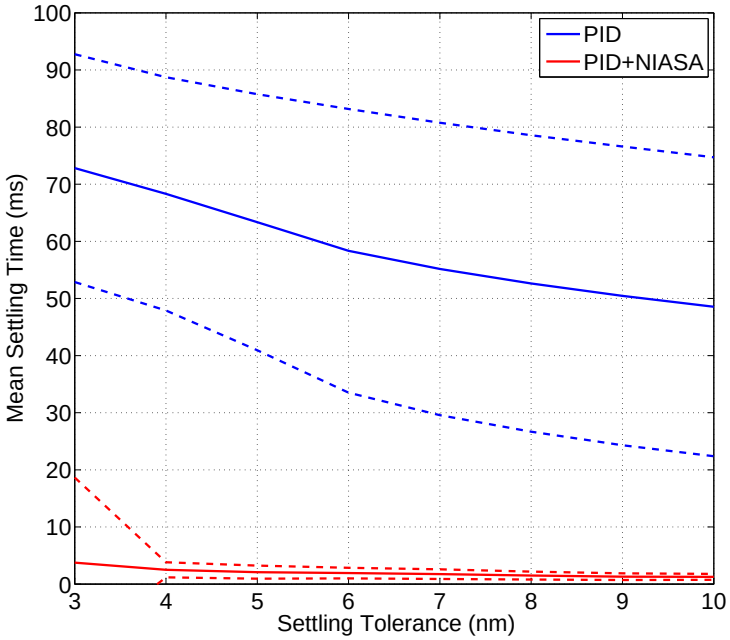

Figure 77: The settling performance for 500 instances of 50 nm steps, with the standard PID controller (frequency cross over of 100 Hz and phase margin of 45 degrees), is shown in this figure. The solid series shows the mean settling time to the given tolerance and the dashed series shows one standard deviation from the mean value. Across all settling tolerances, the NIASA compensator combined with the PID controller demonstrated the ability to reduce servo settling time, as compared to the PID controller by itself.

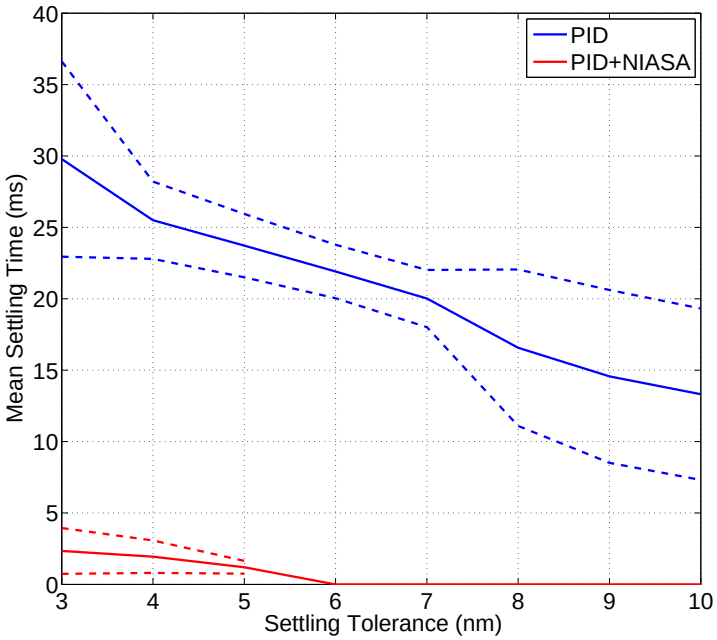

Figure 78: The results of using the high performance PID controller (frequency cross over of 315 Hz and phase margin of 51 degrees), for 500 instances of 50 nm steps, is presented in this figure. The solid series shows the mean settling time to the given tolerance and the dashed series shows one standard deviation from the mean value. For data points where the settling time is stated as 0 ms, the compensator was able to keep the servo within that respective tolerance before the motion profile ends. Thus, the calculated settling time to that given tolerance is 0 ms. Across all settling tolerances, the NIASA compensator combined with the PID controller demonstrated the ability to reduce servo settling time, as compared to the PID controller by itself.

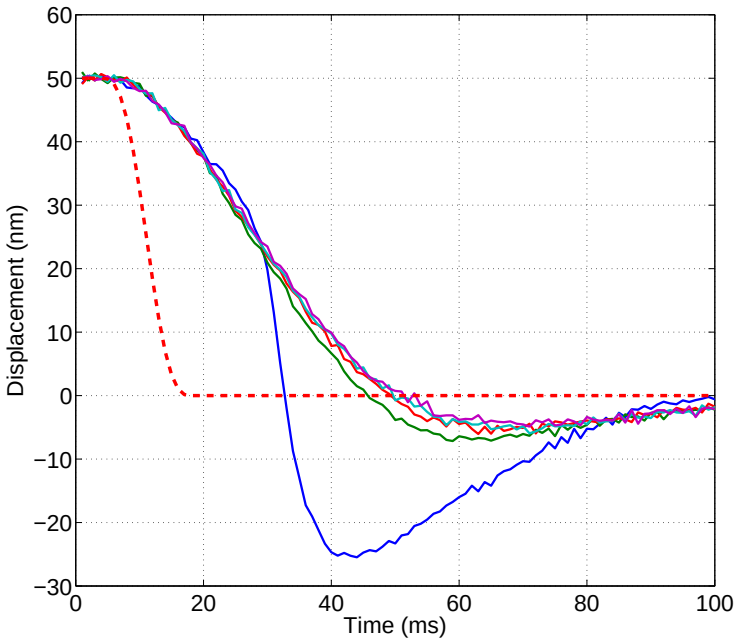

Figure 79: In this figure the dashed red series shows the position reference signal and the solid series show the measured position data. When examining a few examples of the time series of the standard PID controller to a 50 nm step, it appears that there is a delay in the systems response to the motion command. This is followed by an overshoot of the target location and a slow convergence to the desired position reference.

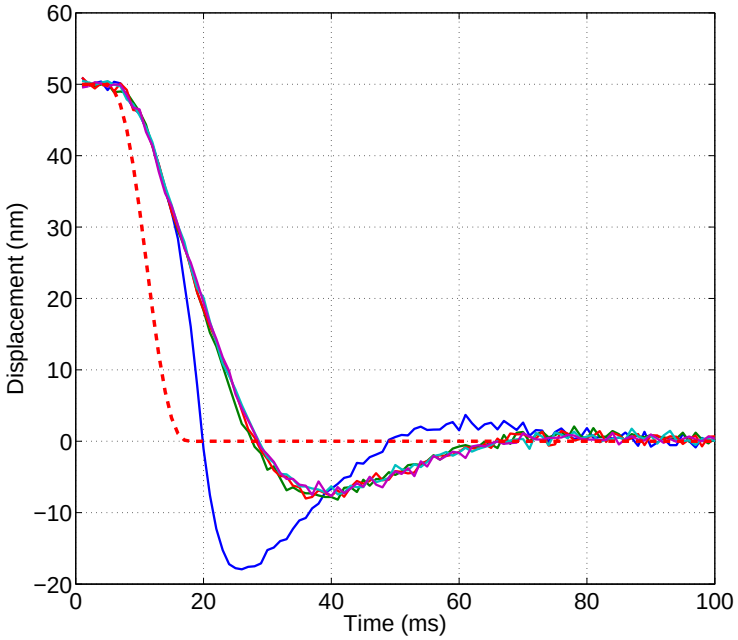

Figure 80: In this figure the dashed red series shows the position reference signal and the solid series show the measured position data. As compared to the standard PID controller presented in figure 79, the high performance PID controller improves upon some of the negative features of the previous plot. The delay in response has been reduced, the overshoot is comparable, and the convergence to the desired location has been expedited. However, even though these features have been reduced, they are still present in the servo response.

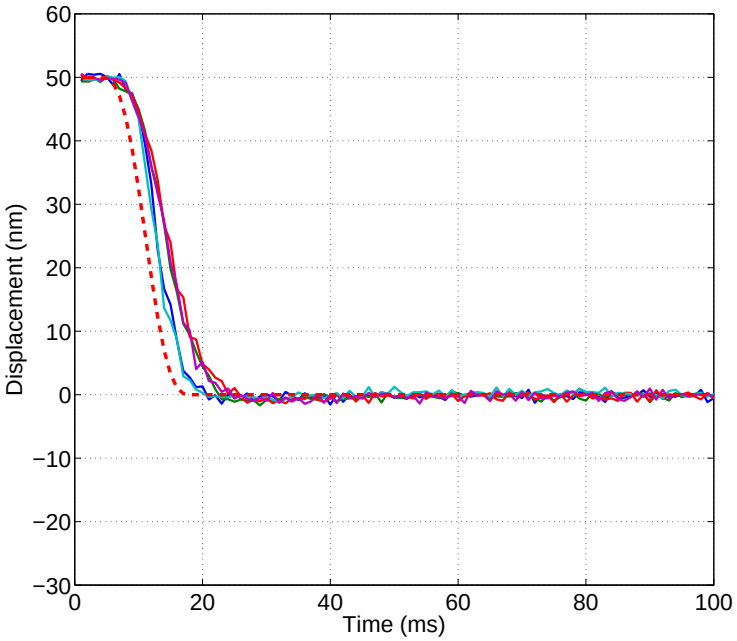

Figure 81: In this figure the dashed red series shows the position reference signal and the solid series show the measured position data. In the case of the standard PID controller combined with the NIASA compensator tracking of the 50 nm step in reference has been improved. The delay in system response has been reduced and overshoot of the target location has also been reduced.

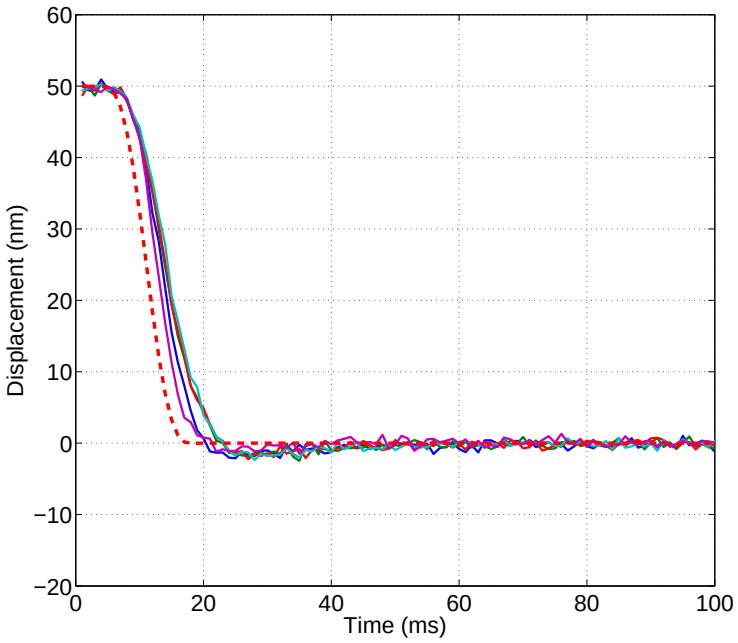

Figure 82: In this figure the dashed red series shows the position reference signal and the solid series show the measured position data. When the NIASA compensator is used in conjunction with the high performance PID controller, the servo response is most similar to that seen in the previous figure. Once again, tracking of the step in reference is improve, compared to only PID control, and servo settling occurs much faster.

tracking the gross motion of the step. This interesting result suggests that future efforts should be made in exploring the utility of this methods in servo tracking applications and that future efforts could evaluate the NIASA compensator as a global method of controlling systems subject to friction.

10.0 CONCLUSIONS

The proposed compensator worked very well to increase ultra precision servo settling performance. In some cases, this method was able to reduce servo mean settling time by up to 87.4%. This effort succeeded in constructing a linear model of the servo mechanism and identifying where this approximation tends to break down. Through a series of small displacement tests and identification procedures, pre-rolling friction is characterized for the servo mechanism. The identified characteristics of pre-rolling friction are found to generalize to observations from real point-to-point motion data. Thus, the potential problems, which occur during system settling, are captured in the identified pre-rolling friction models.

A feedback control algorithm, called the Nonlinear Integral Action Settling Algorithm (NIASA), is designed based on the identified friction model. The NIASA compensator is developed to be robust to parametric uncertainty in the pre-rolling friction process, as compared to other friction compensation methods which rely heavily on model accuracy or are only analyzed in idealized cases. The NIASA compensator is designed to be used in conjunction with conventional control system best practices of properly tuned feed forward control and PID feedback control.

Some basic frequency domain analysis of the behavior of the NIASA compensator is presented. Although this is not the best way to considered a nonlinear system, such as a servo subject to pre-rolling friction, frequency domain analysis provides some perspective how the NIASA compensator functions to those familiar with linear systems tools. This analysis eventually states that the NIASA compensator amounts to a method of increasing low frequency gains for small motions, where pre-rolling friction dominates system response, and for large motion, where the linear components of the system dominate, the desirable frequency domain characteristics are preserved.

In a case study with a reasonably tuned PID controller settling times to $\pm$ 3 to $\pm$ 100 nm, servo settling times are reduced by between 80.5% and 87.4%. As a secondary case study, a high performance PID controller was tuned by an experienced control system engineer to represent the practical limits of linear control methods. When the NIASA compensator is used, servo settling time is still reduced by between 50.5% and 73.0%. Although the NIASA compensator was design to increase settling performance for relatively large point-to-point motions, similar positive results are achieved when the method is applied to smaller step motions. Further, the algorithm appears enhance the ability of the servo mechanism to track nanometer scale point-to-point motion profiles. Thus, experimental data suggests that the NIASA compensator is a viable solution for dealing with friction in ultra precision point-to-point motion for a wide variety of step size. Additionally, the NIASA compensator may prove to be a feasible method of increasing tracking performance of nanometer scale motion profiles.

11.0 FUTURE WORK

With the successes of this work numerous interesting questions are raised. There was not enough time to investigate many of these questions and some where outside of the scope of this effort; to the point where it would be inappropriate to address them in this work. Thus, a brief discussion of potential future work is provided.

This work successfully characterized and improved the point-to-point motion capabilities of one precision servo. For further validation of the ability to increase servo settling performance, it would be useful to conduct the same studies on other precision servo mechanisms. In this study, the precision servo was a linear stage (as in X-axis), there seems to be no reason such methods could not be used on rotational servos. Such studies are proposed for future work.

As another extension to this work, it would be interesting to evaluate the utility of this algorithm in more complex servo configurations. An example of an interesting servo configuration would be a Cartesian X-Y table with a secondary position measurement. The secondary position measurement may come from a sensor such as a laser interferometer. In such a case, there will never be perfect alignment between the two axis of the table and between the X-Y table and the position sensors. Further, neither axis will ever be perfectly straight. Thus, commanding a step on one axis will necessitate a small motion in the other axis to achieve absolute positioning accuracy. It would be interesting to investigate the application of the NIASA compensator to both axes of such a system.

Fortunately, the pre-rolling behavior of this system seemed to be captured rather well by the Dahl model. It is known from the author's own experience and from most efforts related to the GMS model that, not all pre-rolling transition curves can be so accurately captured by the Dahl model. This raises a number of questions. From experience, it appears

that pre-rolling transition curves which are best captured by the GMS model tend to have very sharp slopes near velocity reversal and much more shallow slopes that extend tens of micrometers from velocity reversal. This is the same general behavior as seen in the Dahl model but, a single parameterization of the Dahl model does not capture this behavior with the same measure of accuracy. With transition curves that are well described by the Dahl model there seems to be a point in the settling process where the system response clearly becomes dominated by pre-rolling friction. One question is: For transition curves that are best described by the GMS model, is there a clear point where pre-rolling friction dominates the system response? Also, for these drawn out transition curves which change over several tens of micrometers, how much of this behavior actually influences servo characteristics? Is it only the steepest pre-rolling transition curve sections or is the shape of the entire transition curve important? The $\frac{dF}{dx}$ term of the Dahl model defines the non-linear integration. Could the slope of a section of the GMS model perform similarly? Answers to question such as these could be investigated with further studies on other precision servos with different pre-rolling behavior.

The identification procedure only lead to two numbers, σ and F_C. In unstructured experimentation with the tuning the exact value does not seem to matter very much. It appears quite likely that substantial performance could still be achieve if these number varied by as much as +/- 50%. Thus, the identification procedure seems to involve a large amount of unnecessary effort. How much less identification effort is needed? It seems possible that a large portion of the identification process could be automated, could it be automated to the extent of: a simple selection of bearing or servo model number leads to a good set of settling compensation parameters? Providing answers to these questions is no small task but, this would be neccesary for a full commercialization of the proposed method.

While the NIASA compensator was designed specifically to increase ultra precision, point-to-point settling performance, the frequency domain analysis suggests that the compensator increases the controller bandwidth at low amplitude motion as compared to a conventional linear PID controller. Thus, investigation of the performance of the algorithm in tracking sub-micrometer scale profiles or even large profiles with sub-micrometer features is a topic of future research.

As previously mentioned, the servo studied in this effort had linear crossed roller bearings with an anti-creep mechanism. Anti-creep mechanisms are an available option from most major bearing manufacturers. This mechanism is not supposed to interfere with bearing operation but, some force must be transmitted through the mechanism if it keeps the roller cage from creeping. Studying the effects of this type of mechanism on precision motion equipment could be a topic of future work.

In section 8.1.2 a rationale and method of limiting the rate at which the system integrator grows is proposed. This method is basic but, seems to work quite well. However, a more elegant solution to this concern may be possible.

The proposed application of the NIASA compensator is toward machine tool type of servos. However, it is quite possible that this algorithm or similar methodology could prove useful in other applications. For example, hard disk drive read heads must move rapidly between tracks and they are effected by bearing friction. More generally, this methodology could be useful in controlling other types of systems with hysteresis where the hysteresis shows some measure of parametric uncertainty.

APPENDIX A

GMS FIT

This appendix is included because the process of fitting of GMS models to friction data and explanation of the resulting fit is a topic that may reader may not be familiar with. At the begining of this effort was anticipated that use of the GMS model would be very important to this work. However, the GMS model did not play a key role in this effort. Thus, discussion of GMS model fitting is religated to an appendix chapter.

Fitting a GMS model to friction data is done in a similar fashion to fitting a Dahl model to friction data. In this work a similar genetic algorithm is used to construct the model fit. The difference between the GMS genetic alogorthm and the Dahl model genetic algorithm is that the GMS genetic algorithm adjusts more parameters. The GMS model is stated as

$$\frac{dz}{dt} = v\left(1 - \text{sgn}\left(\frac{F_h(z)}{s(v)}\right)\left|\frac{F_h(z)}{s(v)}\right|^n\right) \tag{A.1}$$

$$F_r = F_h(z) + \sigma_1\frac{dz}{dt} + \sigma_2 v, \tag{A.2}$$

where z is a vector of hidden frictional states, $F_h(z)$ is the hysteresis function, n is a shape factor, v is the relative velocity between the surfaces, and the function $s(v)$ accounts for the Stribeck effect. Since the hysteresis function is likely to contain multiple Maxwell slip elements, the value of the hysteresis function can be written as

$$F_h(z) = \sum_{i=1}^{N} F_i \tag{A.3}$$

where N is the total number of Maxwell slip elements and F_i is the force output of each respective element. The force output of each respective element can be summarized as

$$\begin{aligned} F_i &= k_i z_i \quad when \quad -F_i^{sat} < k_i z_i < F_i^{sat} \\ F_i &= -F_i^{sat} \quad when \quad -F_i^{sat} \geq k_i z_i \\ F_i &= F_i^{sat} \quad when \quad k_i z_i \geq F_i^{sat}, \end{aligned} \tag{A.4}$$

where k_i is the stiffness parameter for each element and z_i is the hidden friction state of each element.

Thus, the parameters to be identified by the genetic algorithm are one stiffness parameter, k_i, for each element, one saturation level, F_i^{sat}, for each element, one micro-damping coefficient, and a Stribeck function. For this work, the micro-damping coefficient was insignificant and not included. The Stribeck function was also insignficant and is replaced by the level of Coulomb friction, F_C. The level of Coulomb friction is defined by

$$F_C = \sum_{i=1}^{N} F_i^{sat}. \tag{A.5}$$

Inuitively, this make sense because one would expect a system be acted upon by friction at the Coulomb level when fully developed rolling occurs and friction has saturated to a nearly constant level. Figure 83 shows an example of the fit of an eight element GMS model to measured friction data. Table 4 shows the specific parameters used to construct this fit.

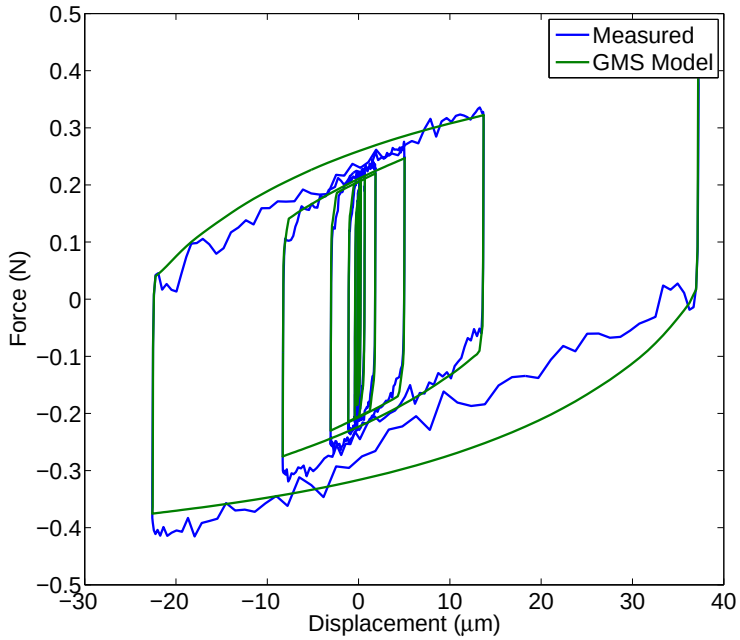

Figure 83: The extra degrees of freedom (N=8), provided by the GMS model, allow for the most accurate approximation of the measured data, compared to the other models which have been presented.

Table 4: This table lists the values of the parameters used to construct the hysteresis function. Note that the sum of all F_i^{sat} values equals 0.4302 N.

Element number	1	2	3	4	5	6	7	8
k_i (N/µm)	6.5408	1.0210	1.6261	0.4352	1.5016	0.6951	0.0605	0.0162
F_i^{sat} (N)	0.0036	0.0156	0.0290	0.0165	0.0675	0.0546	0.0203	0.2230

APPENDIX B

GENETIC ALGORITHM

%This section is presented in a format very close to MATLAB code.

%The % symbol indicates a line that has been commented out.

function [om1, Fc, mse_f]=Dahl_ID_1(v, force_dat, num_genes, new_gen,...

...new_pop, num_iter, par_range)

% v → input velocity data obtained from differentiating position data

% force_dat → input friction force data

% num_genes → number of organisms in each generation

% new_gen → number of fit organisms saved from each generation

% new_pop → number of new organisms to be bread in each generation

% num_iter → number of generations in optimization

% par_range → vector of initial guesses of parameters to be optimized values

% num_pars → number of parameters to be optimized

% min_f → minimum value of measured friction force data

% max_f → maximum value of measured friction force data

% dna → matrix containing the all organisms of a generation

% om1 → genes for initial contact stiffness parameter

% Fc → genes for level of Coulomb friction parameter

% dz → change in modeled friction state per time step

```
% z → modeled friction state
% F → modeled force of friction
% mse → mean square error between modeled and measured force of friction
% breednum → used in randomly selecting from the fittest organisms to breed
% g1 and g2 → selected organisms for breeding
% g1g2 → weight used in crossing genes during breeding
% mut → gene after breeding and mutation
% new_or → new organism after breeding and mutation



num_pars=length(par_range);
min_f=min(force_dat);
max_f=max(force_dat);
%The measured friction force data does not always center about zero force for a variety
% of reasons. This friction model does center about zero force so it helps the model fit
% to center the data.
force_dat=force_dat-(max_f+min_f)/2;

%Initialize random genes. For this problem the parameters are all positive so the abs()
% statement assures that the random genes contain only positive parameters.
for i=1:num_genes
    for j=1:num_pars
        dna(i,j)=abs(par_range(j)+par_range(j)*randn(1));
    end
end

for iter=1:num_iter
    %Evaluate performance
    for i=1:num_genes
        om1(i)=dna(i,1);
```

```
Fc(i)=dna(i,2);

%Creating a vector for the modeled force of friction increases processing speed.
F=zeros(1,length(v));

%This implementation starts the friction state at zero. It could be started at any value.
z=0;

%This loop simulates the friction dynamics with the given parameters.
for k=2:length(v)

dz=v(k)-om1(i)*(abs(v(k))/(Fc(i)))*z;
z=z+dz/1000; % dz is divided by 1000 because data are sampled at 1000Hz
F(k)=om1(i)*z;

%This section prevents the modeled force of friction from becoming greater than
% the magnitude of the Coulomb level of friction because of numerical issues.
% This is very important in this discrete time implementation because this problem
% can occur and leads to numerical instability.
if F(k) ≥ 1*Fc(i)
F(k)=Fc(i);
elseif F(k) ≤ -1*Fc(i)
F(k)=-Fc(i);
end
end

%The mean square error between the modeled force of friction and measured force
% of is computed and used to define the fitness of each organism.
mse(i)=sum((F-force_dat.^2)/length(force_dat);
end
```

```
[err_sort,IX]=sort(mse);
%The fittest organisms of each generation are kept unchanged for the next generation
% incase one happens to be the best solution. These fittest organisms are also used to
% create the next generation.
dna_new=[dna(IX(1:new_pop),:);];

for j=1:new_gen
breednum=randperm(new_pop);

%select for breeding
g1=dna_new(breednum(1),:);
g2=dna_new(breednum(2),:);

for k=1:num_pars
g1g2=rand(1);

%Two fit organisms are blended to make a new one.
new_or(k)=g1g2*g1(k)+(1-g1g2)*g2(k);
flag1=0;

%The new organism is mutuated.
while !flag1
mut=.02*par_range(k)*randn(1)+new_or(k);

%For this problem the parameters are all positive so this statement assures that
%new parameters are always positive.
if mut ≥ 0
new_or(k)=mut;
flag1=1;
end
```

```
        end

        end

        dna_new=[dna_new; new_or;];
    end

    dna=dna_new;

end
```

APPENDIX C

MASSLESS SIMULATIONS

```
%This section is presented in a format very close to MATLAB code.
%The % symbol indicates a line that has been commented out.

%Function to solve ODEs ignoring mass
% tstart → Start time (should usually be zero)
% tend → End of simulation time
% om → Initial contact stiffness
% fc → Level of Coulomb friction
% kp → Proportional Gain
% td → Integral gain or design time constant
% del → Uncertainty
function [t,e] = solve_1gs(om,fc,kp,td,e0,tstart,tend,del)

options = odeset('MaxStep',.001);
(t,e)=ode45(@gs_1stp_gs,[tstart tend],e0,options);

function dedt = gs_1stp_gs(t,e)
%%%%Gain Scheduling
% 1st order model
dedt=-((td*(om*exp(e*(om/fc))*exp(-r*(om/fc))+kp))/...
```

```
.../((om+del)*exp(e*((om+del)/fc))*exp(-r*((om+del)/fc))+kp))*e;

%%%%Observer
%1st order model
% dedt=-(td*kp)/((om+del)*exp(e*((om+del)/fc))*exp(-r*((om+del)/fc))-...
%...-om*exp(e*(om/fc))*exp(-r*(om/fc))+kp);

end
end
```

APPENDIX D

SIMULATIONS INCLUDING MASS

%This section is presented in a format very close to MATLAB code.

%The % symbol indicates a line that has been commented out.

function [tout,eout] = Friction_ODE_observer(om,fc,m,c,kp,ki,f0,f0h,del,r,tstart,tend)

% r → Reference or Settling distance considered

% tstart → Start time (should usually be zero)

% tend → End of simulation time

% om → Initial contact stiffness

% fc → Level of Coulomb friction

% m → Mass

% c → Damping coefficient

% kp → Proportional Gain

% td → Design time constant

% f0 → Actual force initial condition

% f0h → Modeled force intial condition

% del → Uncertainty

e0=[r 0 0]; %State initial conditions <Displacement, Velocity, Acceleration>

tout=tstart; %Make first point of time output data

```
eout=e0; %Make first point of state output data

while tstart < .99*tend
%Solve forward motion, stop at velocity reversal
(t,e,te,ye,ie) = solve_p_ob(om,fc,m,c,kp,td,e0,r,f0,f0h,tstart,tend,del);

%Collect data from positive motion
nt=length(t);
tout=[tout; t(2:nt);];
eout=[eout; e(2:nt,:)];

%set new start time
tstart=t(nt);

%get new error IC
e1=e(nt,:);

%Solve new force IC
f1=fc-(fc-f0)*exp(-((om+del)/fc)*(-e1(1)+e0(1)));
f0=f1;

%Solve new model IC
f1h=fc-(fc-f0h)*exp(-(om/fc)*(-e1(1)+e0(1)));
f0h=f1h;

%set new error IC
e0=e1;

%If simulation is too close to end of specified time stop simulating
if tstart > .99*tend
```

```
break
end

%Solve negative motion, stop at velocity reversal
(t,e,te,ye,ie) = solve_n_ob(om,fc,m,c,kp,td,e0,r,f0,f0h,tstart,tend,del);

%Collect data from negative motion
nt=length(t);
tout=[tout; t(2:nt);];
eout=[eout; e(2:nt,:)];

%set new start time
tstart=t(nt);

%get new error IC
e1=e(nt,:);

%Solve new force IC
f1=-fc+(fc+f0)*exp(((om+del)/fc)*(-e1(1)+e0(1)));
f0=f1;

%Solce new model IC
f1h=-fc+(fc+f0h)*exp((om/fc)*(-e1(1)+e0(1)));
f0h=f1h;

%set new error IC
e0=e1;

end
```

```
end

%Function to solve positive motion
function [t,e,te,ye,ie] = solve_p_ob(om,fc,m,c,kp,td,e0,r,f0,f0h,tstart,tend,del)

options = odeset('Events',@zero_v_ob,'MaxStep',.001);
(t,e,te,ye,ie)=ode45(@gs_1stp_ob,[tstart tend],e0,options);

function dedt = gs_1stp_ob(t,e)

%%%%Gain Scheduling
%dedt = [e(2); e(3); -(1/m)*((td*((fc-f0h)/fc)*om*exp((om/fc)*e(1))*...
% ...*exp(-r*(om/fc))*exp(r*(om/fc))*exp(-e0(1)*(om/fc))+kp)*e(1)+...
% ...+kp*e(2)+((fc-f0)/fc)*(om+del)*exp(((om+del)/fc)*e(1))*...
% ...*exp(-r*((om+del)/fc))*exp(r*((om+del)/fc))*exp(-e0(1)*...
%...*((om+del)/fc))*e(2)+c*e(3))];

%%%%Observer
dedt = [e(2); e(3); -(1/m)*((td*kp)*e(1)+kp*e(2)+...
...+((fc-f0)/fc)*(om+del)*exp(((om+del)/fc)*e(1))*exp(-r*((om+del)/fc))*...
...*exp(r*((om+del)/fc))*exp(-e0(1)*((om+del)/fc))*e(2)+c*e(3)-...
...-((fc-f0h)/fc)*om*exp((om/fc)*e(1))*exp(-r*(om/fc))*exp(r*(om/fc))*...
...*exp(-e0(1)*(om/fc))*e(2))];
end
end

%Function to solve negative motion
function [t,e,te,ye,ie] = solve_n_ob(om,fc,m,c,kp,td,e0,r,f0,f0h,tstart,tend,del)

options = odeset('Events',@zero_v_ob,'MaxStep',.001);
```

```
(t,e,te,ye,ie)=ode45(@gs_1stn_ob,[tstart tend],e0,options);

function dedt = gs_1stn_ob(t,e)

%%%%Gain Scheduling
%dedt = [e(2); e(3); -(1/m)*((td*((fc+f0h)/fc)*om*exp(-(om/fc)*e(1))*...
%...*exp(r*(om/fc))*exp(-r*(om/fc))*exp(e0(1)*(om/fc))+kp)*e(1)+...
%...+kp*e(2)+((fc+f0)/fc)*(om+del)*exp(-((om+del)/fc)*e(1))*...
%...*exp(r*((om+del)/fc))*exp(-r*((om+del)/fc))*exp(e0(1)*...
%...*((om+del)/fc))*e(2)+c*e(3))];

%%%%Observer dedt = [e(2); e(3); -(1/m)*((td*kp)*e(1)+kp*e(2)+...
...+((fc+f0)/fc)*(om+del)*exp(-((om+del)/fc)*e(1))*exp(r*((om+del)/fc))*...
...*exp(-r*((om+del)/fc))*exp(e0(1)*((om+del)/fc))*e(2)+c*e(3)-...
...-((fc+f0h)/fc)*om*exp(-(om/fc)*e(1))*exp(r*(om/fc))*exp(-r*(om/fc))*...
...*exp(e0(1)*(om/fc))*e(2))];
end
end

function [value,isterminal,direction] = zero_v_ob(t,e)

value = e(2);
isterminal = 1;
direction = 0;
end
```

APPENDIX E

NIASA CODE

//This section is presented in a format of AeroBasic code.

//The // symbol indicates a line that has been commented out.

//

//

//

//Experimental Friction Compensation

//Brian Bucci, University of Pittsburgh

//The normal effects of Gains Aff, Vff, Kpi have been disabled.

//Now

//GainAff → level of Coulomb friction (N)

//GainVff → initial contact stiffness (N/um)

//GainKpi → friction compensation design time constant (1/sec)

//Note: As of now the integral action already used in the existing linear PID

// is not considered as of now. So the numbers relating to the design

// time constant and contact stiffness are close but not truly accurate.

//declared a double FrictCoul → [Level of Coulomb Friction]

```
//Applied scaling constants to get to units of current counts (CC)
FrictCoul = (double)(GainAff * 8388608 * 1674);

//declared a double sigmaCon => [Initial Contact Stiffness]
//Applied scaling constants to get units of (current counts)/(displacement counts)
sigmaCon = (double)(GainVff * 8388608 * 0.102170938);

//This variable initialization section really does not belong in the servo loop
//but this is where I could quickly make it work

//For this settling problem, friction compensation is only activated when the
//velocity command has ended.
//This if statement checks to see if the velocity command has ended.

//This if/else has been commmented out to leave the compensator running
//all of the time.
//if (VelocityCmdSubMsec == 0)
//{

//These next two if statements find the actual direction of motion for the system
//Check if motion is in the positive direction
if (VelLoopVelocityFbk > 0)
{
//This if statement detects velocity reversals
//VelDir is the direction of velocity at the previous sample
// 1 = positive velocity, -1 = negative velocity
if (VelDir != 1)
{
//If a velocity reversal occurs the modeled value of the force of friction at
//the velocity reversal must be stored.
```

```
//The (double) FrictIC stores this value.
FrictIC=-FrictCoul+(FrictCoul+FrictIC)*exp((sigmaCon/FrictCoul)*...
...*(-PositionError+ErrorIC));

//This pair of if statements guards against numerical issues that may compute a
//friction initial condition that is greater, magnitude, than the level of Coulomb
//friction. With an unrealistic IC algorithm failure is possible.
if (FrictIC > FrictCoul)
{
FrictIC = FrictCoul;
}
if (FrictIC < -FrictCoul)
{
FrictIC = -FrictCoul;
}

//The position of the velocity reversal, (or in this case position error), must be
//stored.
ErrorIC=PositionError;

//Since a velocity reversal just occurred, set the velocity to the new direction.
VelDir=1;
}
}

//Check if motion is in the negative direction
if (VelLoopVelocityFbk < 0)
{
if (VelDir != -1)
{
```

```
//If a velocity reversal occurs the modeled value of the force of friction at
// the velocity reversal must be stored.
//The (double) FrictIC stores this value.
FrictIC=FrictCoul-(FrictCoul-FrictIC)*exp(-(sigmaCon/FrictCoul)*...
...*(-PositionError+ErrorIC));

//This pair of if statements guards against numerical issues that may compute a
//friction initial condition that is greater, magnitude, than the level of Coulomb
//friction. With an unrealistic IC algorithm failure is possible.
if (FrictIC > FrictCoul)
{
FrictIC = FrictCoul;
t}
if (FrictIC < -FrictCoul)
{
FrictIC = -FrictCoul;
}
ErrorIC=PositionError;

//Since a velocity reversal just occurred, set the velocity to the new direction.
VelDir=-1;
}
}

//This pair of if statements are essentially solving the Dahl model in either
//direction to compute the additional integral gain needed to settle faster
//in the pre-rolling regime.
//GainFrict is a (double) that defines this additional integral gain.

if (VelDir == 1)
```

```
{
GainFrict = ((FrictCoul-FrictIC)/FrictCoul)*sigmaCon*...
...*exp(-(sigmaCon/FrictCoul)*(-PositionError+ErrorIC));
}
if (VelDir == -1)
{
GainFrict = ((FrictCoul+FrictIC)/FrictCoul)*sigmaCon*...
...*exp((sigmaCon/FrictCoul)*(-PositionError+ErrorIC));
}

//The additonal integral gain should always be a positive number so,
//to guard against any numerical issue that would cause this number to be
//negative this if statement is used. (The additional integral
//gain is supposed to approach zero if the system has to move far
//enough from a velocity reversal so it seems possible that a numerical
//issue could lead to a negative value.)
if (GainFrict < 0)
{
GainFrict = 0;
}

//This if statement guards against a numerical issue that could cause
// the additional integral gain to go above its desired maximum value.
if (GainFrict > 2*FrictCoul*sigmaCon)
{
GainFrict = 2*FrictCoul*sigmaCon;
}

//Integrates position error and applied nonlinear gain
//FrictInt += GainKpi*GainFrict*PositionError*(!CurrentCmdClamped);
```

```
//////////////////
//New Section where the rate of integrator is limited
SafetyGain = GainKpi*GainFrict*PositionError;

if (SafetyGain > 25)
{
SafetyGain = 25;
}

if (SafetyGain < -25)
{
SafetyGain = -25;
}

FrictInt += SafetyGain*(!CurrentCmdClamped);
//////////////////////
//Make sure that amplifier is enabled
FrictInt *= AmpEnabled;
//}

//This section is commented out to leave the compensator on all of the time
//The else section is executed if the velocity command is non-zero
//else
//{
// ErrorIC = PositionError;
// FrictIC = 0;
// GainFrict = 0;
//
//}
```

```
//Convert units of counts to +/-1
// CurrentCmd += .0000076293*FrictInt;
}
////////////////////////////////////////////////
////////////////////////////////////////////////
////////////////////////////////////////////////
```

BIBLIOGRAPHY

[1] H. Olsson, K. Åstrom, C. Canudas de Wit, M. Gafvert, and P. Lischinsky. Friction models and friction compensation. *European Journal of Control*, 4:176–195, 1998.

[2] C. Canudas de Wit and P. Lischinsky. Adaptive friction compensation with partially known dynamic friction model. *International Journal of Adaptive Control and Signal Processing*, 11:65–80, 1997.

[3] H. Olsson. *Control of Systems with Friction*. PhD thesis, Lund Institute of Technology, 1996.

[4] R. Stribeck. Die wesentlichen eigenschaften der gleit und rollenlager-the key qualities of sliding and roller bearings. *Zeitschrift des Vereines Seutscher Ingenieure*, 46:1342–1348, 1902.

[5] B. Armstrong-Helouvry, P. Dupont, and C. Canudas de Wit. A survey of models, analysis tools and compensation methods for the control of machines with friction. *Automatica*, 30:1083–1138, 1994.

[6] P. Dahl. A solid friction model. Technical report, Space and Missile Systems Organization Air Force Systems Command, 1968.

[7] C. Canudas de Wit, H. Olsson, K. Åstrom, and P. Lischisnsky. A new model for control of systems with friction. *IEEE Transactions on Automatic Control*, 40(3):419–426, March 1995.

[8] J. Swevers, F. Al-Bender, C. Ganseman, and T. Prajogo. An integrated friction model structure with improved presliding behavior for accurate friction compensation. *IEEE Transactions on Automatic Control*, 45:675–689, 2000.

[9] V. Lampaert, J. Swevers, and F. Al-Bender. Experimental comparison of different friction models for accurate low-velocity tracking. In *Proceedings of the 10th Mediterranean Conference on Control and Automation*, 2002.

[10] B. Bucci, D. Cole, J. Vipperman, and S. Ludwick. Friction modeling of linear rolling element bearings in high precision linear stages. In *Proceeding of the American Society for Precision Engineering*, 2009.

[11] Thomas Beckwith, Roy Marangoni, and John Lienhard. *Mechanical Measurements*. Addison-Wesley, 1995.

[12] Avraham Harnoy, Bernard Friedland, and Simon Cohn. Modeling and measuring friction effects: Physics, apparatus, and experiments. *IEEE Control Systems Magazine*, pages 82–92, 2008.

[13] F. Altpeter, M. Grunenberg, P. Myszkorowski, and R. Longchamp. Auto-tuning of feedforward friction compensation based on the gradient method. *Proceedings of the American Control Conference*, 2000.

[14] S. Chen, K. Tan, and S. Huang. Improvement of tracking performance of servomechanical system by an accurate four-parameter friction modelling and compensation. *IEEE Control Systems Magazine*, pages 28–34, 2007.

[15] Z Jamaludin, H Van Brussel, and J Swevers. Friction compensation of a xy feed table using friction model-based feedforward and an inverse-model-based disturbance observer. PP(99):1–1, 2009.

[16] D. Rizos and S. Fassois. Friction identification based upon the LuGre and Maxwell slip models. *IEEE Transactions on Control Systems Technology*, 17:153–161, 2009.

[17] Friedhelm Altpeter. *Friction Modeling, Identification, and Compensation*. PhD thesis, Lausanne, 1999.

[18] T. Tjahjowidodo, F. Al-Bender, H. Van Brussel, and W. Symens. Friction characterization and compensation in electro-mechanical systems. *Journal of Sound and Vibrations*, 308:632–646, 2007.

[19] Z. Jamaludin, H. Van Brussel, G. Pipeleers, and J. Swevers. Accurate motion control of xy high-speed linear drives using friction model feedforward and cutting forces estimation. *Manufacturing Technology*, 57:403–406, 2008.

[20] H. Olsson and K. Åstrom. Observer-based friction compensation. In *Proceedings of the 35th Conference on Decision and Control*, 1996.

[21] F. Altpeter, P. Myszkorowski, M. Kocher, and R. Longchamp. Friction compensation: PID synthesis and state control. In *European Control Conference*, 1997.

[22] U. Schafer and G. Brandenburg. Model reference position control of an elastic two-mass system with backlash and Coulomb friction using different types of observers. *Power Electronics and Motion Control*, 3:797–801, 1990.

[23] G. Brandenburg and U. Schafer. Influence and partial compensation of simultaneously acting backlash and Coulomb friction in a speed and position controlled, elastic two-mass system. In *Proceedings of the International Conference on Electrical Drives*, 1988.

[24] A. Dixit and S. Suryznarayanan. Adaptive observers for servo systems with friction. *17th IEEE International Conference on Control Applications*, 2008.

[25] J. Martinez-Rosas and L. Alvarez-Icaza. Adaptive compensation of dynamic friction in an industrial robot. In *17th IEEE International Conference on Control Applications*, 2008.

[26] I. Nilkhamhang and Akire Sano. Adaptive friction compensation using the GMS model with polynomial Stribeck function. *Proceedings of International Conference on Control Applications*, 2006.

[27] G. Brandenburg and U. Schafer. Influence and adaptive compensation of simultaneously acting backlash and Coulomb friction in elastic two-mass systems of robots and machines tools. In *International Conference of Control and Applications*, 1989.

[28] C. Walrath. Adaptive bearing friction compensation based on recent knowledge of dynamic friction. *Automatica*, 20:717–727, 1984.

[29] Daniel Helmick and William Messner. Simultaneous control of a precision linear stage in multiple lubrication modes with the complex lag. In *2008 American Control Conference*, 2008.

[30] J. Adams and S. Payandeh. Methods for low-velocity friction compensation: Theory and experimental study. *Journal of Robotic Systems*, 13, 1996.

[31] T. Tjahjowidodo. *Characterization, modelling, and control of mechanical systems comprising material and geometric nonlinearities*. PhD thesis, Department Werktuigkunde Katholieke Universiteit Leuven, 2006.

[32] F. Al-Bender, W. Symens, J. Swevers, and H. Van Brussel. Theoretical analysis of the dynamic behavior of hysteresis elements in mechanical systems. *International Journal of Non-Linear Mechanics*, 39:1721–1735, 2004.

[33] S. Futami, A. Furutani, and S. Yoshida. Nanometer positioning and its micro-dynamics. *Nanotechnology*, 1:31–37, 1990.

[34] S. Yoshida and K. Iizuka. Approaches to nanometer technology: a review of the Yoshida nano-mechanism project. Technical report, Research and Development Corporation of Japan, 1990.

[35] Daniel Helmick and William Messner. Describing function analysis of Dahl model friction. In *2009 American Control Conference*, 2009.

[36] N. Nise. *Control Systems Engineering*. John Wiley & Sons, Inc., 2000.

[37] F. Al-Bender, V. Lampaert, and J. Swevers. The generalized Maxwell-slip model: A novel model for friction simulation and compensation. *IEEE Transactions on Automatic Control*, 50:1883–1888, 2005.